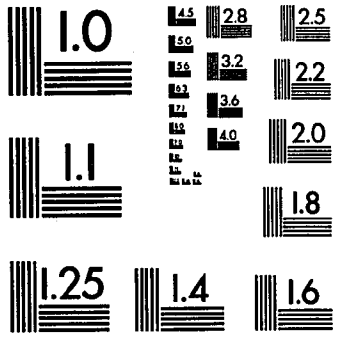

MICROCOPY RESOLUTION TEST CHART
NATIONAL BUREAU OF STANDARDS
STANDARD REFERENCE MATERIAL 1010a
(ANSI and ISO TEST CHART No. 2)

Fernandez-Raone, Elvio Daniel

IRON CATALYST DEACTIVATION BY CARBON DEPOSITION FROM SYNTHESIS GAS

City University of New York PH.D. 1985

PLEASE NOTE:

In all cases this material has been filmed in the best possible way from the available copy. Problems encountered with this document have been identified here with a check mark ✓.

1. Glossy photographs or pages _____
2. Colored illustrations, paper or print _____
3. Photographs with dark background ✓
4. Illustrations are poor copy _____
5. Pages with black marks, not original copy _____
6. Print shows through as there is text on both sides of page _____
7. Indistinct, broken or small print on several pages _____
8. Print exceeds margin requirements _____
9. Tightly bound copy with print lost in spine _____
10. Computer printout pages with indistinct print _____
11. Page(s) _____ lacking when material received, and not available from school or author.
12. Page(s) _____ seem to be missing in numbering only as text follows.
13. Two pages numbered _____. Text follows.
14. Curling and wrinkled pages _____
15. Dissertation contains pages with print at a slant, filmed as received _____
16. Other _____

_____

_____

Iron Catalyst Deactivation by Carbon Deposition from Synthesis Gas

by

E.D. Fernandez-Raone

A dissertation submitted to the Graduate Faculty in Engineering in partial fulfillment of the thesis requirements for the degree of Doctor of Philosophy, The City University of New York.

1985

This manuscript has been read and accepted for the Graduate Faculty in Engineering in satisfaction of the dissertation requirement for the degree of Doctor of Philosophy.

9/24/1985
date

Alberto La Cava
Chairman of Examining Committee

9/25/1985
date

Executive Officer

City University of New York

Abstract

Iron Catalyst Deactivation by Carbon Deposition from Synthesis Gas

by

E.D. Fernandez-Raone

Adviser:Professor Alberto LaCava

The kinetics of C deposition and CO_2 formation from CO over Fe powders, foils and supported pellets was studied at temperatures ranging from 250 to 450 C, using a microbalance tubular flow reactor. Carbon deposition proceeds at constant rates over all catalysts. The dependence of the rates on the CO partial pressure seems to follow a zero order power law kinetics in the range of study. Arrhenius plots show the activation energies for the rates of deposition and formation to be 31-32 Kcal/gmol.

The kinetics of carbon gasification with H_2, from C deposited on Fe supported pellets was studied on the same system, at temperatures in the range 350-450 C. CH_4 was the only detectable gaseous product. Constant rates of C gasification and CH_4 formation could be maintained for 2 to 3 days of continuous operation. Activation energies of 48 Kcal/gmol were obtained for both reactions.

Deactivation of commercial iron pellets by C deposition from pure CO was studied in the range 280 to 320 C. After an initial deactivation process, constant rates of deposition were achieved through filamentous growths. A pore blocking mechanism seems to explain the behaviour of these catalysts for the C deposition reaction.

Non-porous iron pellets were deactivated by C deposition (300-350 C) from pure CO and regenerated by hydrogenation (370-415 C). Both reactions behave similarly. An initial constant high rate is followed by deactivation and a much lower constant final rate. This can be explained by assuming an uneven patch-like iron distribution on the pellet surface.

C deposits from pure CO were readily gasified to methane from porous and non-porous pellets. The order of reaction with respect to hydrogen partial pressure appears to be 1. This seems to be consistent with a mechanism in which the formation of a CH_2M group is the rate limiting step.

Hydrogen increases the rate of C formation from pure CO. The order of reaction with respect to the hydrogen partial pressure varies with the hydrogen partial pressure.

ACKNOWLEDGEMENTS

I would first like to thank Professor Alberto I. LaCava, for his guidance, support and patience throughout this work.

I am also grateful to Professors H. Weinstein, M.K.N. Patell and K. McKeigue and Dr. Rocco Fiato for all the assistance and advice they have provided.

Technical assistance from John Bodnaruk, Bill Hall and the Chemical Engineering Department Shop is grately acknowledged. Special thanks to John Downey, from the Biology Department, for his work on the Scanning Electron Microscope.

My thanks also to Dean P. Karmel, Veneta Nikitiades, Dominick Mazzone, Peter Compo, Shi-Jin Shen, Susan Brandes, John O'Mara, Bill Cassidy, Moliere B., Ellen Floman and Rosa Nazar for various assistance and moral support.

This research was partially supported by grants from Exxon Corporation and The Research Foundation of The City College of New York.

CONTENTS

LIST OF TABLES

LIST OF FIGURES

Chapter I

INTRODUCTION

1.1 CATALYTIC SYNTHESIS OF HYDROCARBONS

As early as 1902, Sabatier et al. observed that methane could be formed catalytically from carbon monoxide/hydrogen mixtures over nickel and cobalt (1). Though scientifically sound and academically interesting, the idea of producing hydrocarbons synthetically was not to be developed for another 20 years. From 1923 to 1926, when Fischer and Tropsch (2-4) published their results and theorized on how to synthesize hydrocarbons over metals, conditions were more favorable to make the process commercially feasible.

Fischer and Tropsch's work opened the door to a new technology. This technology was quickly adopted in the 1930's in an oil-hungry Germany. By the end of World War II, there were 9 plants in operation using this technology in Germany, with an output of 700,000 tons/year (5). The availability of relatively inexpensive oil and natural gas after the war made the process uneconomical, practically all over the world, to the point that today there is only one commercial plant in operation: SASOL in South Africa.

The oil embargo of 1973 reawakened the interest in this field, when it became obvious to western countries that new sources of cheap energy and/or oil were needed in order to sustain and develop independent economies. The Fischer-Tropsch synthesis was one the most suitable choices for various reasons:

1- The world reserves of coal are enormous. They account for 65% of all world's recoverable fossil fuel reserves; while oil is only 10%.

2- The price of oil continues to go up and it is predicted that by the end of the century, if not before, this process can become economically competitive.

3- The Fischer-Tropsch synthesis is a very general commercial method that can be adopted to many local requirements. Different catalysts under different conditions can produce a wide range of products: light olefins, heavy aliphatic chains, oxygenated products, etc.

More than 5,000 publications and 5,000 patents can be found nowadays on the catalytic synthesis of hydrocarbons. This is an indicator of the growing interest of the scientific and industrial communities on the field. This interest has been focused on trying to understand how the process works and the different ways in which it can be improved and made more economic. At a basic level, almost all tools available to surface scientists have been used in search for a mechanism that can explain what happens at a molecular

level on the catalytic surface. Mossbauer (6), Auger (7,14), X-Ray Photoelectron (11) and Infrared Spectroscopies (8,12), X-Ray Diffraction (9) and LEED (10,16), are among the techniques applied recently. In conjunction with this work, several supported and unsupported metals have been tried as catalysts for the reaction. Metal oxides and their alloys have also been inspected. Since 1923, "just about everything but Rasputin's beard has been tried as a catalysts" said one Fischer-Tropsch chemical expert (13).

In spite of the considerable amount of information on the subject, authors do not seem to agree on the answer to some fundamental questions, such as:

1- Does the reaction take place through the formation of carbon oxygenated intermediates, through a carbon hydrogenated intermediate; or through both?
2- How does chain growth take place?
3- Why do certain catalysts deactivate during the reaction and how can this be prevented?
4- What is the link between carbon formation and the way the reaction proceeds over certain metals?
5- What parameters characterizing the catalyst are related to the catalytic activity and selectivity?

These, among others, are not just rethorical questions. The answer to these questions will help transform the art of hydrocarbon synthesis into a science.

1.1.1 The Chemistry

The chemistry of the hydrogenation of carbon monoxide can be described by the following basic reactions:

$$(2n+1)\ H_2 + n\ CO \longleftrightarrow C_nH_{2n+2} + n\ H_2O$$

$$(n+1)\ H_2 + 2n\ CO \longleftrightarrow C_nH_{2n+2} + n\ CO_2$$

$$2n\ H_2 + n\ CO \longleftrightarrow C_nH_{2n} + n\ H_2O$$

$$n\ H_2 + 2n\ CO \longleftrightarrow C_nH_{2n} + n\ CO_2$$

$$2n\ H_2 + n\ CO \longleftrightarrow C_nH_{2n+1}OH + (n-1)\ H_2O$$

$$(n+1)\ H_2 + (2n-1)\ CO \longleftrightarrow C_nH_{2n+1}OH + (n-1)\ CO_2$$

Other reactions that can occur, include the Boudouard reaction:

$$2\ CO \longleftrightarrow C + CO_2$$

and carbon formation:

$$CO + H_2 \longleftrightarrow C + H_2O$$

The above set of reactions (1) to (8), describes the formation of parafins, monoolefins and alcohols. It is generally accepted that these are the only possible products of the Fischer-Tropsch synthesis. Other synthesis, like oxosynthesis and isosynthesis, could include other reactions that will not be discussed here.

1.1.2 The Thermodynamics

The thermodynamics of the $C-H_2-O_2$ system is well known. Values for the heats and free energies of reaction and the equilibrium constants for reactions (1) to (8) are readily available (17,18).

Generally, the reactions forming carbon dioxide have larger equilibrium constants than those forming water. This indicates that products formed by elimination of carbon dioxide are thermodynamically more favorable than those formed by elimination of water. Since the synthesis reactions lead to smaller number of moles of product, the equilibrium conversion at any temperature should increase with pressure. All reactions are not thermodynamically favored above 450 C, except methanation. The higher the temperature, the greater the tendency to form methane. Carbon monoxide rich mixtures favor aldehyde formation, while hydrogen rich feeds favor parafin formation.

The way in which pressure, temperature and composition affect the equilibrium constants has been tabulated and plotted elsewhere (19). Thermodynamic studies can only predict the theoretical limits that bound the production of a desired hydrocarbon. Thermodynamics alone cannot predict product composition or selectivity over different catalysts. This is because real processes generally operate at conditions far from those of equilibrium. Also, the introduction

of a catalytic surface transforms the original $C-H_2-O_2$ system into a $C-H_2-O_2$-catalyst system, whose thermodynamics have to be studied for each catalyst in particular.

1.1.3 The Chemisorption

The chemisorption of reactants, products and intermediates on an active surface plays an important role in any catalytic reaction. An understanding of this role, and the factors affecting it, is essential to the study of a catalytic chemical process. In the case of synthesis of hydrocarbons, information exists on the individual adsorptions of carbon monoxide and hydrogen. Both gases chemisorb at room temperature and low pressures on Co, Cr, Fe, Ir, Mo, Ni, Os, Pt, Rh, Ru, Ta, Ti, V and Zr (20).

Molecular hydrogen is adsorbed rather extensively on a wide variety of metals, even at temperatures as low as 78 K (44). Transition metals are able to adsorb a further amount of hydrogen, provided the hydrogen is made atomic in the gas phase (45,46). The hydrogen atoms appear to locate in the interstices between surface metal atoms or at the intersections of lattice planes (47). Hydride formation and hydrogen dissolution in the metal bulk have been reported (48).

Carbon monoxide has been observed to chemisorb associatively in two different ways on transition metals. In a linear (a) or a bridged (b) structure :

(a) (b)

The monocoordinated form (linear) is the one most frecuently reported in the literature (21-26), though both structures may coexist (27,28). These forms of associative chemisorption can give rise, over metals like Ti, Fe and Mo, to a dissociative adsorption, even at room temperature. Dissociative chemisorption can also occurr at higher temperatures on metals that adsorb carbon monoxide associatively at room temperature. The ability of transition metals to bind carbon monoxide can be correlated to their ability to synthesize different hydrocarbons (section 1.1.5). Metals that readily dissociate carbon monoxide (Co, Ni and Ru) produce mainly hydrocarbons, while those which do not dissociate it (Pt, Pd and Ir) produce alcohols (15). The activation energies for carbon monoxide dissociation on transition metals have been estimated theoretically (29,30). No experimental values can be found in the literature. Values of 23 kcal/mole for nickel and 16 kcal/mole for iron were calculated. Carbon monoxide dissociation is usually accompanied

(at high temperatures) by the release of oxygen as carbon dioxide. This disproportionation reaction (also called Boudouard reaction) leads to carbon formation on the catalyst.

1.1.4 The Mechanism

An explanation on how carbon monoxide/hydrogen mixtures react over a metal surface was first advanced by Fischer and Tropsch in 1926 (4). Their idea was that the metal surface was carbided by the carbon monoxide. The carbide was then hydrogenated to methylene groups which polymerized to longer hydrocarbons. This path for hydrocarbon production was criticized mainly on the ground that it cannot predict the formation of oxygenated products. Other theories tried to account for this fact by suggesting the formation of an oxygenated intermediate (enolic complex), which could undergo further hydrogenation to a methylene group or desorb, after condensation, as an alcohol, aldehyde, acid, etc.

Many more mechanisms can be encountered in the literature and each one accounts satisfactorily for the product distribution obtained experimentally. Apparently, a unique mechanism does not seem to exist and the answer has to be found for each particular metal/support/promoter system. Despite the variety of schemes proposed through the years, all mechanisms can be grouped into one of the following two main categories:

1) Reaction proceeds through a hydrogenated intermediate.

2) Reaction proceeds through an oxygenated intermediate.

In the first category, carbon monoxide is assumed to adsorb dissociatively on the metal. The carbon atoms so formed are individually hydrogenated to CH_x species which combine to form the products. Fischer-Tropsch theory (4) belongs to this first group. Their original hypothesis was refined by Craxford and Rideal (32-34) who suggested that only surface carbide took part in the reaction and that methylene groups formed by hydrogenation of the carbide, react to produce adsorbed macromolecules. Hydrocracking of these macromolecules gave rise to light olefins and paraffins. The carbide theory was subjected to criticism by Anderson (35) and Emmett (36-38). They concluded that bulk phase carbide participates in the synthesis to a negligible extent. Even though the carbon in the carbide phase does not take part in the reaction, the surface carbon has been shown to play an important role in it. Methane and higher hydrocarbons have been produced by hydrogenation of deposited carbon, in the absence of carbon monoxide (15,39-42). Also, deposited labelled surface carbon has been detected in hydrocarbon products by Sachtler et al. (43).

In the second category, carbon monoxide is assumed to adsorb associatively on the metal surface. It is directly hydrogenated to an oxygenated complex. Chain growth occurs by water elimination between neighbour species and/or carbon

monoxide insertion into metal-H or metal-C bonds. The idea that oxygenated species on the catalytic surface were the building blocks under Fischer-Tropsch reaction conditions was first advanced by Elvins and Nash (49). This approach has recieved much theoretical and experimental support (36,37,50-55). Infrared studies have shown the presence of carboxyl, carbonate and carbonyl surface species. Heats of adsorption measurements and temperature programmed desorption studies also suggest the presence of oxygenated intermediates on different catalysts (56,57). This evidence tends to confirm the basic premise on which this theory is based : that carbon monoxide adsorbs associatively on certain metals. At the same time it does not disprove the fact that carbon monoxide can also adsorb dissociatively, even on the same surfaces. Coexistance of both forms has been reported (27,28).

A model that unifies both categories has been proposed by Dry (5). In this scheme, chemisorbed carbon monoxide gives rise to an activated complex that can either be hydrogenated to an oxygenated complex or dissociate to carbon and oxygen atoms. After this initial steps, the main features of both categories remain the same. The strength of the C-O bond in the complex formed upon adsorption will determine whether oxygenated compounds, hydrocarbons or a mixture of both will be obtained as final products.

1.1.5 The Catalyst

A broad spectrum of products may be obtained from the reaction of carbon monoxide/hydrogen mixtures over different catalysts, under different conditions. This flexibility makes the catalytic synthesis process very interesting from a commercial point of view. Recent studies demonstrate that the process can be tailored to specific needs. Pilot plant tests show promising results but further economic improvements must be achieved. The need for a cheap, lasting catalyst is apparent.

The search for a good combination of metal (oxide)/support/ promoter has dramatically increased in the last ten years. Meanwhile, the scope of the search has been narrowed to a few metals and their oxides. Any possible catalyst must satisfy the requirement that either carbon monoxide, hydrogen or both gases chemisorb on the surface under reaction conditions. Also, if adsorption is too strong, or too stable oxides or carbides are formed, reaction cannot take place at reasonable temperatures. These limitations place a great constrain in the number of possible candidates. Among the metals that fulfill the above conditions, Fe, Co, Ni, Ru and Rh have been proved to be the most active catalysts. From a commercial point of view, Fe and Co are the most useful. Ru favors formation of high molecular weight products, Rh produces oxygenates and Ni sythezises

mainly methane. Their high price makes them also less attractive.

Historically, Co was the first catalyst to be used industrially. The German process developed during World War II called for a Co, Mg and Th catalyst supported on Kieselguhr. Nowadays, Fe has replaced Co as the catalyst of choice in many processes. Fischer and Tropsch pioneer work was done on an alkalized Fe catalyst, which deactivated rapidly when operated at low pressures. This setback has been overcome by operation at high pressures and by the use of specific promoters. New technologies, e.g. slurry and fluidized bed reactors, have also helped improving the yields and conversions of the synthesis.

Many species have been tried as promoters over the years. The purpouse of promoter addition is dual. Metal oxides, such as alumina, thoria and magnesia, are added to inhibit active metal recrystallization. Alkali metals appear to be good electronic promoters increasing reactants chemisorption and facilitating complex formation.

The search for the best possible catalysts is still far from over. The activity of noble metals have been investigated with litle success. Other metals like Mo and Cr have been tried. Mo shows reasonable activities at high temperatures (700 K) and those of Cr are even lower. Unless a special product is required, promoted Fe seems to be so far the cheapest and most active catalyst for hydrocarbon synthesis.

1.2 CARBON FORMATION

When carbon bearing gases are contacted with an active metal surface at high temperatures, carbon deposition on the catalyst often occurs. This deposition is usually a reason for catalyst deactivation and can lead to particle swelling and disintegration. Powdering of the catalyst particles results in plugging of fixed bed reactor tubes. In the case of fluidized beds, disintegration can produce low particle density and possible losses of fines in the effluent stream. Also, coking on surfaces of process equipment can reduce heat transfer efficiencies and increase pressure drops in narrow tubes. In order to avoid or minimize these problems of hydrocarbon processing, an understanding of the factors affecting carbon deposition is essential.

Surface carbon formation can be originated in different ways. At sufficiently high temperatures, hydrocarbon cracking is the main source of coke production, through a homogeneous reaction. At lower temperatures, carbon can be formed catalytically on many transition metals. Studies show carbon can be produced from a variety of hydrocarbons : methane, ethane, ethylene, acetylene, propane, benzene and also carbon monoxide and dioxide (58-70).

Recent research on the field has been concentrated in studying the mechanism(s) of carbon formation and the kinetics of the process. Two approaches have been used that com-

plement each other. Microbalance techniques using pure metal foils, metal particles or supported metals have served to establish the kinetics of the reaction and its dependence on the operational variables. Electron microscopy studies, performed under controlled atmosphere conditions have allowed an insight into the morphology and mechanism for the growth of carbon deposits.

1.2.1 Structure and Deposition

Carbon has been observed to deposit in a variety of forms over catalytic and non-catalytic surfaces. The structure of the deposits range from a highly crystalline graphitic form to an almost amorphous state depending on the mechanism and conditions of formation. Carbon filaments have also been obtained from numerous hydrocarbons. Thermodynamic studies have been performed to predict regions where carbon may be formed. Safe H_2/CO ratios, where no carbon formation occurs have been tabulated (71,72). The usefulness of these kind of studies has been cast in doubt as contradicting reports show formation of carbon in regions where thermodynamics would indicate no deposition (73,74). In many circumstances, kinetic considerations rather than thermodynamic equilibrium dictates whether and how carbon will form.

Laminar graphite, with a crystalline structure of numerous single crystals oriented with their basal planes paral-

lel to the substrate surface, has been obtained at high temperatures (600-1200 C) under low deposition rates. Non-crystalline deposits seem to be formed at lower temperatures or higher deposition rates. Filamentous carbon deposits have been observed at both low and high temperatures. Carbon fibers of different shapes and structure have been reported from a diversity of hydrocarbons over transition metals. Helically twisted filaments, hollow thin-skinned tubes and straight strands are among the forms encountered in the literature (75-78). A (carbided) metal particle usually appears at the tip or middle of the carbon filament. An explanation for filamentous carbon growth has been advanced by Baker (67) (section 1.2.2), though a clear picture of the whole process is not available yet.

When carbon monoxide or synthesis gas react over metals like Fe, Co or Ni, a modification of the catalytic surface occurs, sometimes leading to the formation of carbon and/or a metal carbide. Even at the low temperatures (250-350 C) at which hydrocarbon synthesis are carried out, substantial amounts of carbon deposits have been detected. Similarly to deposition from hydrocarbons, filamentous carbon and lamellar forms (crystalline or amorphous) have been reported (75,77,80).

1.2.2 Kinetics and Mechanism

A literature survey on carbon formation from hydrocarbons, synthesis gas and carbon monoxide indicates that some common features are present in different systems:

1- Carbon deposition can be maintained for extended periods of time. Carbon is usually produced in the form of filaments.

2- The presence of hydrogen has been found to increase the rates of deposition from hydrocarbons.

3- Metal particles are included in or within the filamentous growths.

4- Metal carbides have been observed in many cases.

5- The rate determining step has been associated with a solid-state diffusion mechanism.

These similarities suggest that a general mechanism for carbon formation must apply in many instances.

Baker et al. (67) tried to explain carbon filament formation in the following way: gaseous carbon containing species are adsorbed on the catalytic metal surface where they undergo a series of reactions (hydrogenolisis, dehydrogenation, etc.) to produce active carbon atoms. These carbon atoms, in term, dissolve into the bulk metal and migrate to regions of active growth. Metal crystals are pushed out of the surface by the growing accumulation of atomic carbon and are carried with(in) the filament, catalyzing further pro-

duction of carbon. This allows for the surface reaction to propagate, eventhough the amount of carbon produced this way would be more than enough to cover all the available active sites. Diffusion of carbon through the metal particles has been suggested to be the rate limiting step, as activation energies for the whole deposition process agree well with published values for carbon diffusion. Baker's idea was that a temperature gradient was the driving force behind carbon diffusion. Rostrup-Nielsen and Trimm (78) concluded that the concentration difference was the result of equilibrium established between the gas phase and the growth crystal.

Boehm et al. (75) proposed a mechanism similar to Baker's, in which carbon filaments can only grow from certain crystal faces of a carbided catalyst, the growth rate being controlled by the difussion of carbon to these specific crystal faces. Disorganized or poorly crystalline carbon in contact with other crystal faces of the carbide phase would be transported to the thermodynamically more favorable carbon phase. The regions were this is thought to happen are the grain boundaries, where carbon atoms are trapped and accumulate disrupting the metal surface. Similarities of crystallite sizes of the original metal foils and crystallites contained in the carbon filaments support these conclusions (81).

Hydrocarbon pyrolysis studies in the absence of hydrogen show that carbon deposition terminates after a fixed amount of carbon has been incorporated into the catalyst. Not surprisingly, the amount of carbon uptake corresponds closely to the solubility of carbon in the metal at the deposition temperature (66,67). Metal particles appear to be inmobilized in these experiments, preventing therefore filament formation. The particle surface will become encapsulated and the fiber will not be able to grow.

Carbon formation always brings about structural changes in the surface and bulk of the metal used as catalyst. Surface rearrangement in the case of Ni (82) and carbide formation in Fe catalysts have been observed under carbon deposition conditions. Although Co and Ni carbides do exist, their presence in the metal bulk has not been detected during hydrocarbon synthesis. The complexity of the C-Fe phase diagram is reflected in the many C-Fe species encountered under reaction conditions. Cementite (Fe_3C), Hagg carbide (Fe_5C_2), Fe_7C_3 and other non-stoichiometric Fe-C compounds are among the ones reported in the literature (9,77,79). Different models have been proposed trying to account for Fe carbide formation and its role in the synthesis of hydrocarbons:

1- Carbide model

2- Competition model

3- Slow activation model

In the carbide model, the real catalyst is the iron carbide bulk with active sites on its surface. This explanation was first proposed by Fischer and Tropsch (4). Recently, some other authors have come to support this theory (6,83,84), eventhough this model cannot account for the formation of oxygenated products. Iron carbide has also been shown to be inactive for hydrocarbon synthesis (85). The competition model assumes iron atoms on the surface to be the active sites. Once carbon atoms are formed, they can either combine with iron to form carbides (i), react with hydrogen to hydrogenated compounds (ii), or become inactive carbon (iii). The carbidation reaction stops eventually when the bulk iron is completely carbided. At this point, the surface carbon can take part in two competing reactions : (ii) and (iii). As long as surface active carbon production is the slowest step, competition for its use will be present. When carbon monoxide adsorption and dissociation are faster than all subsequent reactions, enough carbon will be available for hydrogenation and carbidation and the processes will proceed autonomously. This is the basis for the slow activation model. Here, hydrogenation is believed to occur at surface complexes consisting of carbon, hydrogen and iron in a certain configuration. These complexes are thought to form slowly, hence the name of the model.

1.2.3 Deactivation and Regeneration

Catalysts used in hydrocarbon synthesis can deactivate as a result of different factors:

1- Loss of active area due to crystalline growth (sintering).

2- Loss of active area due to deposition of carbon or carbonaceous compuonds (fouling).

3- Chemical poison of metal.

When supported metals are used as catalysts, the initial active area usually decreases with usage. Metal particles tend to agglomerate into bigger ones with the consequent loss of activity. Temperature has a marked effect upon sintering as at high temperatures metal mobility is enhanced. This has been observed for iron catalysts under hydrocarbon synthesis conditions. Precipitated iron catalysts show a lowering in the area and also crystal growth after many days of continuous operation (5).

Both carbon and carbonaceous compounds can be formed in many petroleoum and petrochemical processes. These deposits, when strongly adsorbed on the metal catalyst, somehow block the active sites leading to losses in activity. This is an important cause for deactivation in Fischer-Tropsch catalysts. Carbon deposits have been observed to form over iron catalysts from carbon monoxide and carbon monoxide/hydrogen mixtures. Inert carbon lowers the metal area. Particle

swelling and disintegration may result from prolonged carbon deposition. A decrease in activity can also be produced by high molecular weight hydrocarbons. At reaction temperatures, these products are present as liquids, filling wholly or partially the catalyst pores. Diffusion limitations will therefore slow down the overall rate of reaction. This is not truly a fouling problem. Fouling of the metal surface results from strong adsorption of some of the waxes formed. Those waxes not soluble in the liquid product will tend to remain on the catalytic surface, covering useful sites. Reactivation can only be achieved by the removal of those heavy components attached to the catalyst.

Among the chemicals that poison Fischer-Tropsch synthesis catalysts are sulphur, halogens and some metals. Even at low levels, these contaminants can readily deactivate iron catalysts. Reactivation has proven to be lenghty and difficult (35). Regeneration of fouled commercial catalysts has been more succesfull. Burning of the heavy residues with hydrogen at high temperatures removes almost all deposits. Aged iron catalysts treated this way recover their original activity (5).

Quantitative analysis of catalyst deactivation have been attempted by many authors (86-90). In the case of cristallite sintering, the rate of decay of exposed metal surface, S, has been found to obey an equation of the form:

$$dS/dt = -k.S^n$$

where the range of the exponent n is in between 2 and 8 (91).

Deactivation by coking or fouling of porous catalysts has been described by a simple equation of the form:

$$dA/dt = -K.A^n$$

where A is the activity defined as the fraction of active sites that remain active, and K is a function of the reaction conditions. By assuming different functionalities of A with time, many previously proposed decay equations can be generalized by this representation (92). Another approach takes into account the time dependency of activity with time, through the way in which the poison is produced (93). Activity function is defined so that:

$$dC_c/dt = r_c.A(C_c)$$

where r_c is the initial coking rate and C_c is the carbon concentration at time t. $A(C_c)$ will depend on C_c in a way to be determined experimentally. Several expressions have been proposed:

$$A(C_c) = \exp(-K.C_c)$$

$$A(C_c) = 1-K.C_c$$

$$A(C_c) = 1/(1+K.C_c)$$

Possible models for the mechanism of carbon formation can be checked by fitting kinetic (r_c) and activity data ($A(C_c)$) for a particular catalyst.

1.3 PRESENT WORK

The literature survey presented in the previous sections reveals the need for more quantitative information on the kinetics of carbon formation from synthesis gas and its relationship (if any) to the hydrocarbon synthesis process. The present work was initiated in order to provide kinetic data under specific conditions and to help elucidate the mechanism of carbon and hydrocarbon formation over pure iron catalysts from synthesis gas. By using unpromoted catalysts, a baseline can be established and the role of additives be better understood. The following rections were thus investigated:

1- Carbon formation from pure carbon monoxide and CO/H_2 mixtures over Fe catalysts (powders, foils and supported pellets).

2- Gasification with hydrogen of the deposits obtained on supported pellets.

3- Deactivation of iron pellets by carbon formation from carbon monoxide and synthesis gas.

4-Observation of carbon deposits by scanning electron microscopy.

The studies were carried out in a microbalance tubular flow reactor, as described in the next chapter, and kinetic data was collected on different catalysts for various experimental conditions.

Chapter II

EXPERIMENTAL

2.1 INTRODUCTION

All kinetic experiments were carried out in a thermogravimetric flow system. It consisted of a microforce balance attached to a tubular flow reactor, a feed system for reactants and a gas chromatograph.

The catalyst samples were suspended from the balance and reduced in hydrogen. After flushing with helium, reactants were admitted into the reactor and weight changes of the sample were continuously recorded. The flow rate of inlet gases was controlled by needle-valves and measured by calibrated rotameters. Gas compositions of reactants and products were analyzed with a gas chromatograph. Metal surface areas were measured using the hydrogenation of ethylene from 50% hydrogen and 50% ethylene mixtures as a reference reaction.

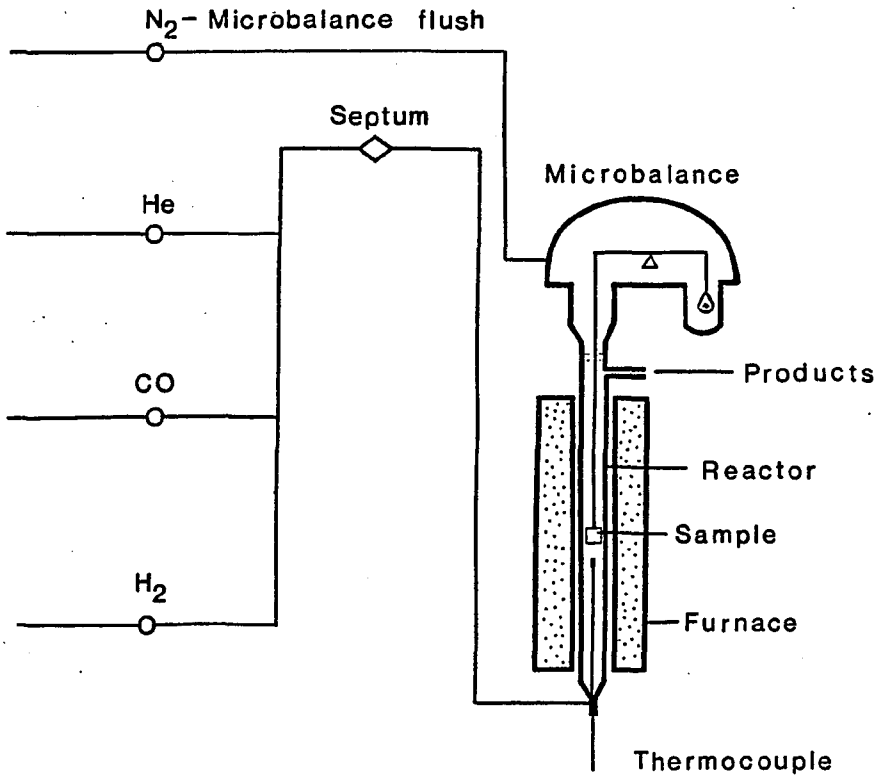

Figure 1. Schematic of flow microbalance reactor.

2.2 EQUIPMENT

2.2.1 Microbalance and Reactor

A C.I. Electronics (MARK 2B) vacuum microbalance head was used in connection with a Vycor tubular reactor (Fig. 1). The balance electric control cabinet was attached to a Cole-Palmer recorder model 8372-20.

The microbalance characteristics were the following:

Capacity	1 gm sample
	1 gm counterweight
Sensitivity	0.5%
Ranges	0-25 microgm
	0-250 microgm
	0-2.5 mg
	0-10 mg
	0-100 mg.

The microbalance-reactor system was suspended from a metal structure bolted to the floor. Vibrations were minimized by mounting the balance on rubber shockers. The microbalance head was continuously flushed with helium to prevent corrosion of the electrical parts. Calibrated weights, used as counterweights, were placed on an aluminum pan hanging on one arm of the balance. Catalyst samples were suspended from the other arm, at the end of a series of quartz suspension fibres. Short segments, 3 to 6 cm, were preferred because they reduced oscillatory noise.

Powdered catalysts were located in a small quartz basket. Metal foils were suspended through a hole from a quartz fiber hook. Pellets were suspended by fastening a piece of copper wire (.1 cm diameter) around them. A blank run to test copper wires showed the copper to be inactive under reaction conditions.

The microbalance head was connected to the reactor by a ball-joint. This made the centering of the sample inside the reactor a simple task. The connections were sealed with Dow Corning silicon grease. The reactor was made out of Vycor tubing, 2.54 cm external diameter and 50 cm long. At operating conditions, conversion levels were low enough to allow the reactor to be treated as differential.

2.2.2 Furnace and Temperature Control

The furnace used in these experiments was a Lindberg, Type 123-12. Its internal resistence of 18 ohms allowed operation at temperatures up to 1000 C. The dimensions were: length 30 cm, 12 cm external diameter and 3 cm internal diameter. Power to the furnace was controlled by a Lindberg Temperature Controller, in conjuction with a chromel-alumel thermocouple. By placing the thermocouple inside the reactor, close to the catalyst sample, very accurate measurements of the reaction temperature were possible.

2.2.3 Feed System for Reactants

Gases were supplied from cylinders, through two-stage pressure regulators, calibrated rotameters and fine control needle-valves. The rotameters were calibrated with a bubble flow meter. Purification of the reactants was not attempted because of the high purity of the gases used. Delivery of the gases was done through stainless steel and PVC tubing, periodically checked for leaks.

2.2.4 Gas Chromatograph

Gas compositions were analyzed with a Hewlett-Packard, F&M Scientific 700, gas chromatograph. Nitrogen was employed as a carrier at a flow rate of 60 cc/min. The detector operated at a temperature of 200 C and at a constant current of 110 mA. Its signal was recorded by a Cole-Palmer recorder, model 8373-20. Two chromatographic columns were needed for complete analysis of samples. They were installed in such a way that each one served as the reference column to the other one. Samples could be injected into either column as required by the analysis to be performed. Hydrogen and carbon monoxide were separated by a 2 m long, 0.6 cm internal diameter, stainless steel column filled with 30-60 mesh Matheson silica gel. Carbon dioxide, methane and higher hydrocarbons were analyzed with a Poropak Q, 180-200 mesh, column of .6 cm internal diameter and 36 cm long. Both columns were oper-

ated at room temperature. Injections were made with a Hamilton syringe, gas tight, 1 ml capacity.

Calibration charts were obtained by injection of known amounts of pure gases and plotting the volume injected as a function of recorded peak heights. Measurement of peak areas was not necessary as the peaks were quite sharp and their heights gave a linear calibration in the range of interest (Fig. 3 and 4). Calibration charts and retention times (Fig. 2) were checked regularly.

2.2.5 Scanning electron microscope

Foils and pellets were observed by means of scanning electron microscopy. The microscope used in these studies was a Cambridge S4, with a maximum power of 30 KV. Samples were mounted on a disk holder and coated with gold. This improved the sharpness of the image by eliminating electric overcharging.

2.2.6 Materials

Iron foils, powders and supported iron pellets were used in this work. Iron powder was provided by Fisher Scientific Company, in the form of ferric oxide of 99.7% purity. Polycritalline iron foils were obtained from Johnson Matthey Chemicals. They were provided in the form of 10x10 cm sheets, 0.1 mm thick and a purity of 99.99%. Silica-alumina

supported iron catalysts were supplied by United Catalysts Inc.. The spherical pellets, 0.6 cm diameter, had an iron content of 2.5% in weight and a total surface area of 5 m^2/gm. Gases were purchased from Matheson Company and were of the highest purity available. Non-porous pellets were obtained from Alcoa Chemicals. They were made out of alumina in the shape of spheres 1/8 " diameter. The commercial name is Tabular Alumina T 162. Impregnation of the pellets was done with ferrous chloride supplied by Mallinckrodt Chemical Works with a purity of 99.98%.

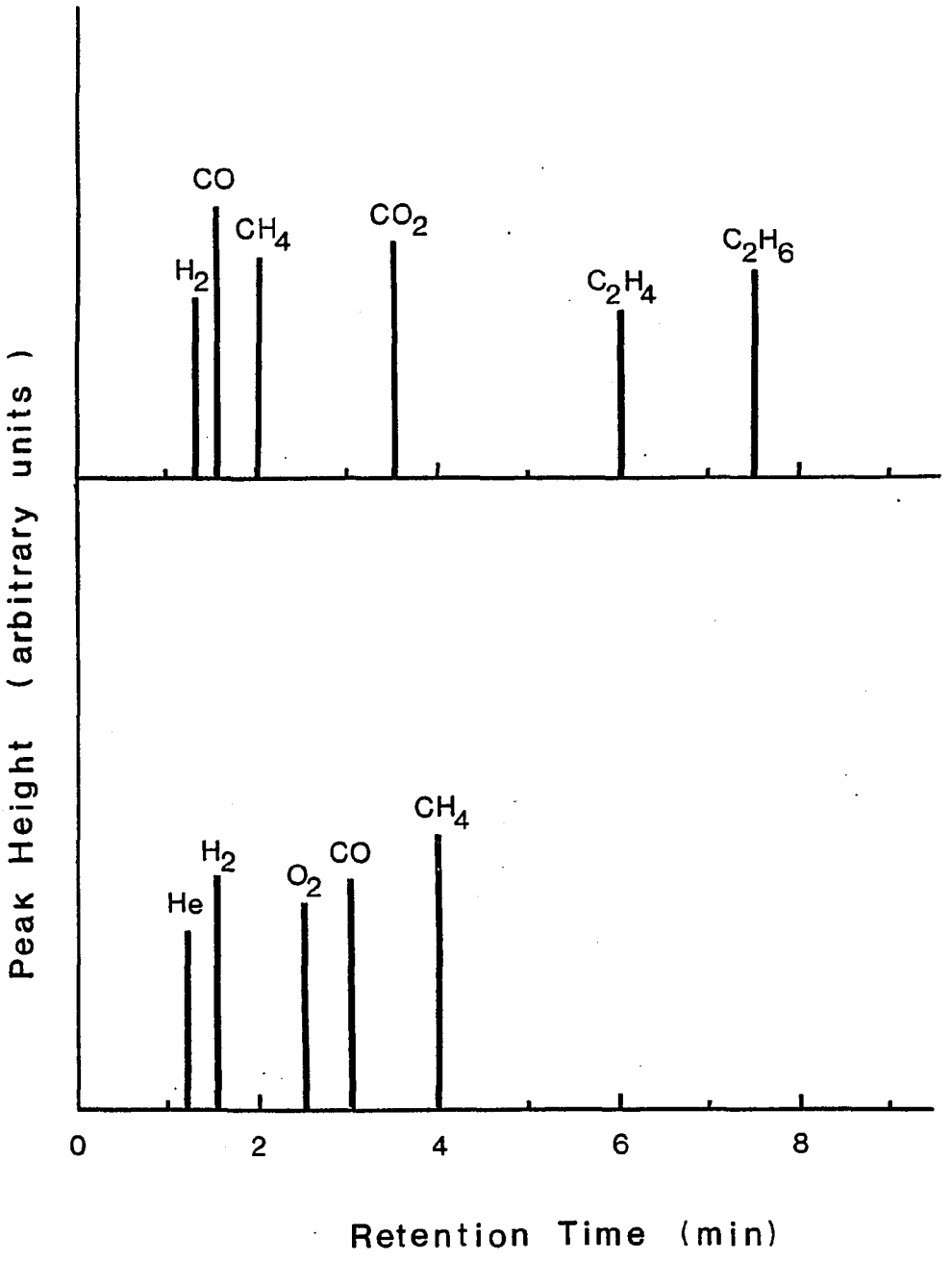

Figure 2. Retention times for gas Chromatography. Key: top, Poropak Q column; bottom, silica gel column.

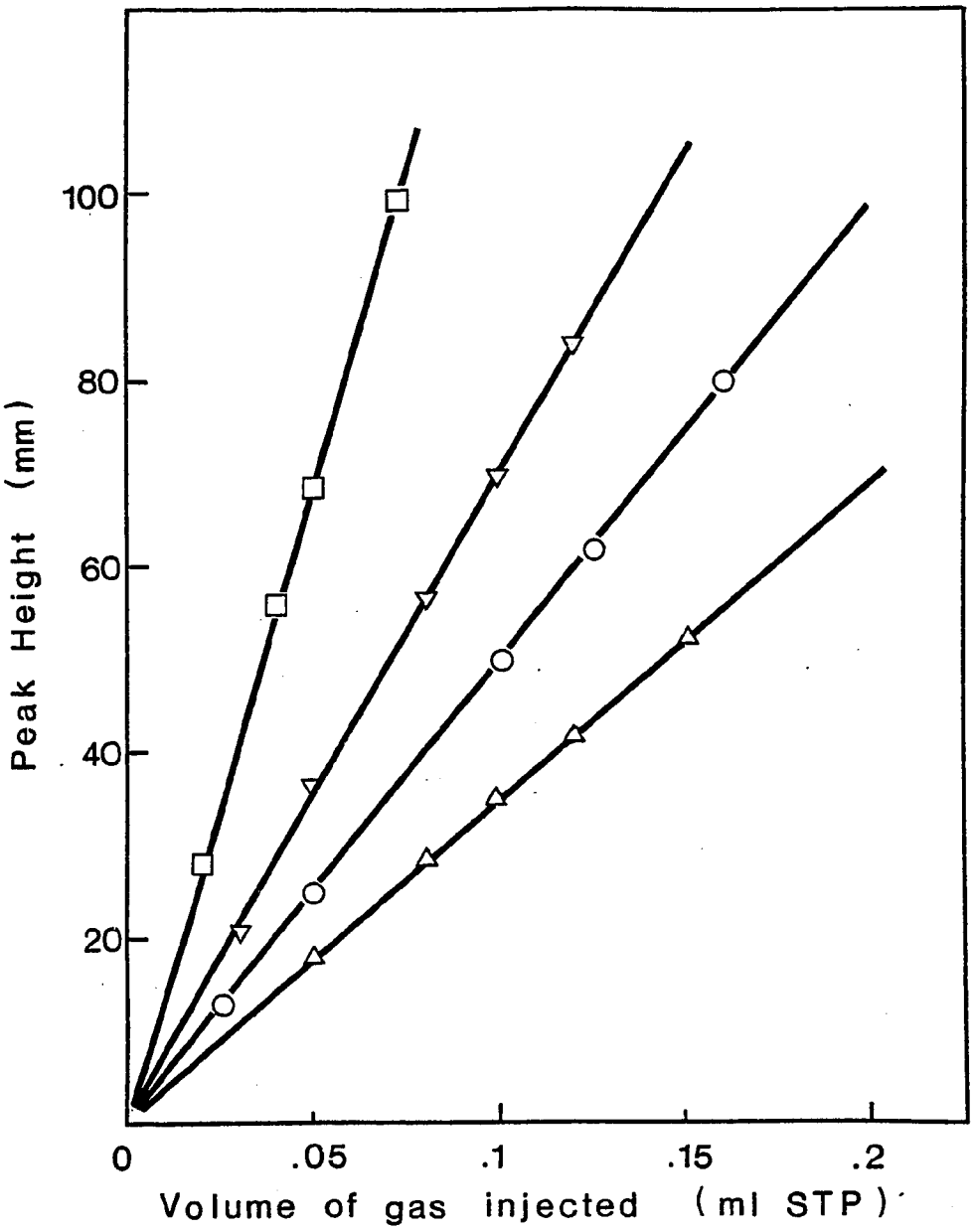

Figure 3. Calibration chart for silica gel column.

○ : H_2, attenuation 20

△ : CO, attenuation 1

□ : CH_4, attenuation 5

▽ : He, attenuation 10.

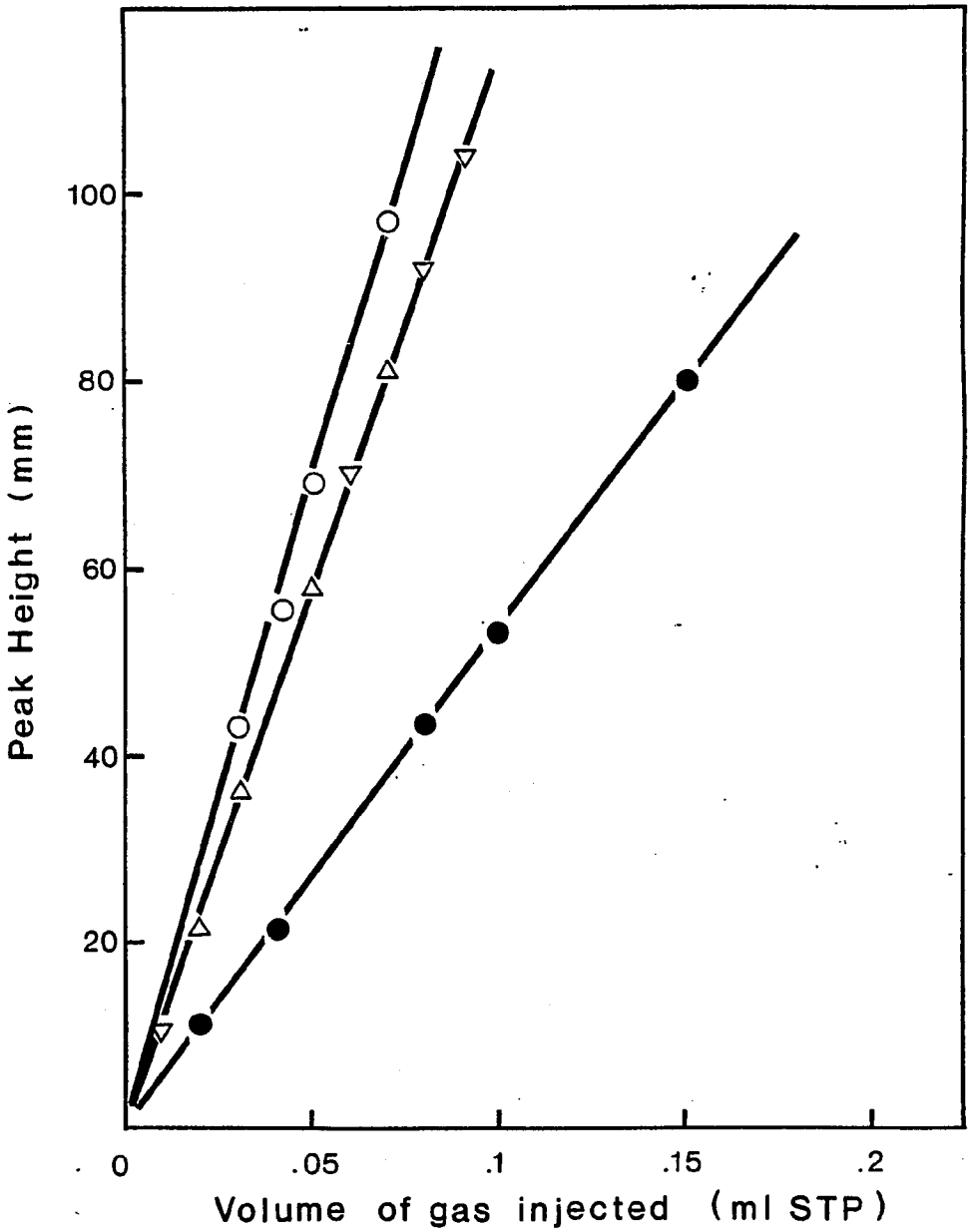

Figure 4. Calibration chart for Poropak Q column.

○ : CH_4, attenuation 5

● : CO_2, attenuation 5

△ : C_2H_4, attenuation 2

▽ : C_2H_6, attenuation 2.

2.3 PROCEDURE

2.3.1 Catalyst preparation

Non-porous alumina pellets were inmersed in a 12% solution of ferrous chloride. The solution was evaporated to dryness while stirring continuously. The resulting pellets had an Fe content of .5% in weight and a metal area of cm2/gm. Catalyst samples were treated with He at 400 C. At this temperature the ferrous chloride decomposes leaving the Fe on the pellet surface.

2.3.2 Catalyst Pretreatment

Iron oxide powder was sieved into two different fractions:

(a) 120-150 mesh (120-105 microns)

(b) 24-28 mesh (700-600 microns)

A portion of either catalyst was weighed and suspended in a quartz basket from the microbalance. Iron foils were cut from a large metal sheet and their geometric area was determined by weighing. Areas in the range 1 to 10 cm^2 were used. After rinsing in acetone, they were suspended from the balance. Catalyst pellets were weighed and suspended by a copper wire to one arm of the balance. After mounting of the sample, the same experimental procedure was followed in all cases. The system was flushed with helium and brought to 450 C. Helium was replaced by hydrogen and reduction of the

catalyst proceeded for 10 to 12 hours. Weight changes were continuously recorded. Flushing with helium preceded admittance of reactants at the desired temperature. Areas were measured prior to reaction for powders and pellets catalysts.

2.3.3 Measurement of Metal Areas

The metal areas of different samples were measured using the hydrogenation of ethylene as a reference reaction. Iron foils of known geometric areas were used as catalysts for the hydrogenation reaction from mixtures 50% hydrogen / 50% ethylene at 220 C. The same foils were treated with pure carbon monoxide at 300 C and the rate of carbon deposition was correlated to the geometric area of the foils. Linear plots were obtained in both cases (Fig. 5 and Table 4). It was concluded, as the hydrogenation reaction is a facile one, that metal areas could be measured by determining the rate of carbon deposition at the preestablished conditions. Surface areas of powders and pellets were obtained from their rates of carbon production from pure carbon monoxide at 300 C and the calibration chart for iron foils.

2.3.4 Kinetic Experiments

After the reduction treatment and area measurement, reaction was initiated by allowing reactants into the reactor,

up from the bottom. Gas compositions were varied by changing component flow rates. Helium was used as a diluent. Inlet and outlet compositions were measured chromatographically.

A record of the amount of carbon deposited was obtained and rates of carbon deposition were calculated from the slopes of the plots. Outlet flow rates were measured with a bubble flow meter. Rates of formation of gaseous products were evaluated from each flow rate and its correspondent gas composition.

Rate of formation
of component i = y(i).Fo.MW(i)

y(i) = mole fraction of component i in outlet stream
Fi = inlet flow rate (gmol/min)
Fo = outlet flow rate (gmol/min)
MW(i)= molecular weight of component i

Because of the low conversions attained in most cases (less than 3%), Fo and Fi were almost identical. The difference between the flow rates was smaller than the experimental error and therefore impossible to be measured under the reaction conditions of this work. Values for the rates of carbon monoxide disproportionation reaction could be checked for consistency knowing that the molar rate of carbon depo-

sition should be equal to that of carbon dioxide formation. A similar analysis should be valid for the rates of carbon gasification and methane formation: their molar rates should be equal. A comparison of molar rates of reaction for selected runs is shown in Table 1. It can be concluded from the good agreement of results that the experimental data obtained in the equipment used is reliable.

TABLE 1

Stoichiometric analysis of experimental data.

Run#	Rate of CO	Rate of C	Rate of CH	Rate of CO	Rate of C	Rate of CH
	(mg/min.cm^2)			(gmol/min)		
121*	1.5E-3	3.7E-3	-	1.9E-6	2.0E-6	-
708@	8.6E-2	2.4E-2	-	6.2E-6	6.1E-6	-
710	-	1.6E-2	2.1E-2	-	4.1E-6	4.06E-6
712	-	2.9E-3	3.9E-3	-	7.5E-7	7.6E-6
713	-	1.5E-3	2.1E-3	-	3.9E-7	4.06E-7

* Reduced Fe powder, 5.9 cm^2.
@ Supported Fe pellets, 3.1 cm^2.

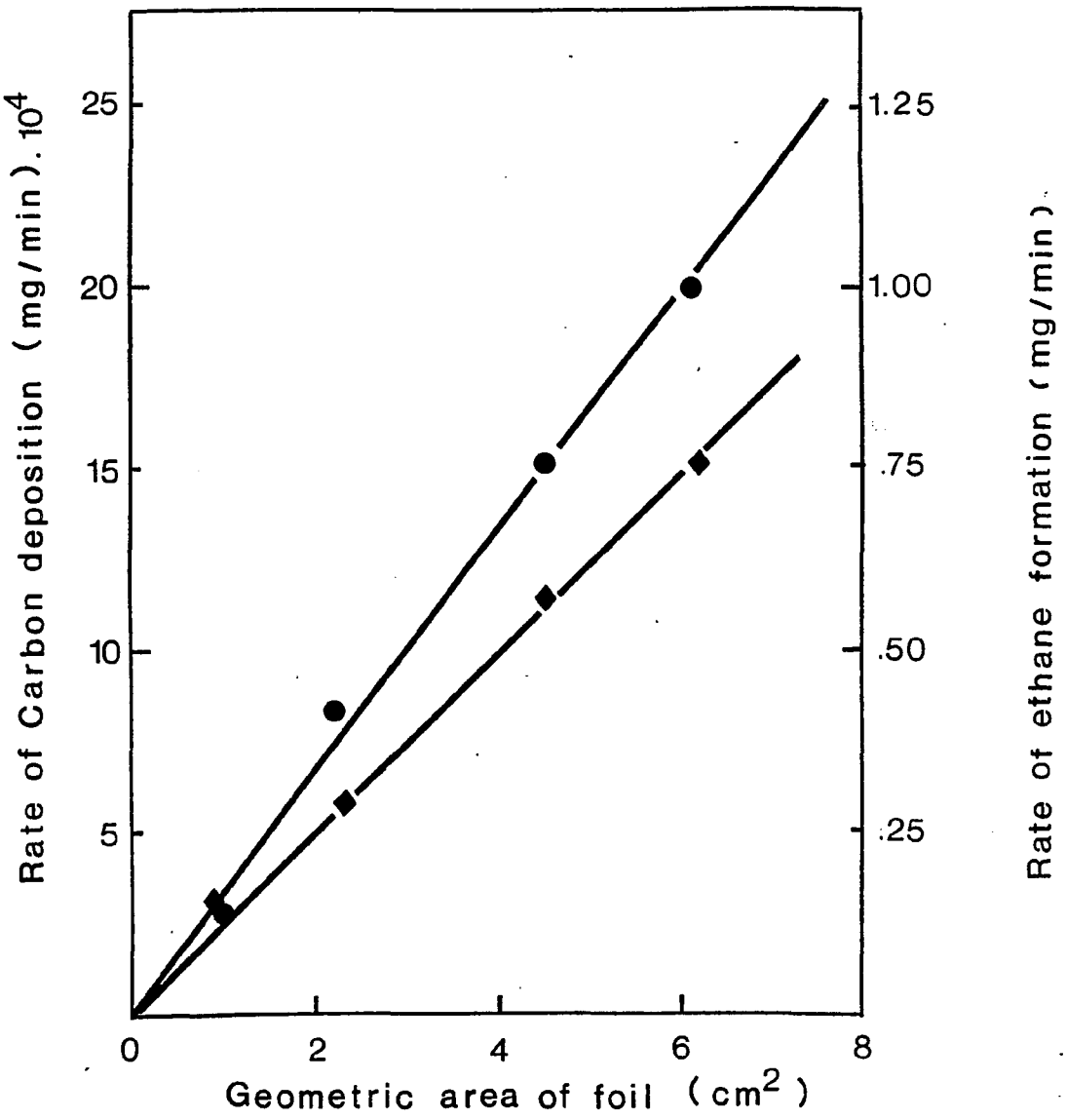

Figure 5. Calibration chart for iron foils of different geometric areas. Reference reaction :

- ● carbon deposition from pure CO at 300°C
- ◆ ethane formation from 50% H_2 / 50% C_2H_4 at 220°C.

2.3.5 Deactivation and regeneration studies

Iron pellet deactivation by carbon formation from pure CO was studied over commercial porous and impregnated non-porous pellets. After pretreatment of the sample, CO was admitted into the microbalance reactor system. Amounts of carbon deposited were continuously recorded until constant rates of formation were achieved. At this point, gasification of the carbon deposits with hydrogen was attempted. The amounts of carbon gasified were continuously monitored. Rates of carbon deposition and gasification could be calculated from the slopes of the plots mg C vs. time.

Rates of formation of gaseous products could not be established for the non-porous pellets. The amounts produced were hard to detect and even harder to measure. Consistency of results was extremely poor. Methane appears to be the main gaseous product of the gasification reaction; carbon dioxide that of the CO disproportionation reaction. After the rates of gasification became constant, kinetic measurements were possible. Helium was used as a diluent. Rates were measured as described above. Gas compositions were varied by changing the component flow rates.

2.3.6 Effect of hydrogen on C formation

The effect of hydrogen on the carbon formation reaction was studied on the non-porous pellets. Once final constant rates of carbon deposition from pure CO were achieved, hydrogen was admitted to the system. Partial pressures of hydrogen and CO were varied by using helium as diluent. Gaseous product could not be measured accurately. Carbon deposition proceeded at constant rates.

Chapter III

RESULTS

3.1 INTRODUCTION

Carbon deposition from carbon monoxide over iron oxide powders was studied in the temperature range 250-450 C. The same reaction was tested over iron foils and supported iron pellets. Deactivation of the catalytic pellets was followed under reaction conditions. Gasification of carbonaceous deposits was attempted with hydrogen. The differential method for the analysis of results was possible since conversions were low enough and steady state rates were usually observed.

3.2 CARBON FORMATION FROM CARBON MONOXIDE

3.2.1 Carbon Deposition on Iron Oxide Powders

3.2.1.1 Description

Carbon formation over reduced iron oxide powders could be detected even at temperatures as low as 250 C. Steady state rates of carbon deposition could be maintained for extended periods of time. The effect of flow rate, carbon monoxide partial pressure and temperature were studied for powders of different sizes. At constant total pressure of 1 atm, carbon

monoxide partial pressure was varied from .03 to 1 atm., for temperatures in between 290 and 370 C. Conditions used in all experiments are given in Table 2, together with the steady state rates of reaction.

3.2.1.2 Preliminary Experiments

Reduced iron oxide powders were treated with carbon monoxide and carbon monoxide/helium mixtures. Carbon deposition started in all instances after an induction period of 2 to 3 hours. Reproducibility of this induction period was poor, even though great care was taken to follow the same pretreatment procedure. This did not seem to affect the steady state rates of carbon deposition eventually obtained.

Once deposition was initiated, constant rates of reaction were observed for 1 to 2 days and sometimes even longer periods. The rates were not proportional to the weight of powder used, but to the exposed metal area (Table 3). Diffusion limitations were checked by changing the flow rate of reactants, keeping other variables constant. Results presented in Fig. 6 show that mass transfer limitations can be considered negligible in the range tested (5-150 cc/min). Most runs were carried out with a flow rate of 5 to 15 cc/min, measured at room temperature and atmospheric pressure.

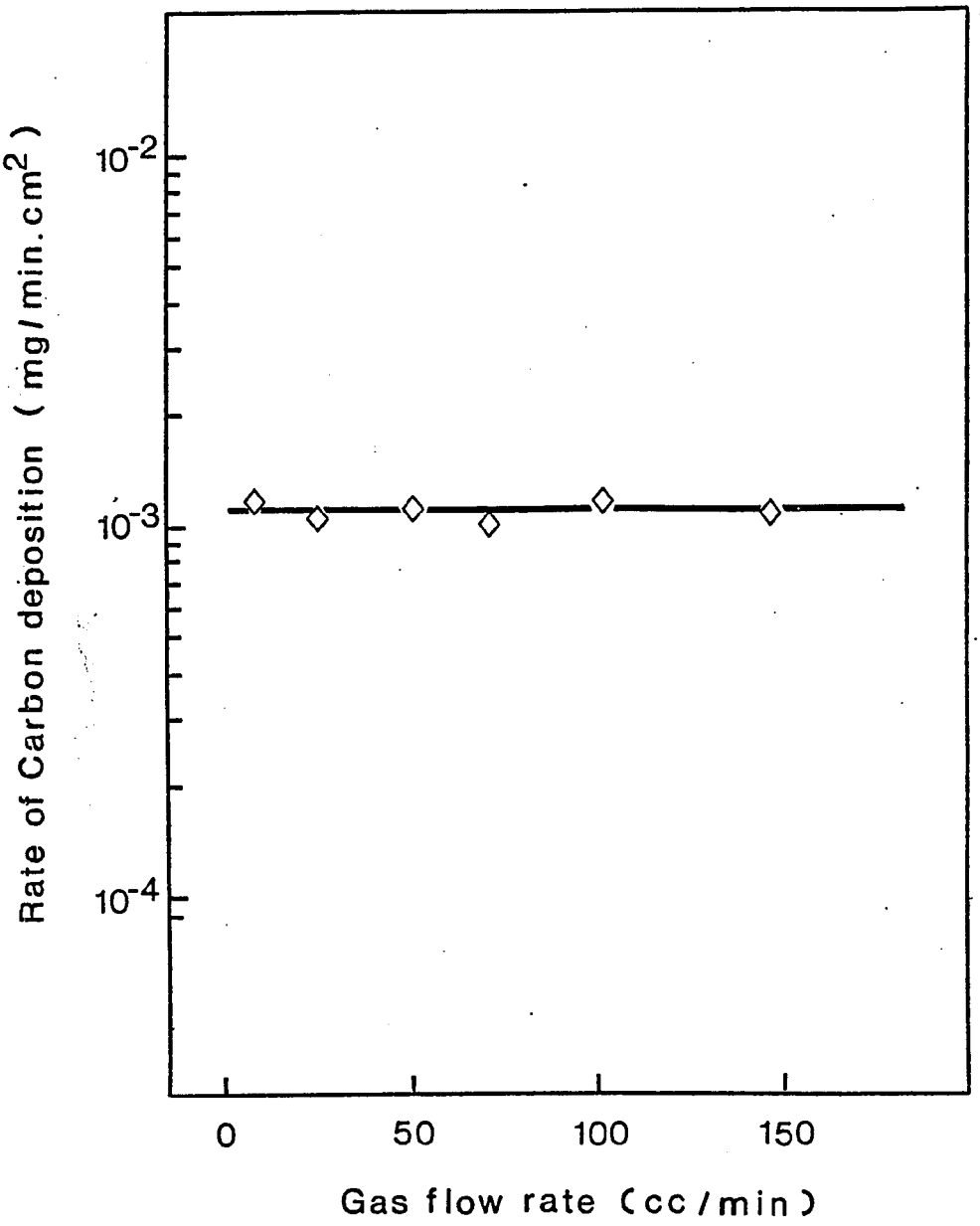

Figure 6. Effect of gas flow rate on the rate of carbon deposition from pure CO on iron powders, at 325°C and 1 atm total pressure.

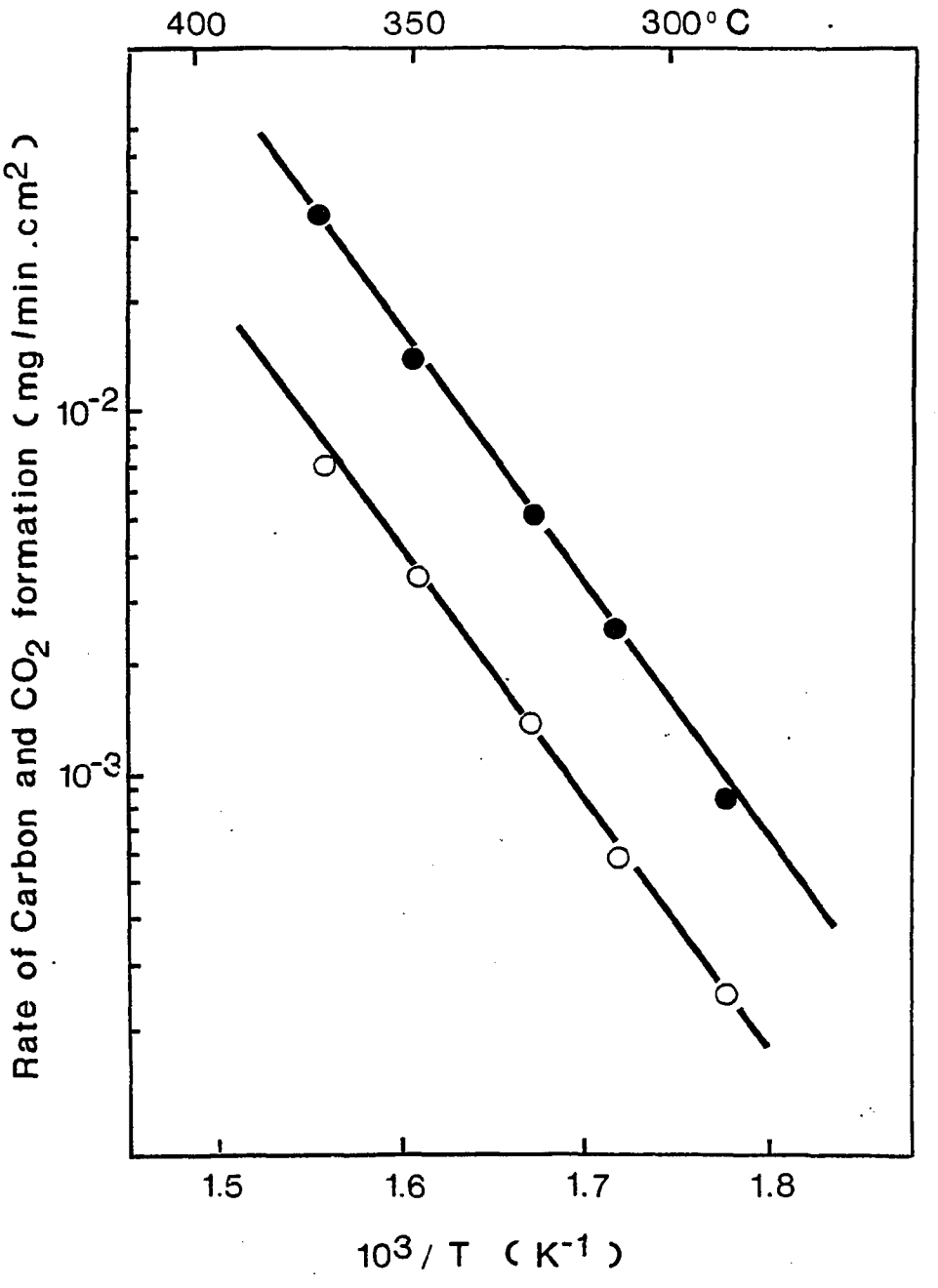

Figure 7. Arrhenius plot for the rates of C and CO_2 formation from pure CO on iron powders, at 1 atm total pressure. Key : ○, C deposition; ●, CO_2 formation.

TABLE 2.

Experimental conditions and results for iron powders.

Run#	Temp. (C)	%CO	%He	Rate of C deposition (mg/min.cm)	Rate of CO formation (mg/min.cm)	Flow rate (cc/min)	Amount of powder (mg)
101	300	100	0	3.5E-4	-	10	12.2
102	300	100	0	3. E-4	-	26	12.2
103	300	100	0	4. E-4	-	51	12.2
104	300	100	0	3.2E-4	-	100	12.2
105	300	100	0	4.2E-4	-	120	12.2
106	325	100	0	1.2E-3	-	7	12.2
107	325	100	0	1.0E-3	-	24	12.2
108	325	100	0	1.1E-3	-	50	12.2
109	325	100	0	9.8E-4	-	72	12.2
110	325	100	0	1.2E-3	-	99	12.2
111	325	100	0	1.1E-3	-	145	12.2
121	300	100	0	3.7E-3	1.5E-3	14	18.5
122	290	100	0	2.5E-4	9.1E-4	14	18.5
123	310	100	0	5.5E-4	2.5E-3	14	18.5
124	325	100	0	1.4E-3	5.1E-3	14	18.5
125	350	100	0	3.5E-3	1.4E-2	14	18.5
126	370	100	0	7.2E-3	3.5E-2	14	18.5
144	300	100	0	3.6E-4	1.4E-3	10	27.3
145	325	100	0	1.5E-3	5.0E-3	10	27.3
146	325	63	37	1.6E-3	5.1E-3	10	27.3
147	325	41	59	1.6E-3	5.4E-3	10	27.3
148	325	22	78	1.4E-3	4.8E-3	10	27.3
149	325	5	95	1.5E-3	5.1E-3	10	27.3

TABLE 3

Effect of powder metalic area on the rates of deposition.

Run#	Powder size (mesh)	Rate of carbon deposition (mg/min)	Amount of powder (mg)	Specific rate of carbon deposition (mg/min.cm^2)
101	120-150	1.4E-3	12.2	3.5E-4
121	120-150	1.8E-3	18.5	3.3E-4
144	120-150	2.6E-3	27.3	3.1E-4
155	24-28	9.8E-4	9.6	3.2E-4
167	24-28	2.1E-3	16.7	3.3E-4

Carbon was deposited from pure carbon monoxide at 300 C.

3.2.1.3 Kinetic Results

Activation energies were determined for several carbon monoxide/helium feed ratios as shown in Fig. 7. In all cases, the activation energies were found to be 31 Kcal/gmol in the range of temperatures studied. The order of reaction with respect to carbon monoxide partial pressure was determined at different temperatures and found to be close to zero for concentrations as low as 3% in carbon monoxide (Fig. 8). At lower concentrations, the order of reaction should change (at zero carbon monoxide concentration there should be no deposition) though this could not be observed because of limitations in the detection system used.

Carbon deposited in the form of small particles below and around the iron powder, pushing the catalyst up in the container. Losses of active material and deposits usually occured because of overflowing of the basket. At this point, fresh catalyst had to be loaded. The only gas product for this reaction was carbon dioxide. Activation energies for carbon dioxide production were determined from the same runs by measurement of outlet flow rates and carbon dioxide concentrations in it (Fig. 7). The apparent order of reaction with respect to carbon monoxide partial pressure appears to be zero also (Fig. 8). Admission of hydrogen to the system resulted in a lowering of the rate of carbon deposition.

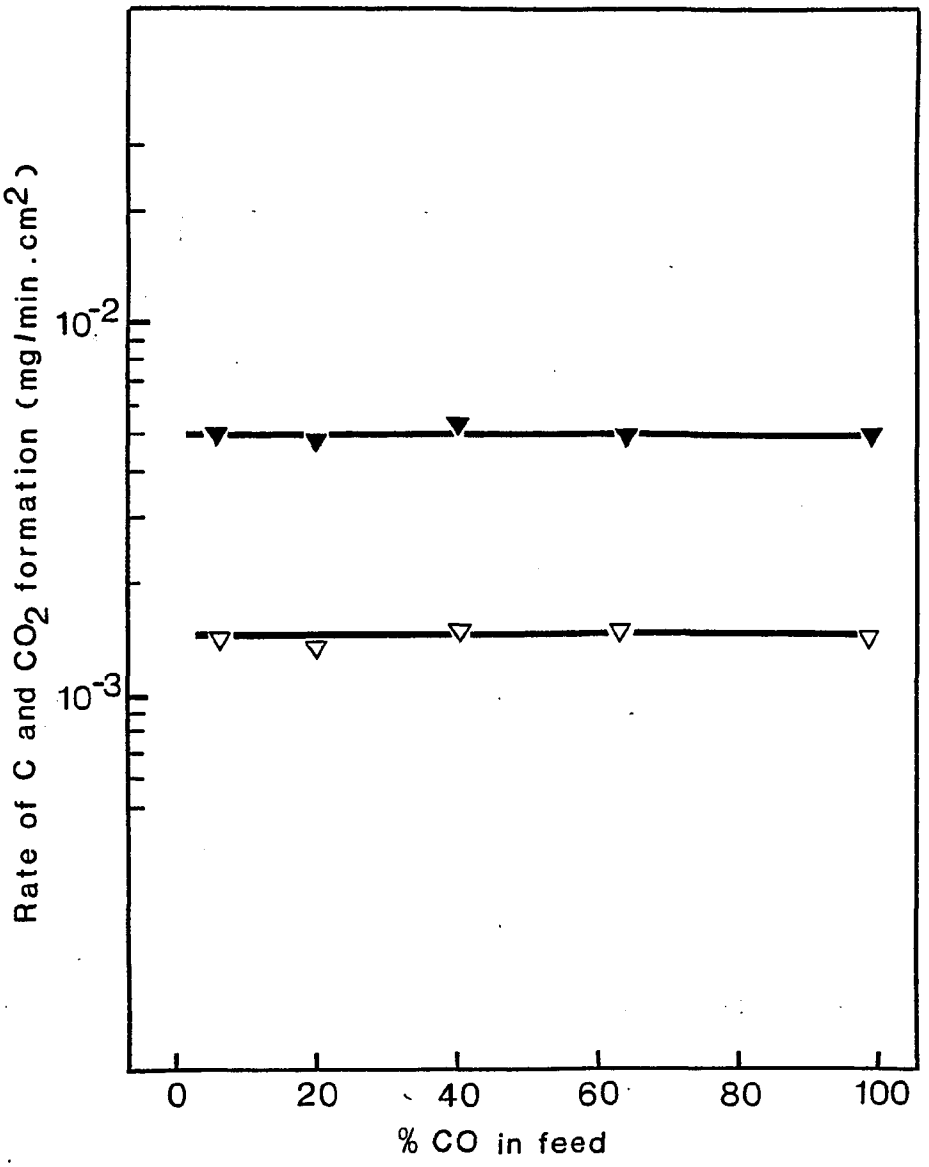

Figure 8. Effect of CO on the rates of C and CO_2 formation from pure CO on iron powders at 325°C and 1 atm . Key : ▽, C deposition; ▼, CO_2 formation. He used as diluent.

3.2.2 Carbon Deposition on Iron Foils

3.2.2.1 Description

Carbon monoxide decomposition over iron foils was characterized by constant rates of carbon deposition for long periods of time. Induction periods for foils were longer than those for powders, in the order of 20 to 30 hours. Shortening of the period was achieved by raising the initial deposition temperature. Once carbon started depositing, temperatures were lowered to the desired working value without affecting or stopping the formation of carbon. The effect of gas flow rate, carbon monoxide partial pressure and temperature were studied for iron foils of different geometric areas, in a similar way to that for iron powders. Conditions and rates are given in Table 4. Mass transfer limitations were checked the same way as for powders (Fig. 9) and were also negligible.

3.2.2.2 Kinetic Results

Rates of carbon formation were found to be proportional to the geometric area of the foil used, as can be seen on Table 5. The order of reaction with respect to carbon monoxide partial pressure seems to be near zero as for iron powders (Fig. 10). Activation energies for carbon monoxide decomposition were determined for different carbon monoxide/helium ratios (Fig. 11) and its value of 32 Kcal/

gmol is in good agreement with that obtained for iron powders. Carbon filaments were observed to form over the foil allowing for the deposition reaction to take place at a steady state rate. Unfortunately their fragility permitted only a limited growth. Filaments broke down under their own weight or because of perturbances in the system. This produced a net loss in the active area and indicated that a new foil had to be used. Deactivation of the foils was not detected. The active area was determined at the beginning and end of each set of experiments (usually 1 or 2 days). Variations were in the order of +/- 4%.

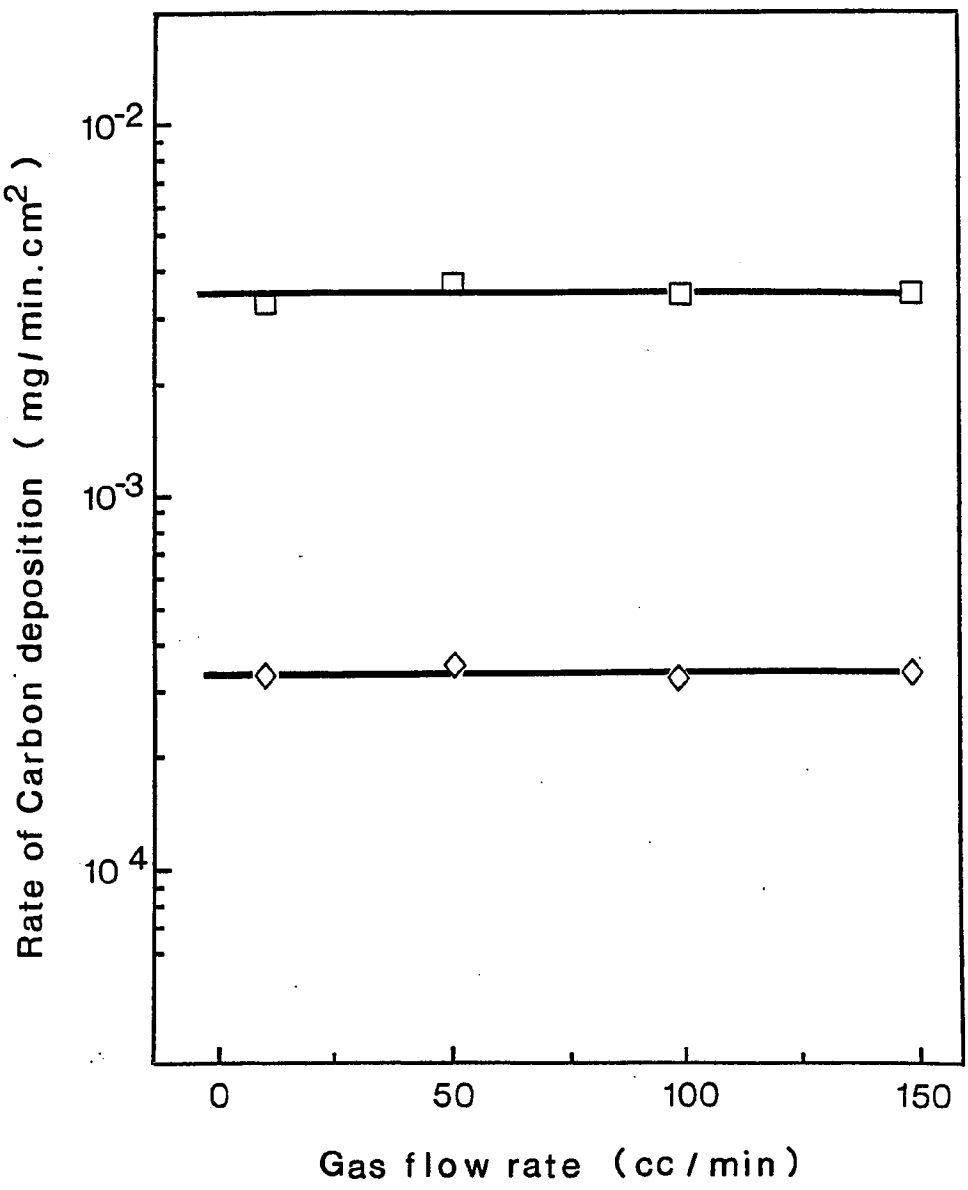

Figure 9. Effect of gas flow rate on the rate of C formation from pure CO on iron powders at 1 atm total pressure. Key : ◇ , 300°C; □ , 350°C.

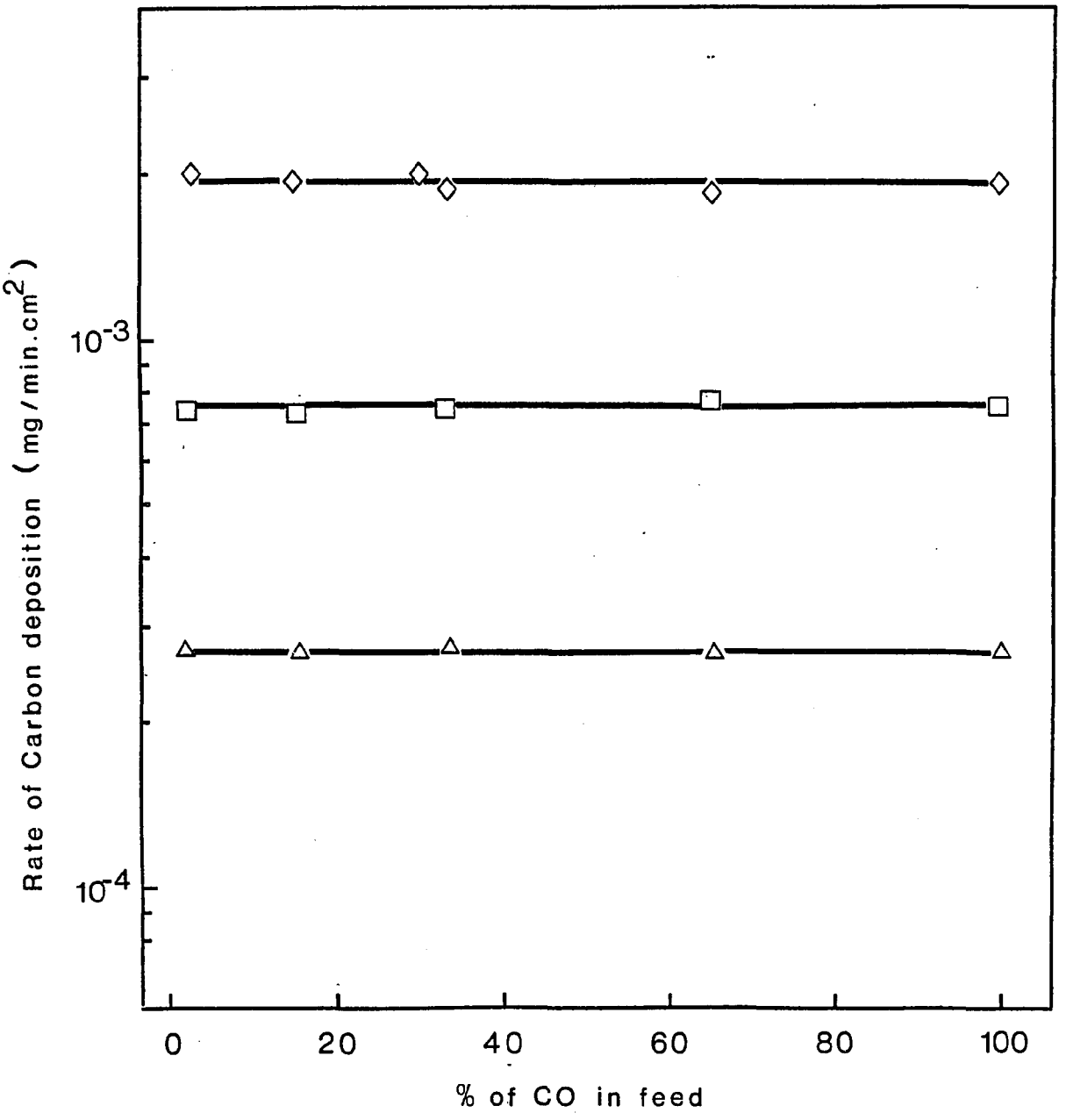

Figure 10. Effect of CO on the rate of carbon deposition from pure CO on iron foils at 1 atm total pressure. Key : △ ,300°C; □ ,320°C; ◇ ,340°C. He used as diluent.

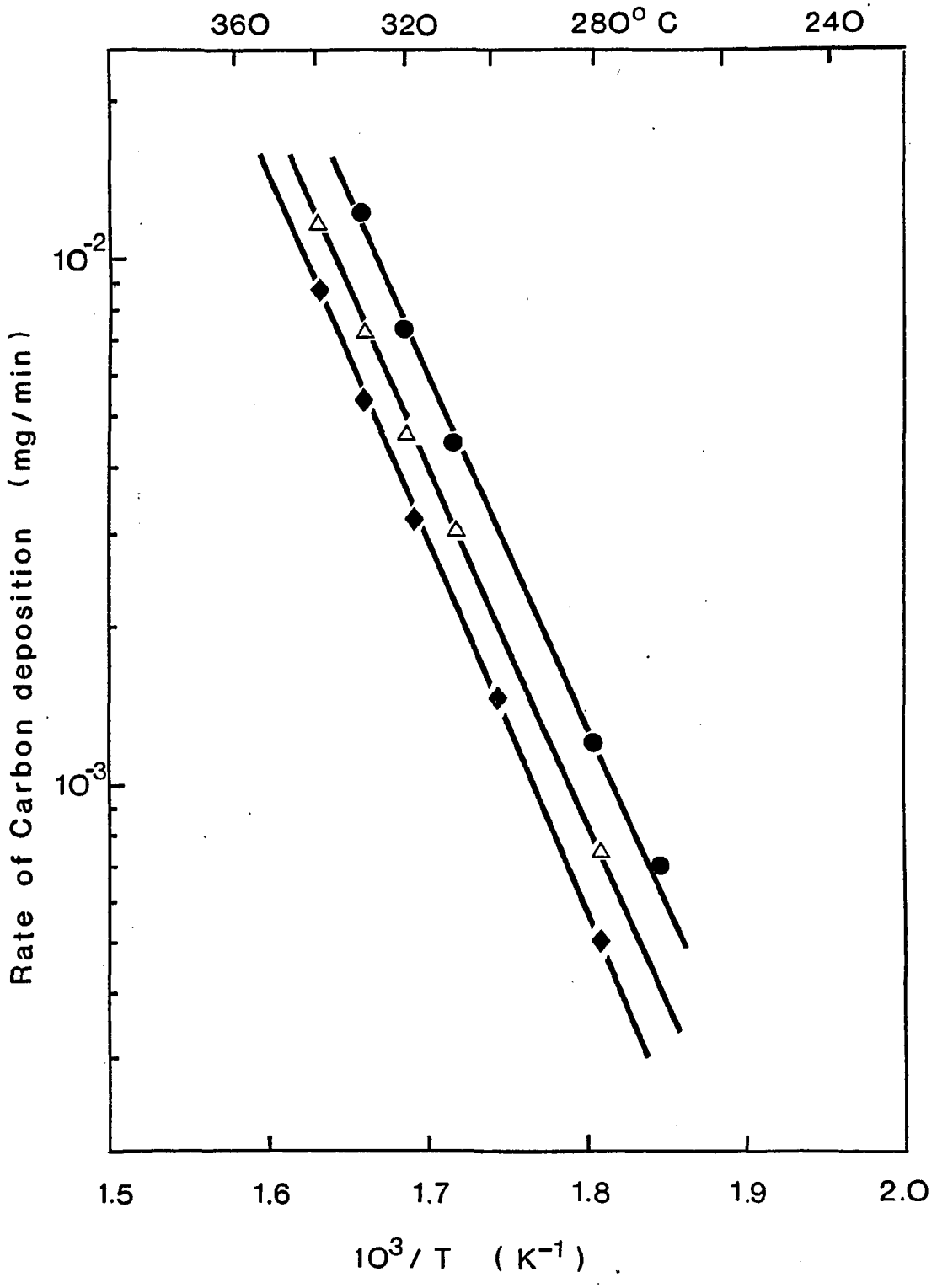

Figure 11. Arrhenius plot for the rate of carbon deposition from pure CO on iron foils of different geometric areas at 1 atm total pressure. Key : ● , 9.4 cm^2; △ , 6.1 cm^2; ◆ , 4.6 cm^2.

TABLE 4

Experimental conditions and results on iron foils.

Run#	Temp. (C)	%CO	%He	Rate of carbon deposition (mg/min.cm^2)	Flow rate (cc/min)	Geometric area (cm^2)
F115	300	100	0	3.3E-4	10	4.6
F116	350	100	0	3.1E-3	10	4.6
F117	300	100	0	3.6E-4	51	4.6
F118	350	100	0	3.8E-3	51	4.6
F119	300	100	0	3.2E-4	102	4.6
F120	350	100	0	3.5E-3	102	4.6
F121	300	100	0	3.4E-4	147	4.6
F122	350	100	0	3.4E-3	147	4.6
F135	300	100	0	2.9E-4	12	1.1
F136	320	100	0	7.6E-4	12	1.1
F137	340	100	0	1.9E-3	12	1.1
F138	300	66	34	2.7E-4	12	1.1
F139	320	66	34	7.8E-4	12	1.1
F140	340	66	34	1.8E-3	12	1.1
F141	300	37	63	2.8E-4	12	1.1
F142	320	37	63	7.5E-4	12	1.1
F143	340	37	63	1.9E-3	12	1.1
F144	340	30	70	2.1E-3	12	1.1
F145	300	18	82	2.6E-4	12	1.1
F146	320	18	82	7.4E-4	12	1.1
F147	340	18	82	2.1E-3	12	1.1
F148	300	3	97	2.8E-4	12	1.1
F149	320	3	97	7.6E-4	12	1.1
F150	340	3	97	2.2E-3	12	1.1
F166	300	100	0	3.6E-3	9	9.4
F167	270	100	0	7.1E-4	9	9.4
F168	310	100	0	4.4E-3	9	9.4
F169	320	100	0	7.3E-3	9	9.4
F171	330	100	0	1.3E-2	9	9.4
F180	300	100	0	4.1E-4	15	2.2
F181	325	100	0	2.7E-3	15	2.2
F188	300	100	0	3.5E-4	13	6.1
F189	310	100	0	5.1E-4	13	6.1
F190	320	100	0	8.5E-4	13	6.1
F191	330	100	0	1.4E-3	13	6.1
F193	340	100	0	2.3E-3	13	6.1

TABLE 5

Effect of foil geometric area on rates of reaction.

Run#	Rate of C deposition (mg/min)	Rate of ethane formation (mg/min)	Geometric area (cm^2)	Specific rate of deposition (mg/min.cm^2)
F135	2.9E-4	.15	1.1	2.9E-4
F180	8.9E-4	.29	2.2	4.1E-4
F115	1.5E-3	.54	4.6	3.3E-4
F188	2.1E-3	.72	6.1	3.5E-4
F166	3.4E-3	1.15	9.4	3.6E-4

Carbon was deposited from pure CO at 300 C. Ethane was formed by reacting a mixture 50% H_2/50% C_2H_4 at 220 C.

3.2.3 Carbon Deposition on Commercial Porous Pellets

3.2.3.1 Description

Carbon deposition readily occured over the pellets used. The induction period was in general shorter than 30 minutes. Deactivation of the catalyst was appreciable in the first day of operation. Constant rates of formation could be achieved after 2 to 3 days of continuous running. The low conversions attained insured availability of reactants everywhere on the catalyst. Though internal diffusion limitations may be present initially, their effect on the rate of reaction is minimal after a certain period of time (2 to 3 days). See Fig. 14.

Once the reaction proceeded at a steady state rate, kinetics studies could be performed on the pellets. This was done by alternating deposition with gasification of the deposits on a day to day basis.

3.2.3.2 Kinetic Results

The behaviour of the supported iron catalysts was identical to that of iron powders and foils for the carbon monoxide decomposition reaction. Activation energies for the carbon and carbon dioxide formation reactions were measured from the Arrhenius plots shown in Fig. 12. Values of 32 Kcal/gmol were calculated, in good agreement with values of 31 and 32 Kcal/gmol for powders and foils. The order of the carbon and carbon dioxide formation reactions appear to be zero with respect to carbon monoxide partial pressure, as can be seen in Fig. 13. Experimental conditions are given in Table 5.

Disintegration of the pellets resulted after 7 to 10 days of operation. Carbon filaments formed on the surface, or grew from the pores inside. The breaking of filaments produced irreversible losses of catalytic material.

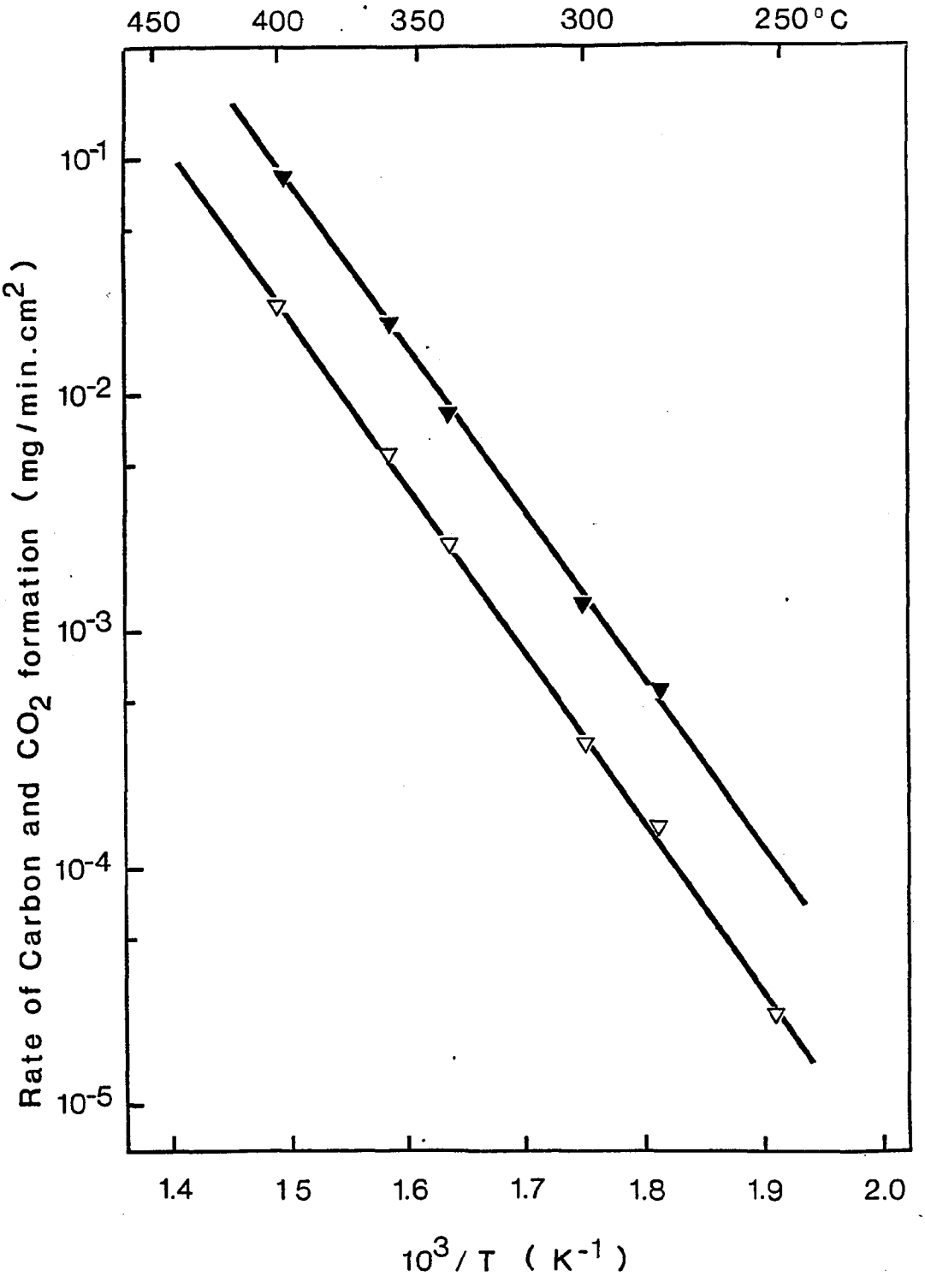

Figure 12. Arrhenius plot for the rates of C and CO_2 formation on supported iron pellets at 1 atm total pressure. Key : ▽ , carbon deposition; ▼ , CO_2 formation.

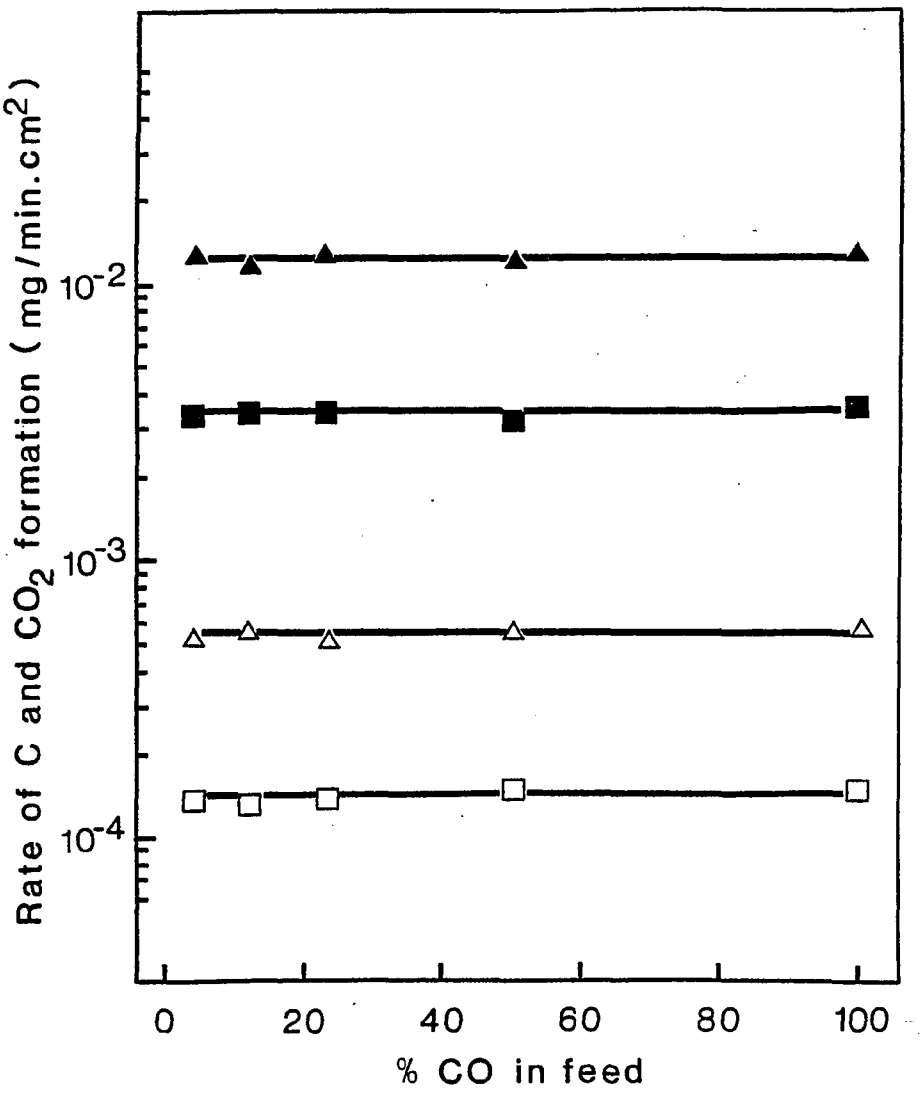

Figure 13. Effect of CO on the rates of C and CO_2 formation on supported iron pellets at 1 atm total pressure. Key : □, C deposition at 280°C; ■, C deposition at 300°C; △, CO_2 formation at 280°C; ▲, CO_2 formation at 300°C.

TABLE 6

Experimental conditions and results for iron pellets.

Run#	%H	%CO	%He	Rate of C formation	Rate of CO formation	Rate of CH formation	Temp.
					(mg/min.cm)		(C)
701	-	100	-	2.4E-5	8.9E-5	-	250
702	-	100	-	1.5E-4	5.4E-4	-	280
703	-	100	-	3.4E-4	1.3E-3	-	300
704	-	100	-	1.3E-3	4.9E-3	-	325
705	-	100	-	2.3E-3	8.5E-3	-	340
706	-	100	-	5.4E-3	2.0E-3	-	360
707	-	100	-	9.2E-3	3.5E-2	-	375
708	-	100	-	2.4E-2	8.6E-2	-	400
710	100	-	-	1.6E-2	-	2.1E-2	425
711	100	-	-	7.3E-3	-	1.0E-2	410
712	100	-	-	2.9E-3	-	3.9E-3	400
713	100	-	-	1.5E-3	-	2.1E-3	390
714	100	-	-	3.7E-4	-	4.4E-4	375
715	100	-	-	4.7E-5	-	6.6E-5	350
716	-	100	-	3.5E-4	-	-	300
717	70	30	-	7.0E-3	-	-	375
718	70	30	-	3.6E-3	-	-	360
719	70	30	-	1.1E-3	-	-	340
720	70	30	-	4.4E-4	-	-	325
721	70	30	-	8.5E-5	-	-	300
805	-	100	-	3.1E-4	-	-	300
806	100	-	-	3.0E-3	-	-	400
807	65	-	35	1.7E-3	-	-	400
808	50	-	50	1.3E-3	-	-	400
809	33	-	67	1.0E-3	-	-	400
810	23	-	77	8.4E-4	-	-	400
811	12	-	88	6.3E-4	-	-	400
812	5	-	95	4.1E-4	-	-	400
813	-	100	-	1.4E-4	-	-	280
814	-	100	-	3.2E-4	-	-	300
815	-	100	-	3.5E-3	-	-	350
816	-	100	-	2.7E-2	-	-	400
903	-	100	-	3.3E-4	-	-	300
904	-	50	50	1.5E-4	-	-	280
905	-	50	50	3.3E-4	-	-	300
906	-	50	50	3.4E-3	-	-	350
907	-	50	50	2.6E-2	9.8E-2	-	400
908	-	23	77	1.3E-4	5.0E-4	-	280
909	-	23	77	3.1E-4	1.1E-3	-	300
910	-	23	77	3.5E-3	1.3E-2	-	350

TABLE 6 contd.

Run#	%H	%CO	%He	Rate of C formation	Rate of CO formation (mg/min.cm)	Rate of CH formation	Temp (C)
911	-	23	77	2.7E-2	1.0E-1	-	400
912	-	12	88	1.3E-4	6.0E-4	-	280
913	-	12	88	3.2E-4	1.2E-3	-	300
914	-	12	88	3.4E-3	1.2E-2	-	350
915	-	12	88	2.8E-2	8.6E-2	-	400
916	-	4	96	1.4E-4	5.0E-4	-	280
917	-	4	96	3.1E-4	1.2E-3	-	300
918	-	4	96	3.5E-3	1.3E-2	-	350
919	-	4	96	2.6E-2	1.0E-1	-	400
920	-	100	-	3.3E-3	-	-	300

3.2.4 Carbon Deposition on Non-porous Pellets

3.2.4.1 Description

Carbon deposition from pure CO could be detected as soon as reactant gases were contacted with the pellets. Carbon formation rates remained constant for periods of 2 to 3 hours. Deactivation of the catalyst could then be observed. After 1Ø to 12 hours, constant rates of formation could be achieved and maintained for days. Kinetic studies were then performed. This was done by alternating deposition with gasification of the deposits on a day to day basis. After gasification of the carbon with hydrogen catalyst activity was completely recovered to the initial values.

3.2.4.2 Kinetic Results

Non-porous pellets behaved as the porous pellets did for the CO disproportionation reaction. Arrhenius plots for the final rates of carbon deposition (Fig. 14) show an activation energy of 32 Kcal/gmol. Rates of formation of gaseous products could not be measured accurately. Carbon dioxide appears to be the the only product. The amounts produced were enough to allow for detection but not for consistent measurements. Reproducibility for the carbon formation reaction was good.

TABLE 7

Arrhenius plots for the rates of C deposition

Temperature (C)	Rate of C deposition or gasification (mg/hr)	
	Deposition	Gasification
250	0.04	-
275	0.15	-
290	0.28	-
300	0.49	-
310	0.62	-
325	1.3	-
350	3.1	0.19
360	4.7	-
375	7.0	0.54
390	-	1.12
400	16.1	1.63
410	-	2.51
425	36.2	4.4
440	-	8.0
450	-	12.1
480	-	43.3

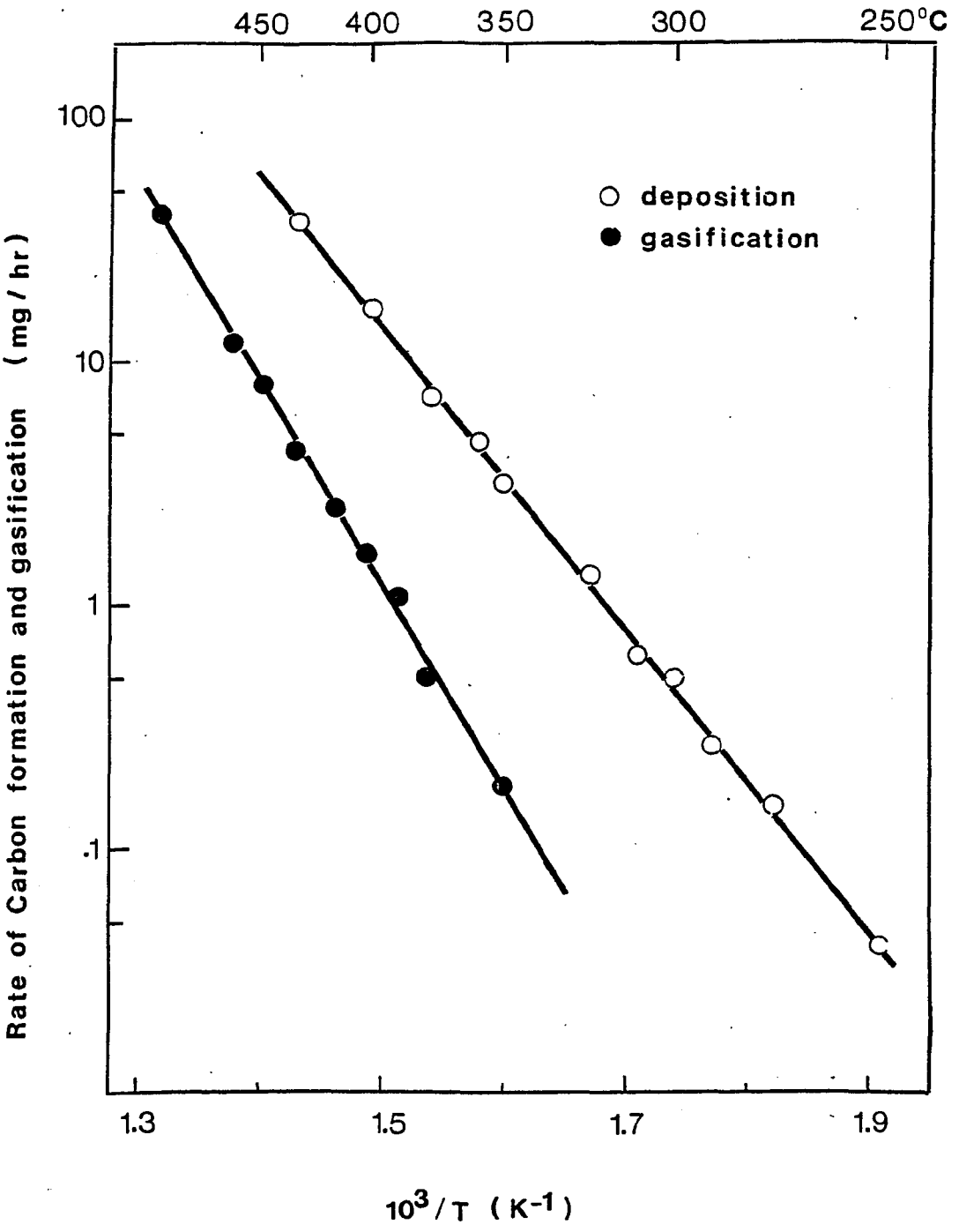

Figure 14. Effect of Temperature on the Rates of C Deposition and Gasification over Impregnated Non-Porous Pellets.

3.3 STUDIES OF PELLET DEACTIVATION

3.3.1 Commercial Porous Pellets

Carbon deposition lowered the pellet activity for the carbon monoxide decomposition reaction. Weight changes of the catalyst were continuosly recorded (Fig. 15). Rates of reaction were calculated periodically from these plots. See Table 8. The rate of reaction dependency with time could then be obtained (Fig. 16). The way in which the rate varies with the amounts of carbon formed could also be obtained and is depicted in Fig. 17. The activity function can be calculated at each temperature for different amounts of carbon deposited. Results are shown in Fig. 18. A mechanism of pore blocking by the carbon formed appears to be a plausible explanation of these deactivation experiments. The void fraction of the pellets was .2 for pores bigger than 29 Amstrongs, and less than .1 for pores smaller than 29 Amstrongs. After all small pores are filled and a certain amount of active material blocked out, the reaction takes place at a constant rate until disintegration or irreversible losses prevent further studies.

TABLE 8

Results for porous pellet deactivation study

Time (hr)	Amount of C deposited (mg)		
	280 C	300 C	320 C
2	.72	1.92	4.32
4	1.3	3.0	5.92
6	1.78	3.9	7.2
8	2.14	4.64	8.32
10	2.72	5.31	9.32
14	3.44	6.56	11.23
20	4.40	8.14	12.7
30	5.1	10.36	14.4
40	5.83	12.16	-

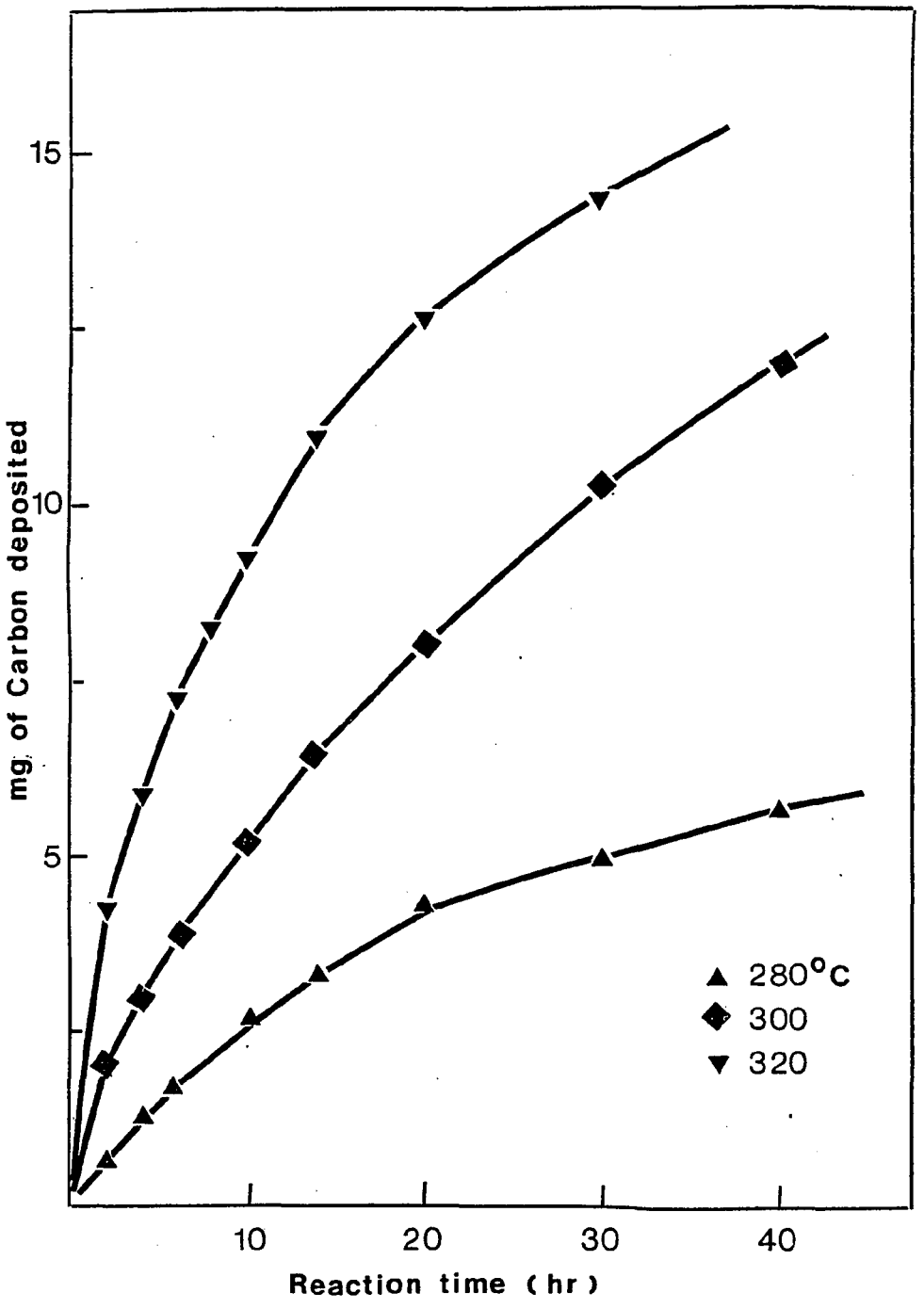

Figure 15. Deactivation of Porous Pellets by C Deposition from Pure CO.

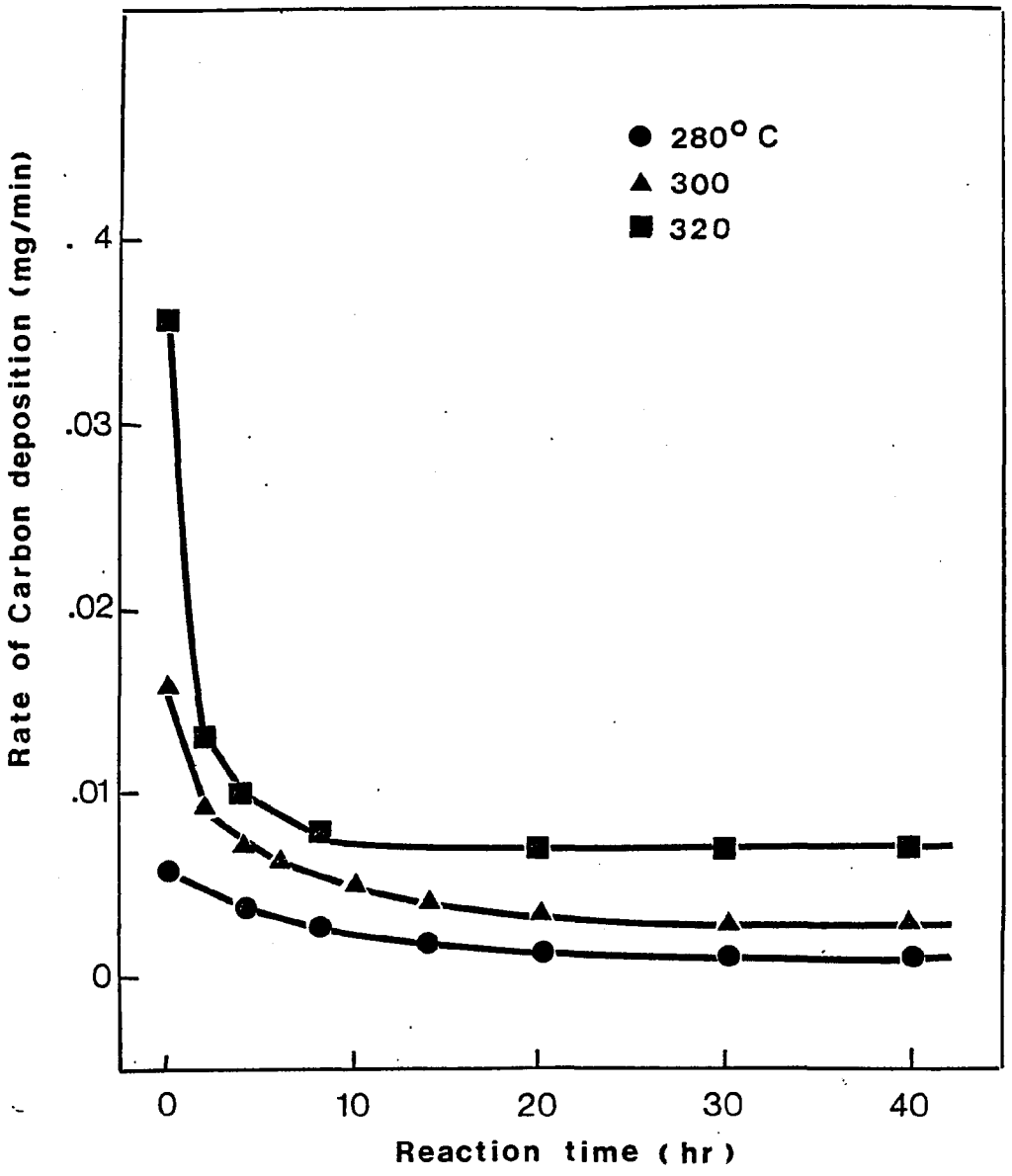

Figure 16. Time Dependence of the Rate of C Deposition from from pure CO over Commercial Porous Pellets.

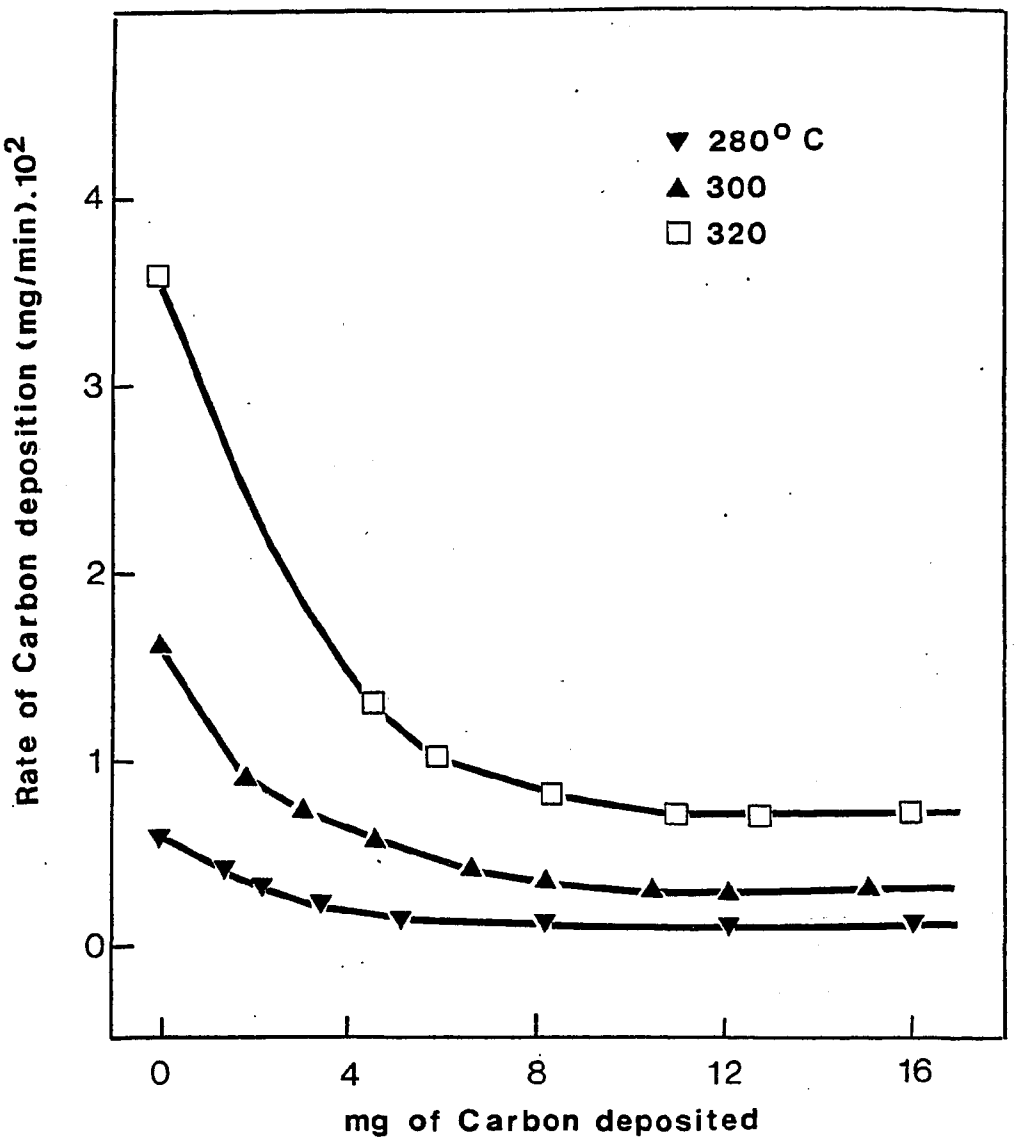

Figure 17. Dependence of the Rate of C Formation from Pure CO with the Amounts of C Formed. Commercial Porous Pellets.

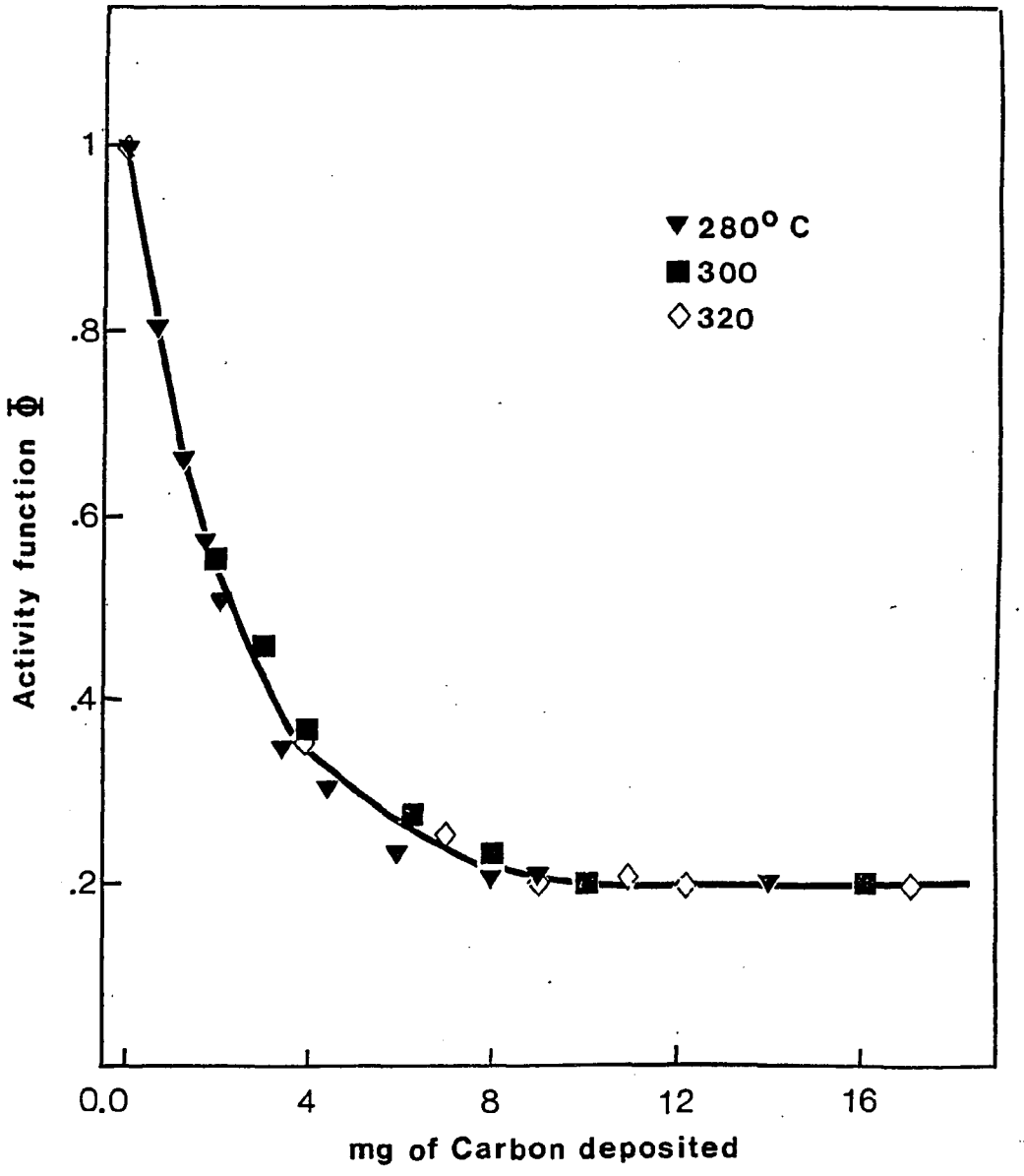

Figure 18. Activity Function Dependence with the Amounts of C Deposited from pure CO over Porous Pellets.

3.3.2 Non-porous Pellets

Carbon from pure carbon monoxide was initially produced at constant rates (Fig. 19). Deactivation of the pellets occurred after a period of 2 to 3 hours of continuous deposition. Constant rates of carbon formation were achieved in 10 to 12 hours. Initial and final rates follow Arrhenius plots, as shown in Fig 20. Experimental conditions are given in Table 9. The activation energy values for both rates is identical and equal to 32 Kcal/gmole. The way in which rates of deposition change with time and with the amounts of carbon formed were obtained from the deactivation graphs. Results are shown in Figures 21 and 22. The activity function was plotted vs. the amounts of carbon deposited in Fig. 23.

TABLE 9

Deactivation of non-porous pellets by C deposition

Time (hr)	Amount of C deposited (mg)				
	300 C	320 C	330 C	340 C	350 C
1	.2	.35	.6	.72	1.3
2	.4	.65	.9	1.45	2.1
3	.45	.8	1.2	1.75	2.4
4	.55	.9	1.4	2.01	2.65
5	-	1.02	1.6	2.25	2.85
6	-	1.1	1.7	2.45	3.05
8	-	1.20	1.85	2.7	3.45
10	-	1.3	2.0	3.0	-
12	.85	1.4	2.15	3.2	4.15
14	.9	1.55	2.35	3.4	-
18	1.01	1.7	2.6	3.8	5.13
20	1.06	-	-	4.0	5.65

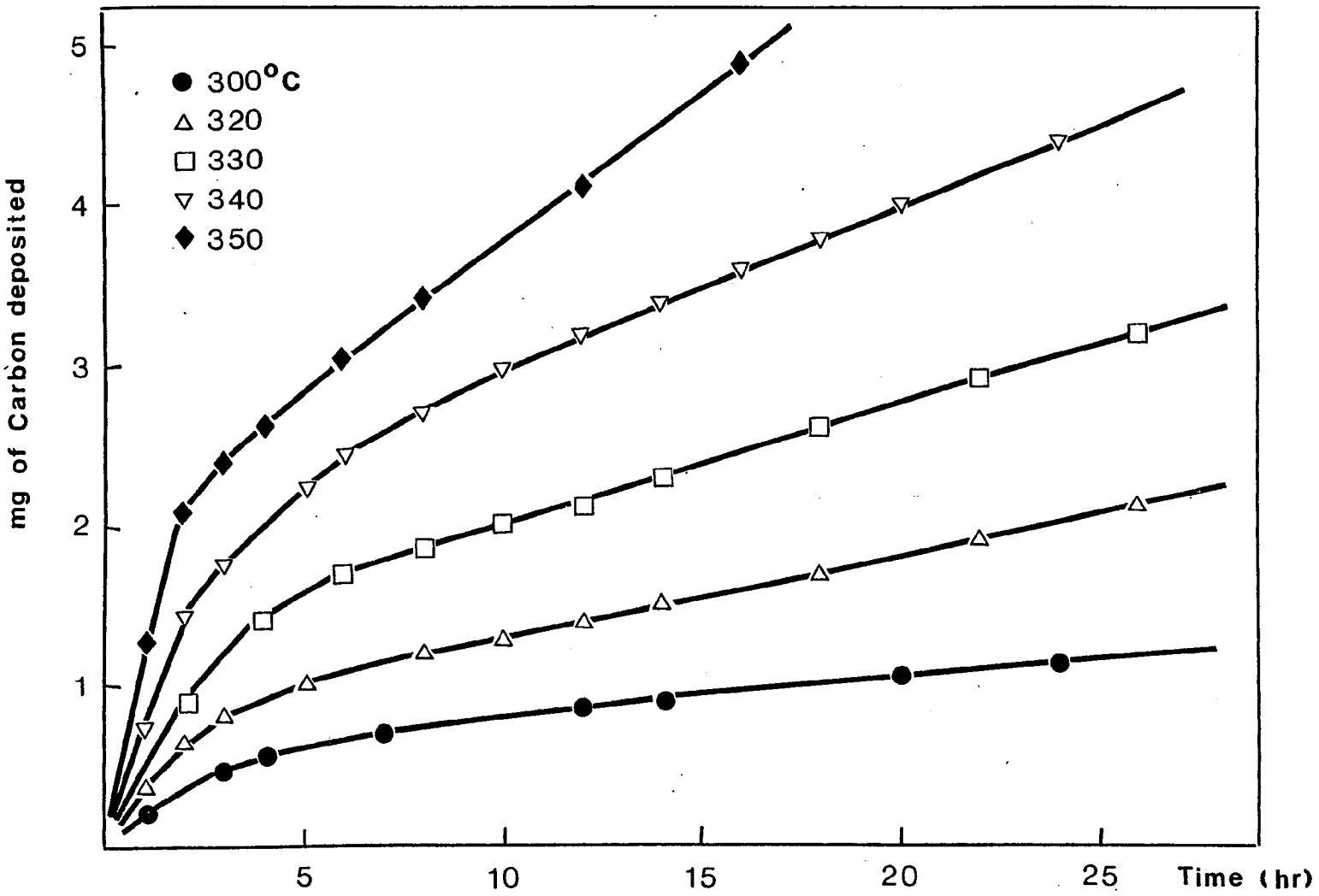

Figure 19. Deactivation of Impregnated Non-Porous Pellets by C Deposition from Pure CO.

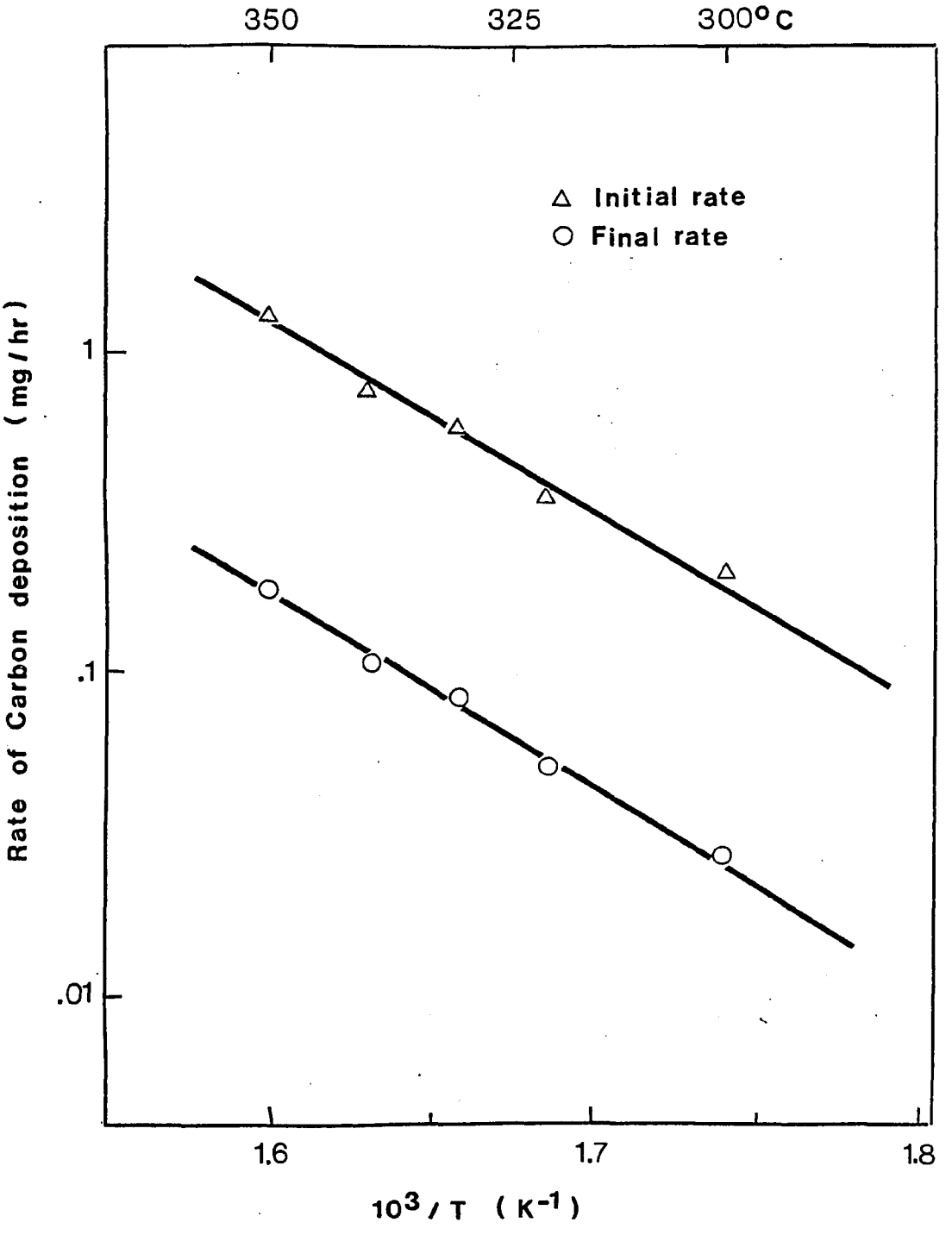

Figure 20. Effect of Temperature on the Initial and Final Rates of C Deposition from pure CO on Non-Porous Pellets.

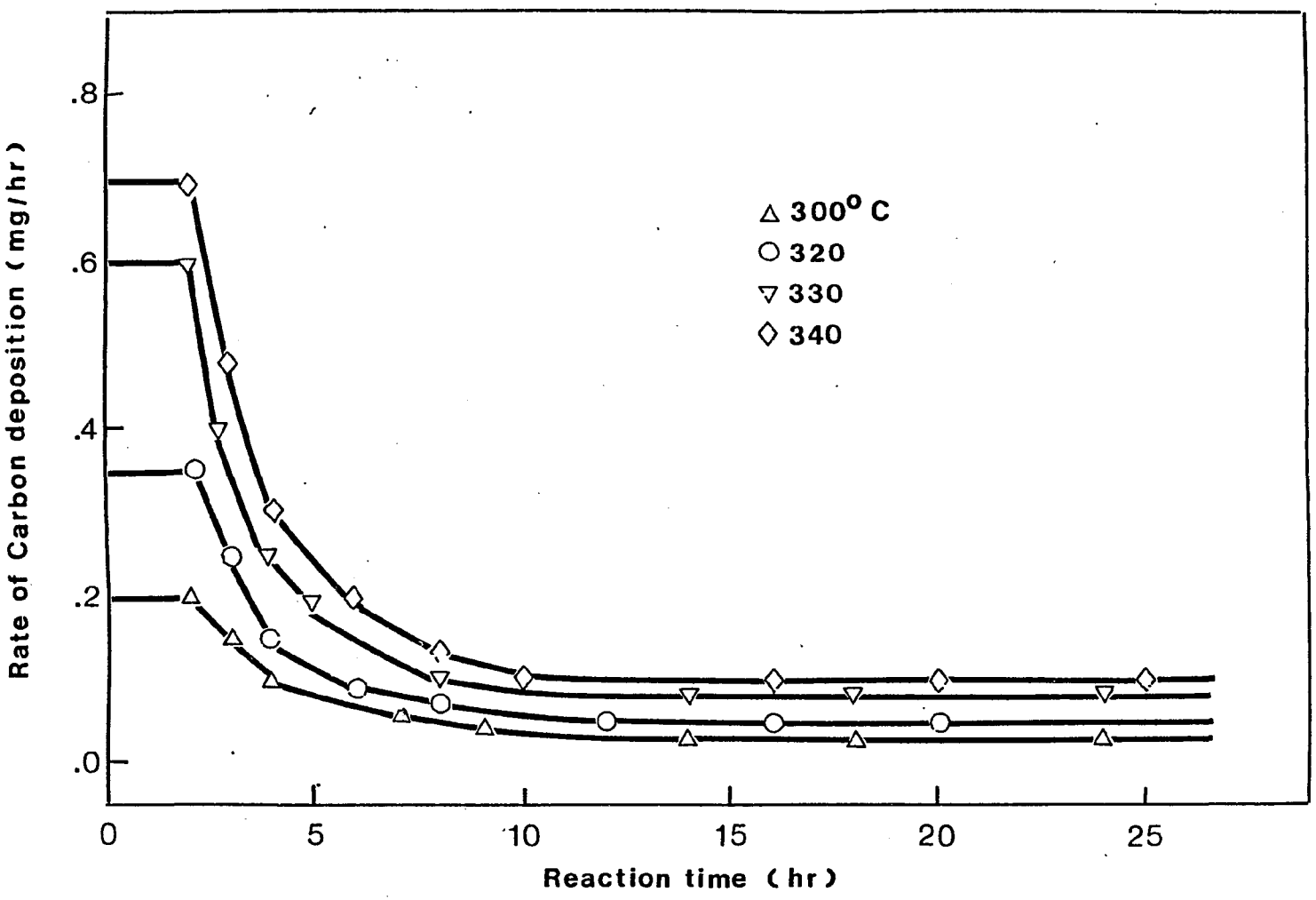

Figure 21. Time Dependence of the Rate of C Deposition from pure CO over Non-Porous Pellets.

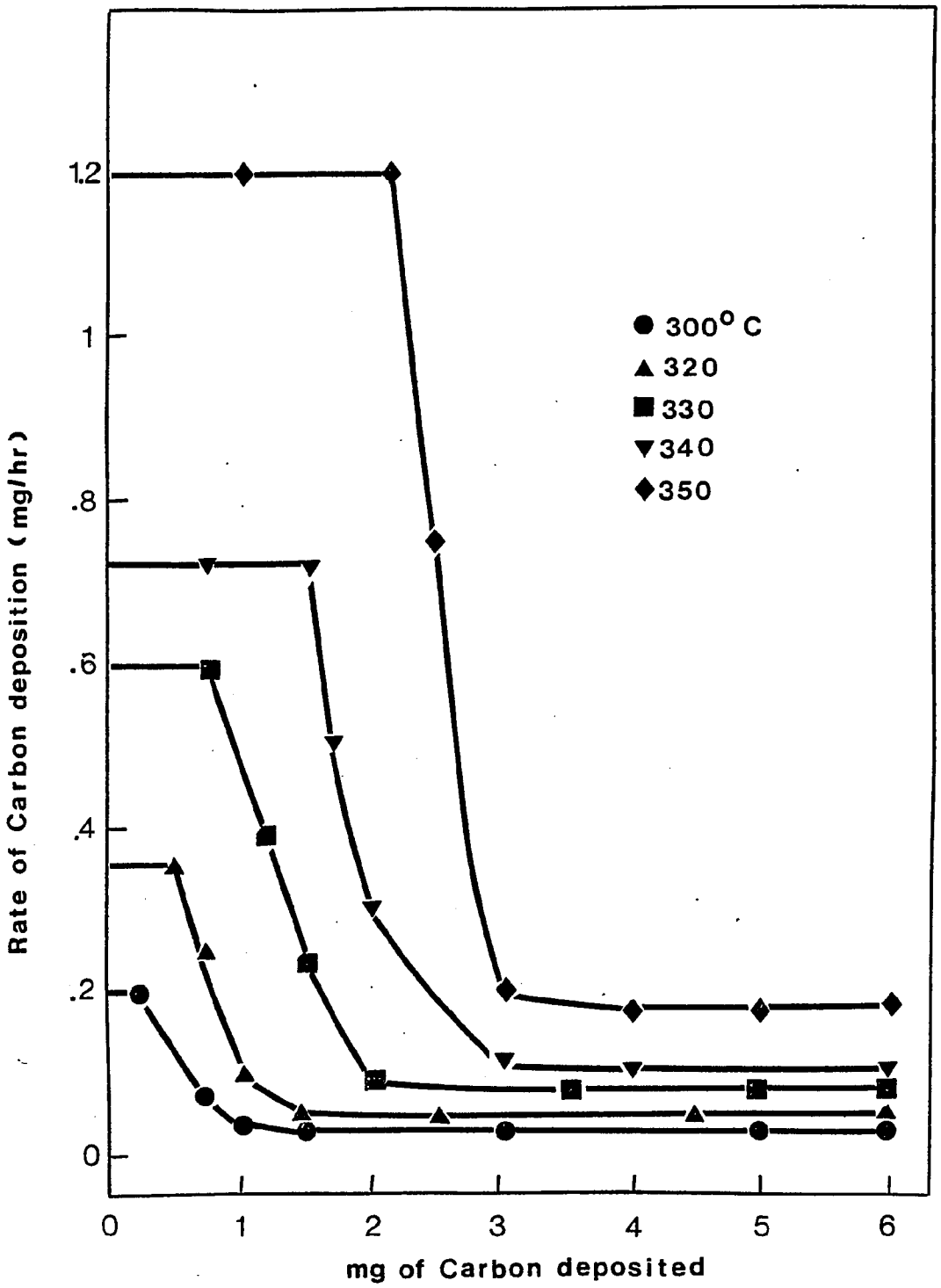

Figure 22. Dependence of the rate of C Deposition with the amounts of C Deposited from Pure CO over Non-Porous Pellets.

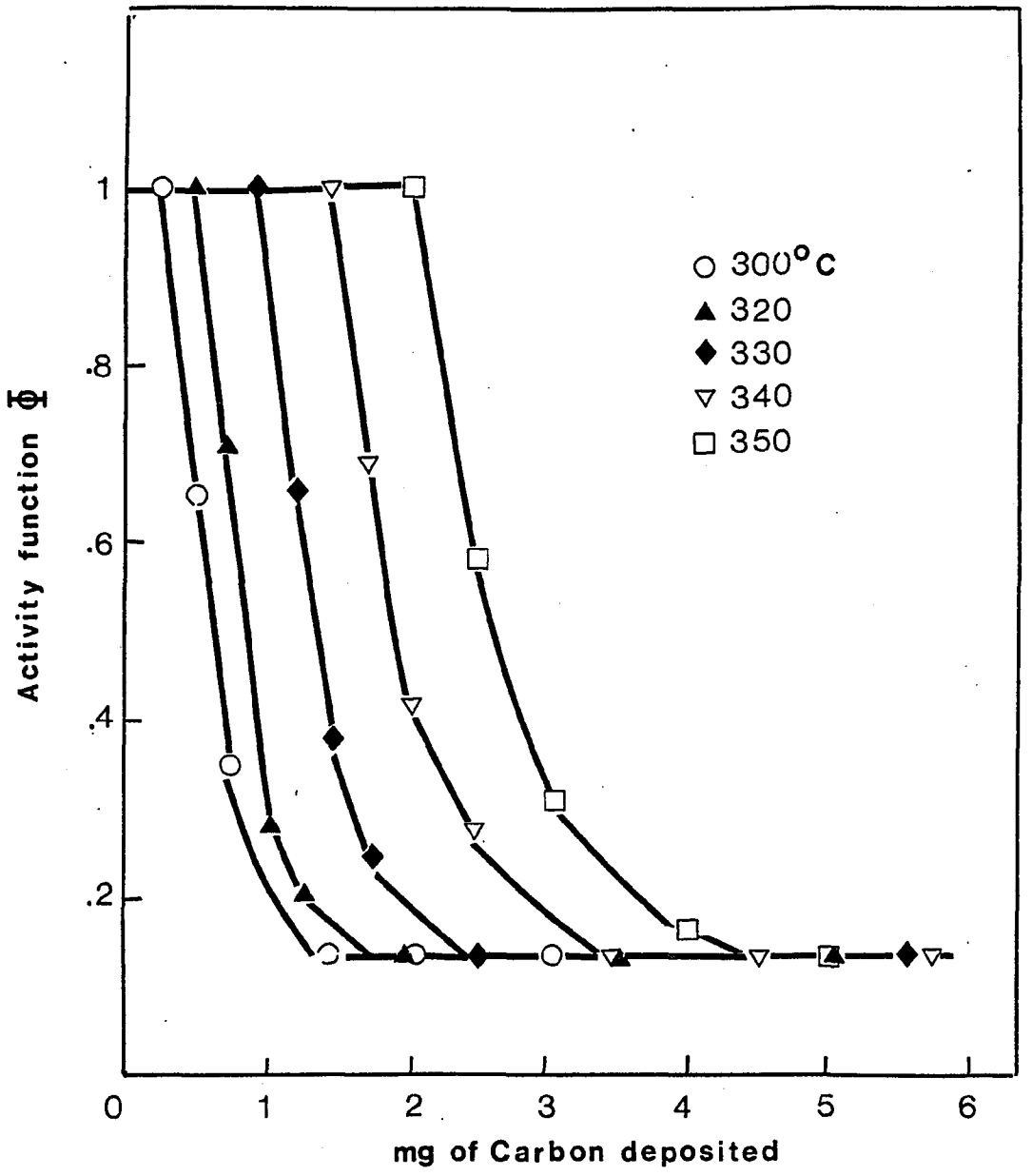

Figure 23. Activity Function Dependence on the Amounts of C Formed from Pure CO over Non-Porous Pellets.

3.4 GASIFICATION OF CARBON DEPOSITS WITH HYDROGEN

3.4.1 Description

Gasification of carbon deposits was attempted on both foils and pellets. Constant rates of gasification on foils were difficult to achieve and reproducibility of results extremely poor. Constant values could be sustained on pellets for periods of 2 to 3 days. By alternating carbon deposition with gasification, good agreement was possible for values of rates of reaction (see Table 5). Temperatures of reaction were varied in between 350 and 500 C and the hydrogen partial pressure changed from .05 to 1 atm.

3.4.2 Kinetic Results

Constant rates of carbon gasification could be maintained for both porous and non-porous pellets. The temperature dependence of the rate of gasification was then measured. Results are shown in Fig. 24 for porous pellets and Fig. 25 for non-porous pellets. The Arrhenius plots give values of 48 Kcal/gmol for the activation energy of the gasification reaction for both kinds of pellets. The only detectable gaseous product was methane. The amounts produced by the non-porous pellets were too small to be measured accurately. The order of reaction with respect to hydrogen partial pressure appears to be 1 in the range of this study (Fig. 25).

TABLE 1Ø

Effect of H on the rate of C gasified from pellets

% H in feed	Rate of C gasification (mg/min)		
	375 C	4ØØ C	425 C
9	.Ø38	.13	.35
18	.Ø85	.3	.73
27	.135	.42	1.Ø5
34	.15	-	-
38	.17	-	-
48	.25	-	-
55	.28	-	-
62	.3	.94	2.5
75	.4	-	-
1ØØ	.5	1.53	4.Ø

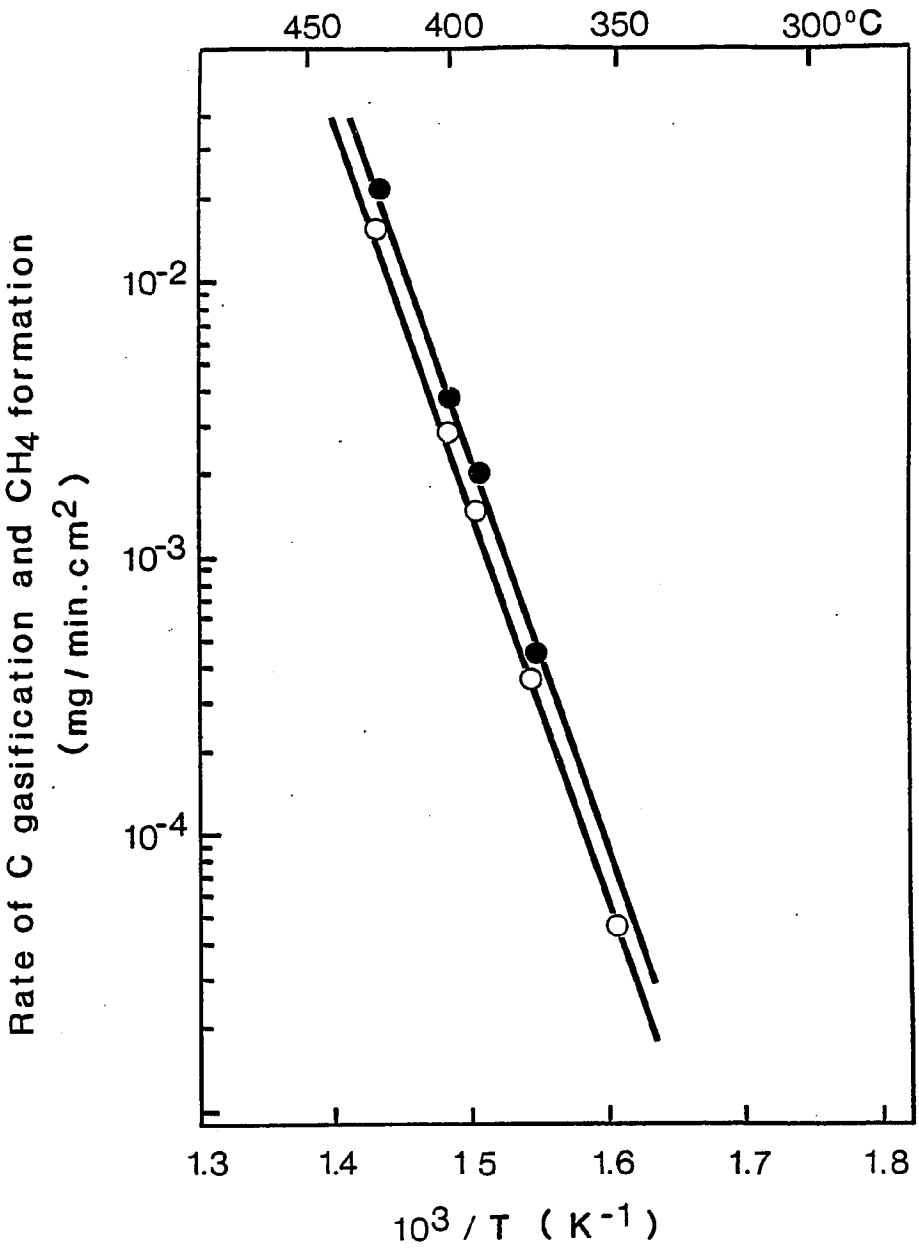

Figure 24. Arrhenius plot for the rates of carbon gasification and CH_4 formation from carbon deposits on supported iron pellets. Reactant : H_2 at 1 atm total pressure. Key : ●, CH_4 formation ; ○, carbon gasification.

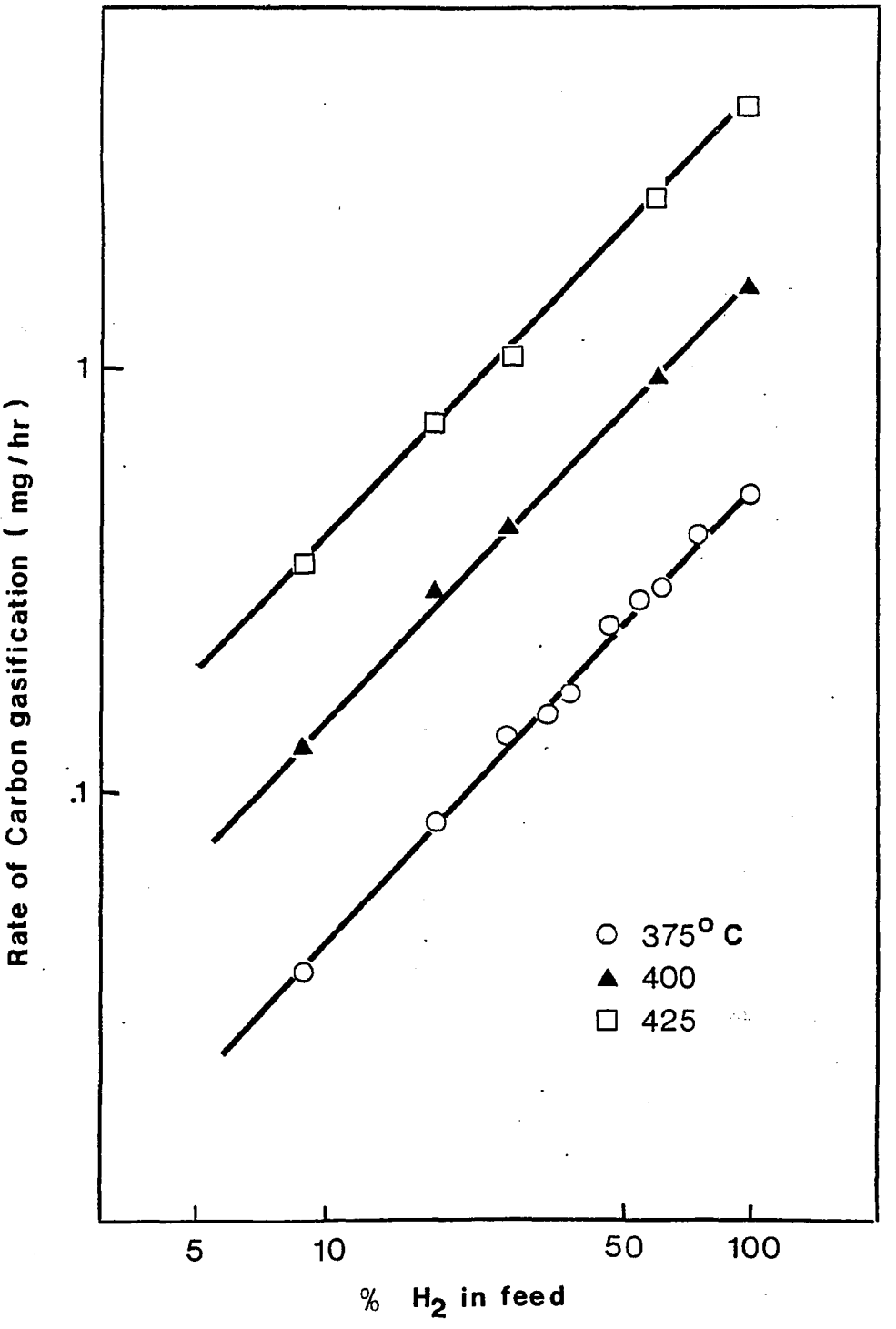

Figure 25. Effect of H_2 on the Rate of Gasification of C Deposited on Non-Porous Pellets.

3.4.3 Regeneration Studies

Carbon deposits on non-porous pellets were readily gasified on contact with hydrogen. The initial rates of gasification were constant for periods of 10-12 hours. A decrease in the rates could be observed afterwards. Constant lower rates were achieved after 20 to 22 hours of continuous gasification. Results are shown in Table 11 Fig. 26. Reactivation of the pellets with hydrogen lead to initial activity levels for the carbon monoxide decomposition reaction.

The dependence of the rates of regeneration with time (Fig. 27) and with the amounts of carbon gasified (Fig. 28) were obtained from the reactivation plots. This was done by numerical derivation. The activity function was calculated for different amounts of carbon gasified. Results are plotted in Fig. 29. Arrhenius plots for the initial and final rates of gasification give straight lines of identical slopes (Fig. 30) The activation energies for both reactions is 48 Kcal/gmol, equal to that obtained on porous pellets.

TABLE 11

Gasification of C deposited on non-porous pellets

Time (hr)	Amount of C gasified (mg)				
	370 C	380 C	390 C	400 C	415 C
1	-	-	.3	.4	.8
2	.25	.4	.6	.8	1.6
3	-	-	.9	1.25	2.4
4	.5	.8	1.15	1.65	3.2
6	.75	1.2	1.75	2.5	4.7
8	.95	1.55	2.35	3.3	6.1
10	1.2	2.0	2.95	4.1	7.6
12	1.4	2.2	3.35	4.9	8.9
14	1.6	2.4	3.65	5.3	9.5
16	1.7	2.55	3.8	5.5	9.8
18	-	2.65	3.9	5.7	10.1
20	1.75	2.70	4.0	5.8	10.3
24	-	2.80	4.15	6.0	10.7
28	1.9	2.9	4.3	6.2	11.1

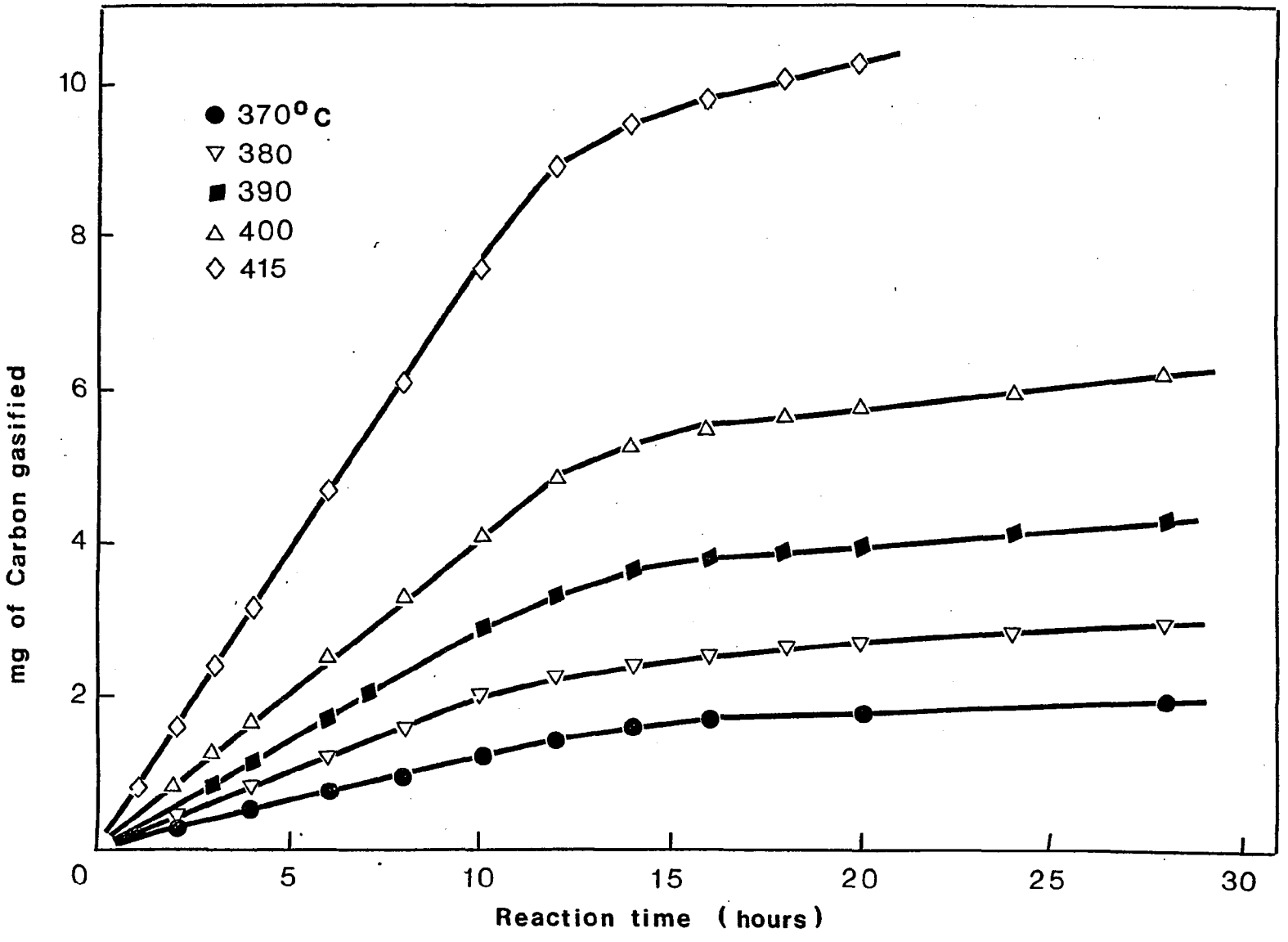

Figure 26. Regeneration of Non-Porous Pellets by Hydrogenation of C Deposition from Pure CO.

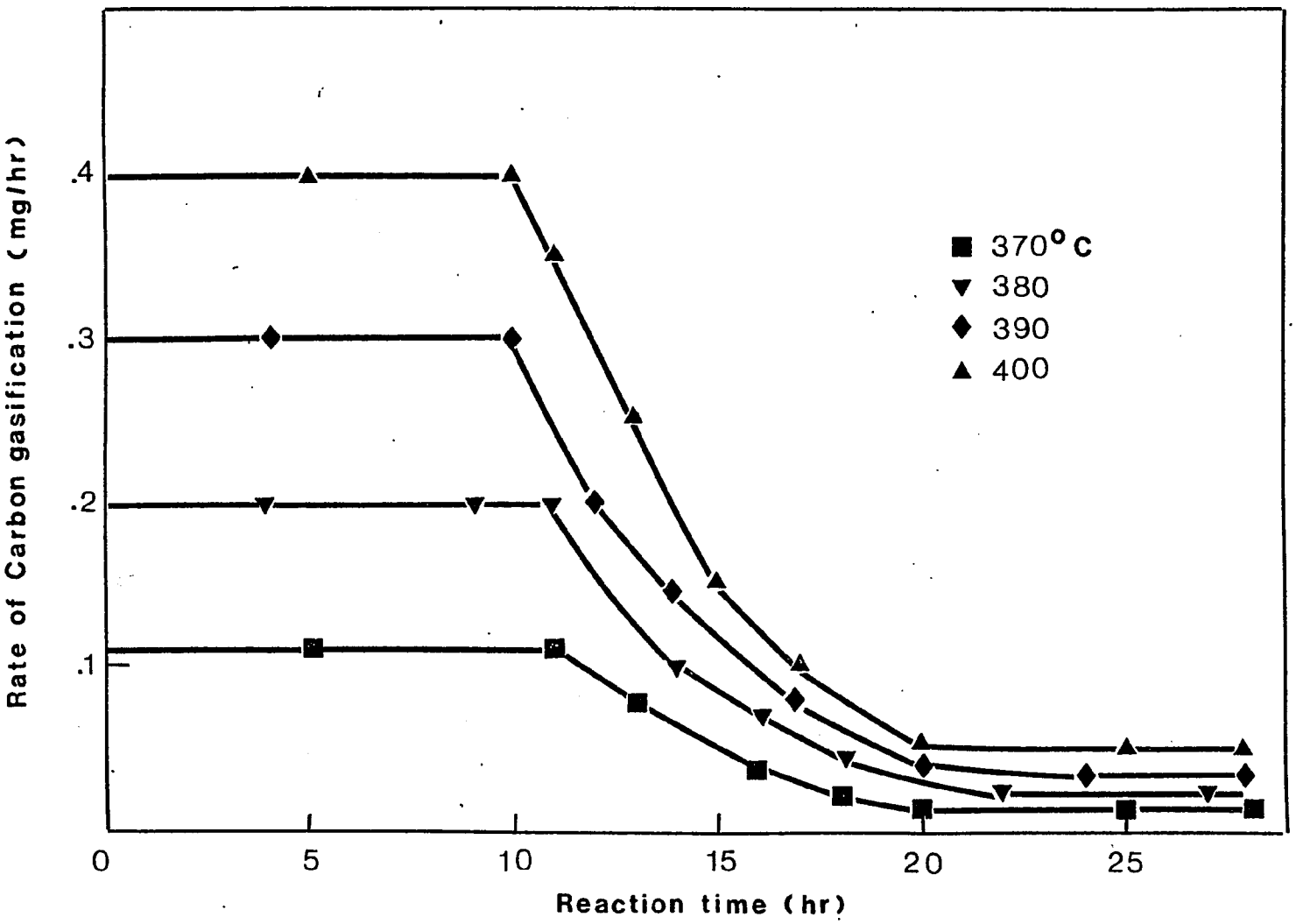

Figure 27. Time Dependence of the Rate of C Gasification of C Deposited on Non-Porous Pellets.

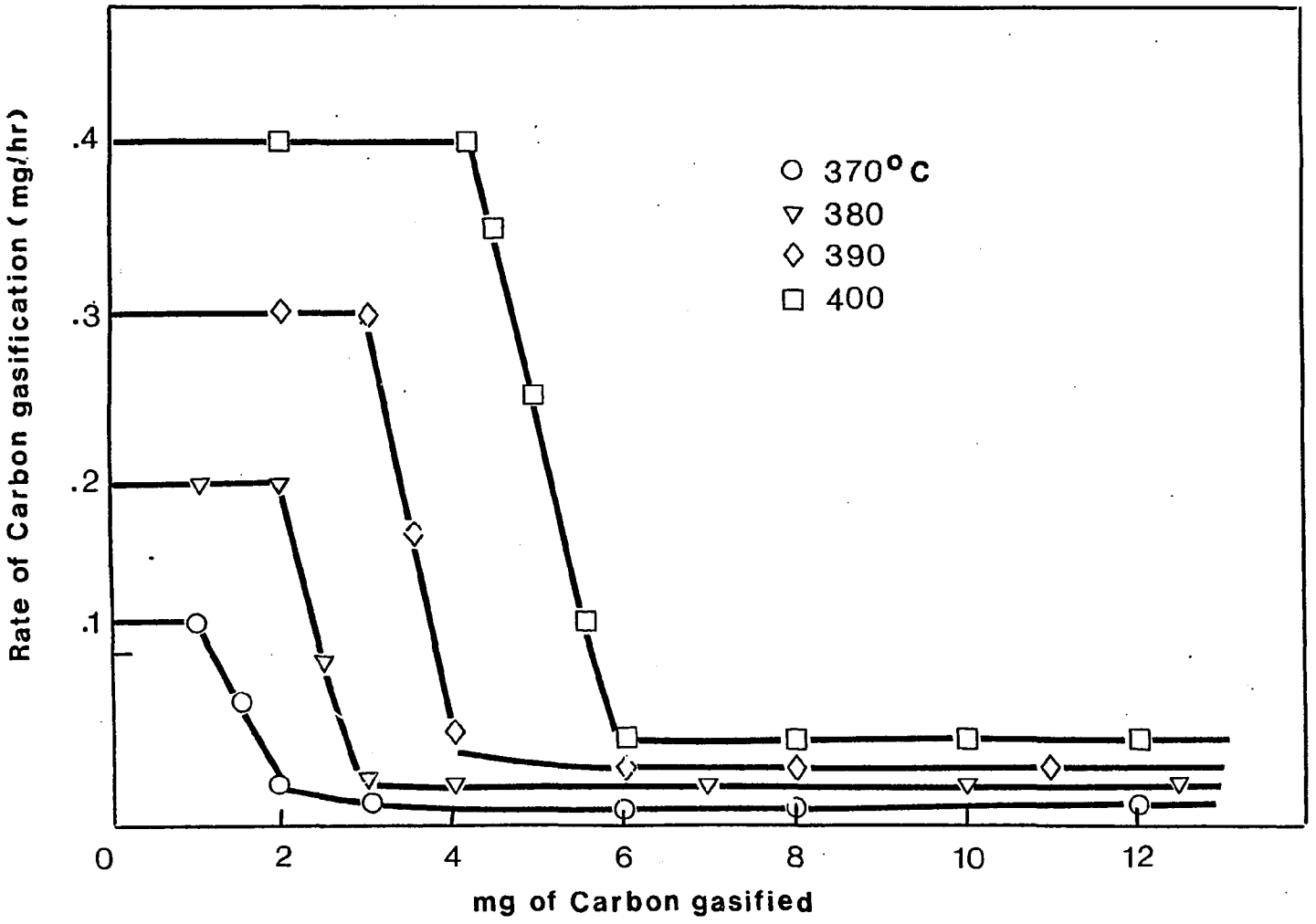

Figure 28. Dependence of the Rate of C Gasification with the Amounts of C Gasified from Non-Porous Pellets.

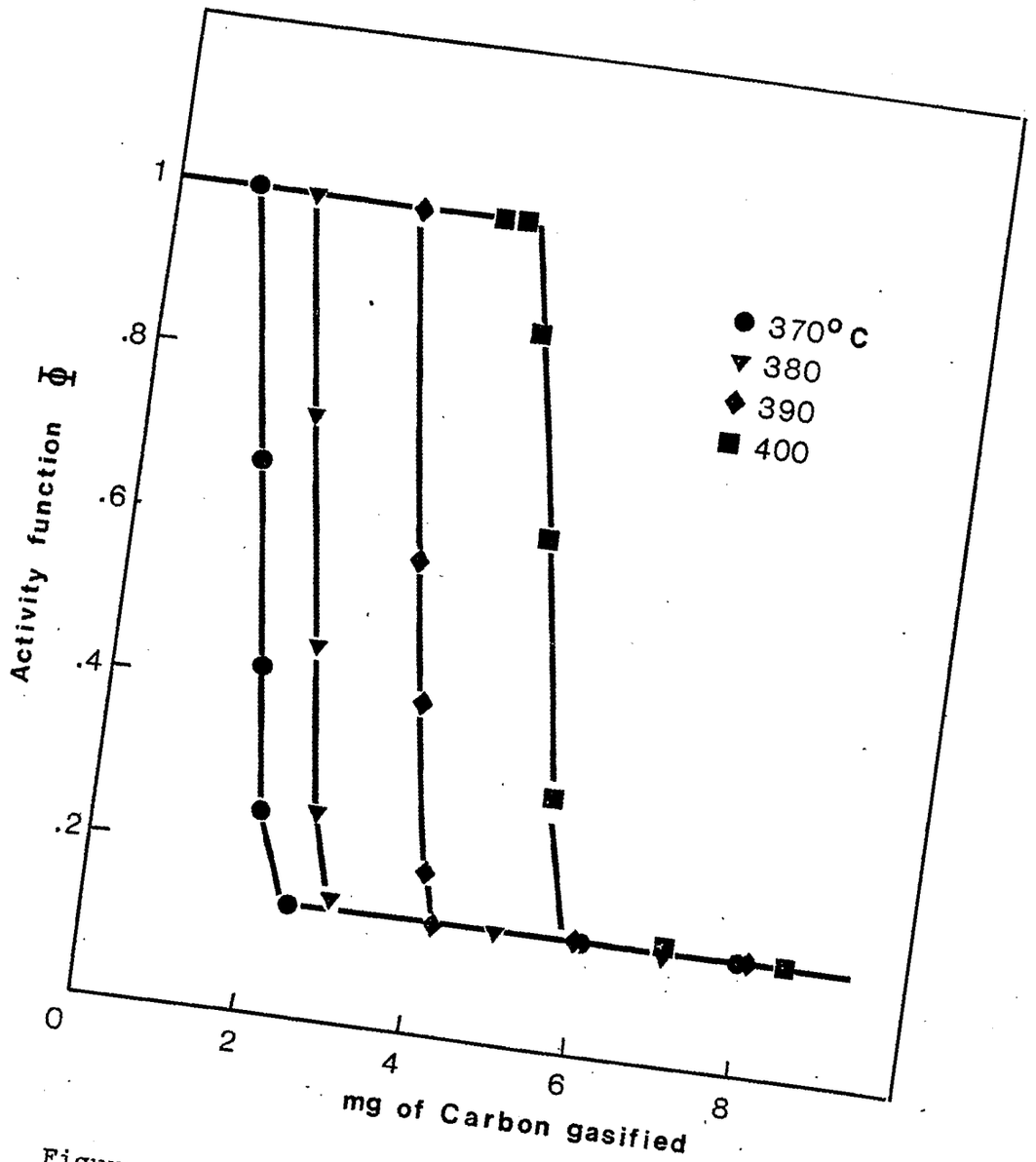

Figure 29. Activity Function Dependence on the Amounts of C Gasified with H_2 from Non-Porous Pellets.

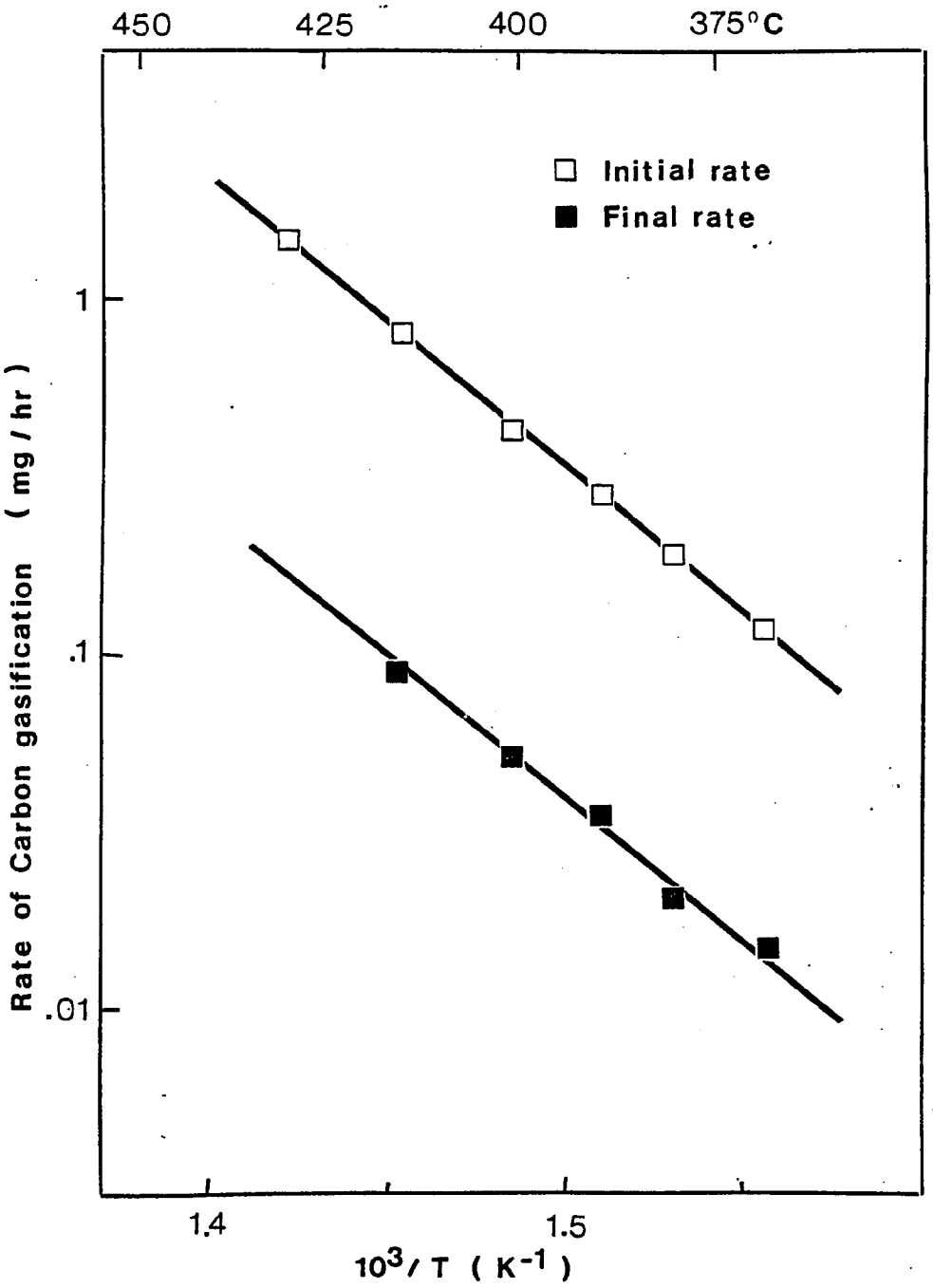

Figure 30. Effect of Temperature on the Initial and Final Rates of C Gasification from Non-Porous Pellets.

3.5 EFFECT OF HYDROGEN ON THE RATE OF CARBON FORMATION

Admission of hydrogen to the system resulted in an increase of the rate of carbon deposition at the temperatures of this study. The temperature dependence of the rate of formation was examined for different compositions of carbon monoxide and hydrogen. Results are shown in Fig. 31. Temperatures were varied in between 300 and 400 C. Hydrogen concentrations were changed while keeping carbon monoxide partial pressure constant. The effect of hydrogen partial pressure on the rate of deposition was then studied. See Fig. 32.

3.6 ELECTRON MICROSCOPY STUDY

Carbon deposits on foils and pellets were inspected by electron microscopy using a scanning electron microscope (SEM). Pictures taken with this apparatus are shown in Figures 33 to 38. Carbon filaments are present in all of the samples observed. Those for foils appear to have a metal particle at the tip (see Fig. 36). The size of the iron crystal and filament is 0.2 microns. Carbon deposits on pellets show a different type of formation. They resemble more a carbonaceous growth with the metal at the outskirt. Carbon seems to form on patches on the pellet surface, presumably

where iron clusters were originally. Metal particle sizes were measured to be 0.1 microns.

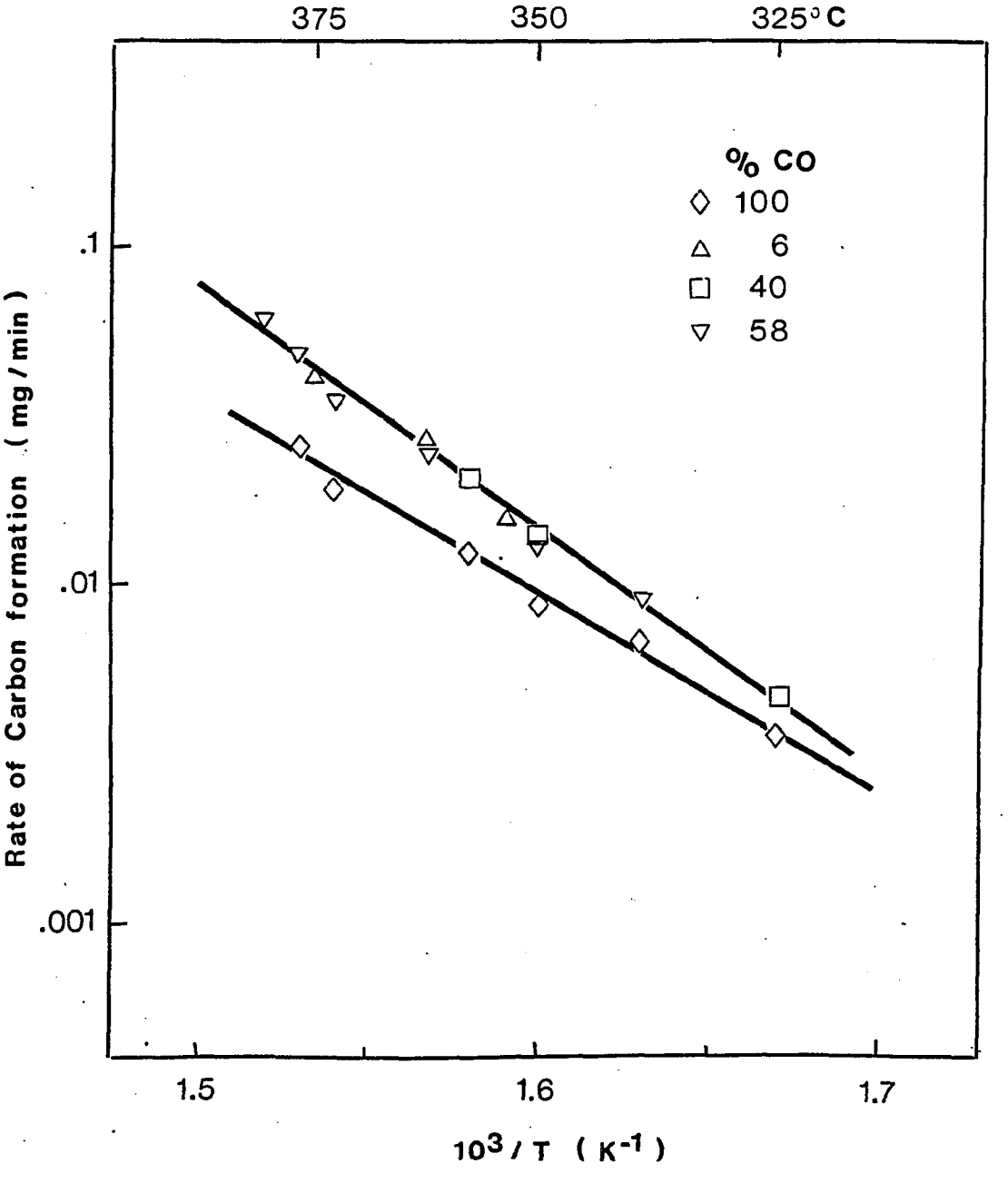

Figure 31. Effect of Temperature on the Rates of C Formation from Pure CO and CO/H_2 Mixtures over Non-Porous Pellets ($\%H_2$= 42).

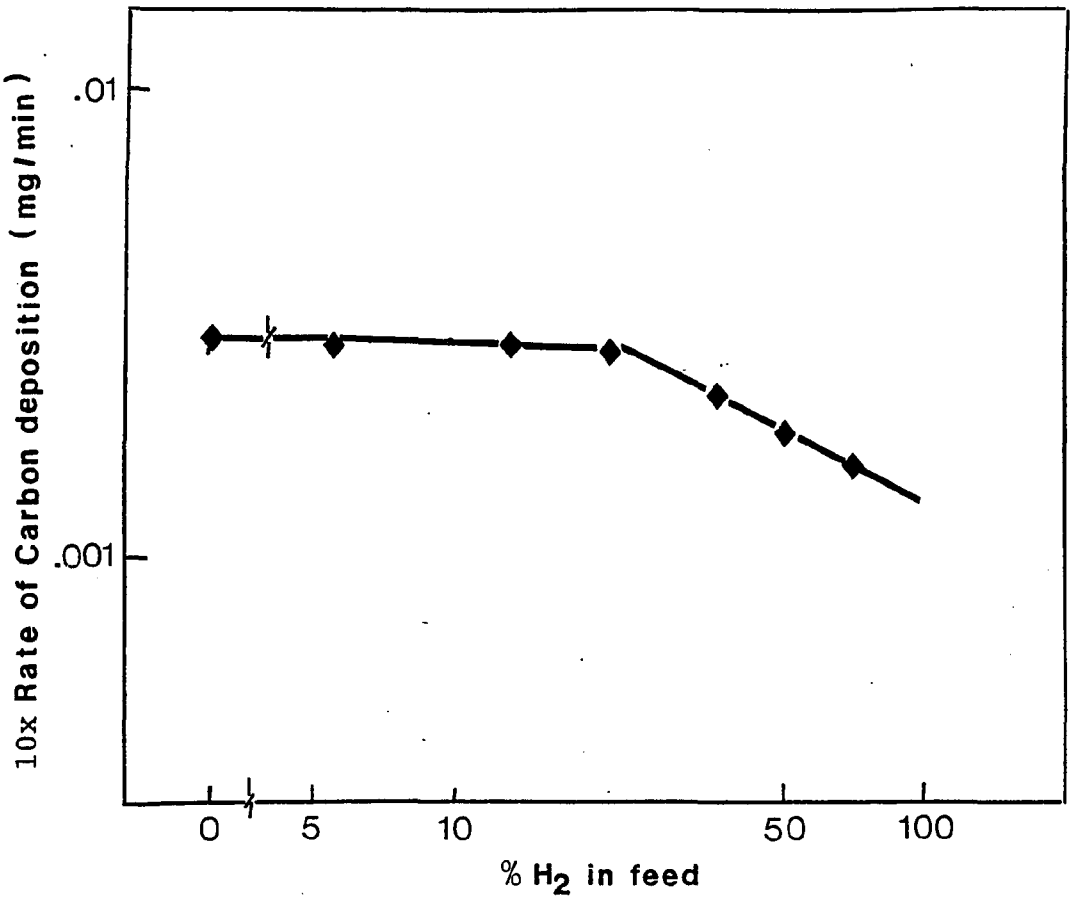

Figure 32. Effect of H_2 on the rate of CO Deposition from CO/H_2 mixtures (%CO = 30), at 260°C.

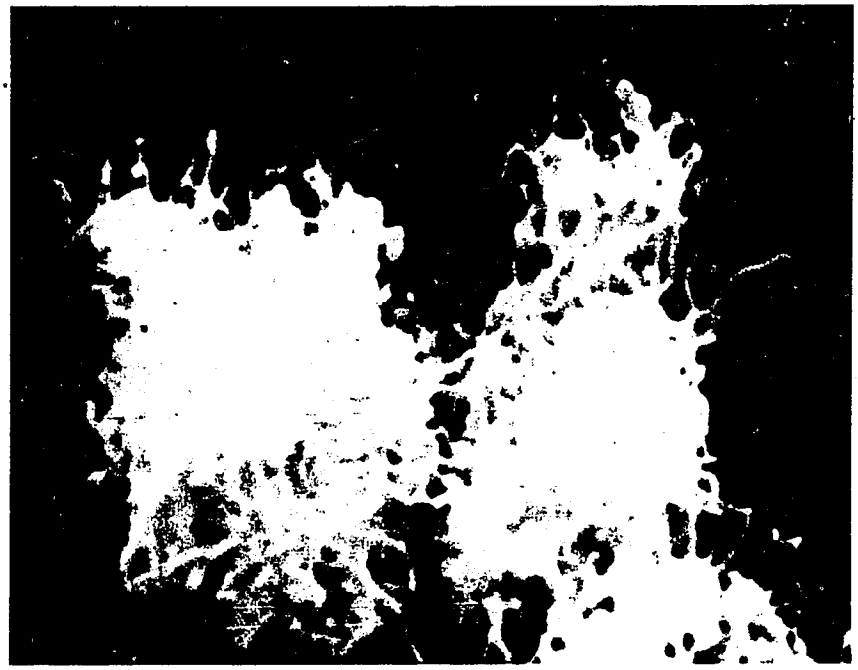

Figure 33. SEM photograph of carbon deposited on an iron foil showing filament growth. Magnification 10,800x.

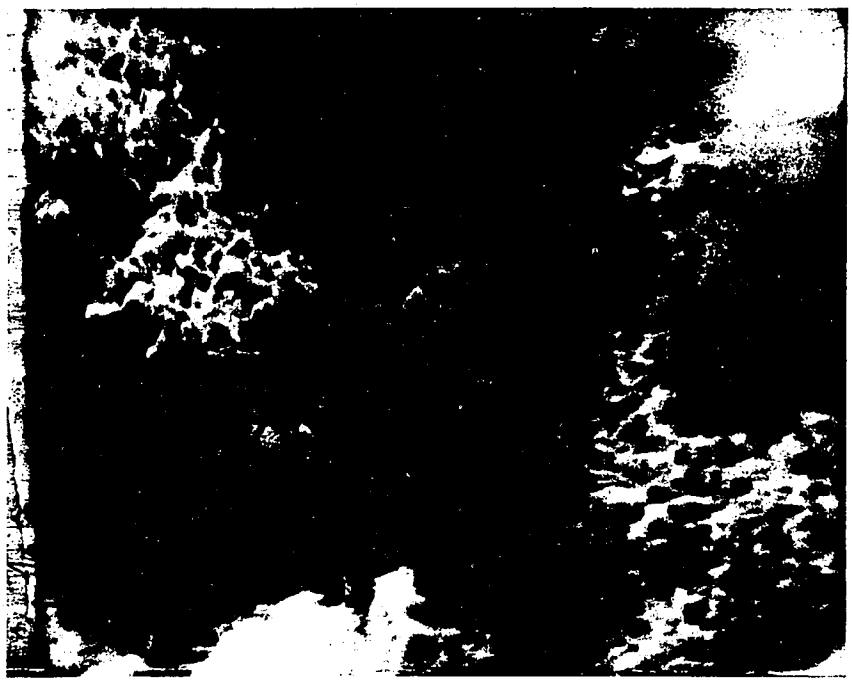

Figure 34. SEM photograph of carbon deposited on an iron foil showing filament growth. Magnification 6,600x.

Figure 35. SEM photograph of carbon deposited on an iron foil showing filament growth. Magnification 7,300x.

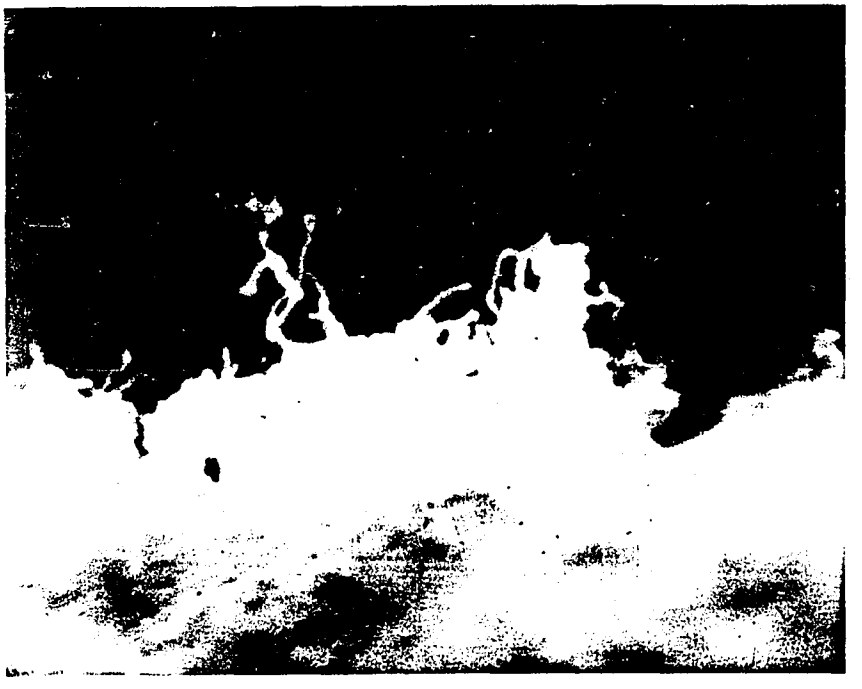

Figure 36. SEM photograph of carbon deposited on an iron foil showing filament growth. Magnification 10,000x.

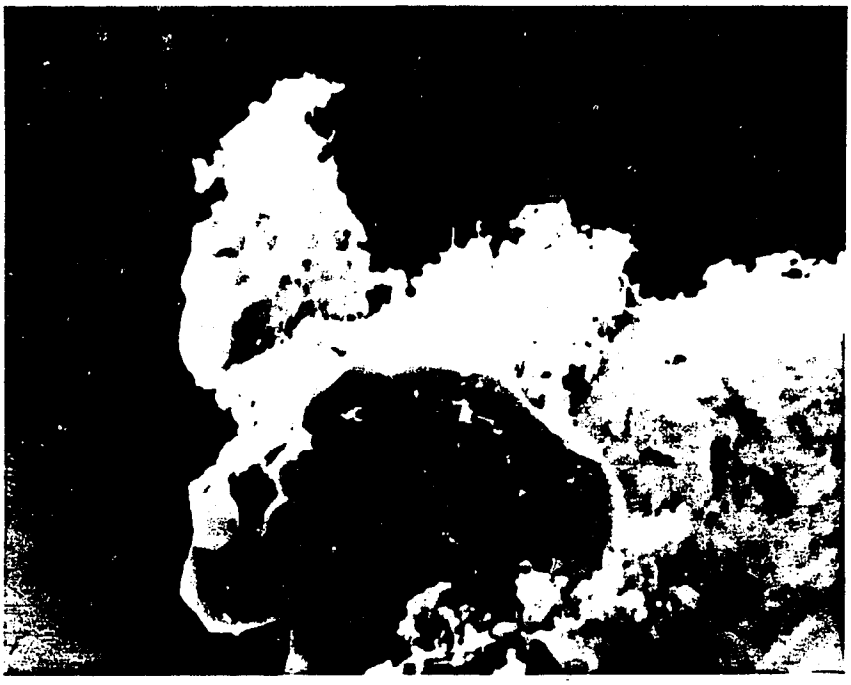

Figure 37. SEM photograph of carbon deposits on a porous iron pellet. Magnification 5,700x.

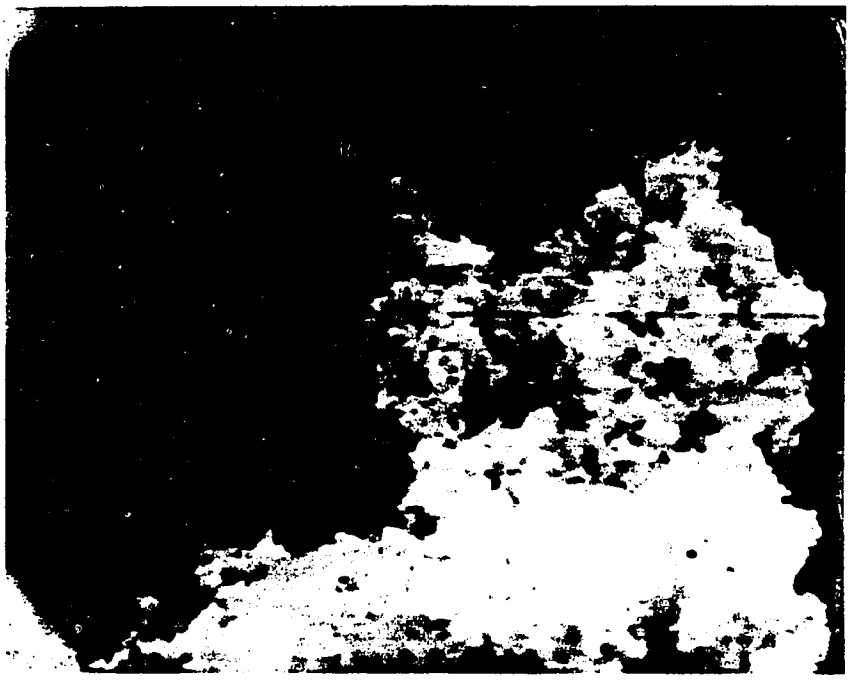

Figure 38. SEM photograph of carbon deposits on a porous iron pellet. Magnification 15,200x.

Chapter IV

DISCUSSION

4.1 CARBON FORMATION FROM PURE CARBON MONOXIDE

The partial pressure of carbon monoxide appears to have no effect on the rates of carbon and carbon dioxide formation. This can be described by a surface mechanism in which the CO adsorption and dis-association on the catalytic surface is fast (and reaches equilibrium) and the filament growing step is rate limiting. The following sequence of reactions can be proposed:

$$CO + M \longleftrightarrow CO\text{-}M \qquad (1)$$

$$CO\text{-}M + M \longleftrightarrow CM + OM \qquad (2)$$

$$CO\text{-}M + OM \longleftrightarrow CO_2\ (g) + 2M \qquad (3)$$

$$CM \longrightarrow C\ (\text{filament}) + M \qquad (4)$$

Reactions (1) to (3) can be considered to be in quasi-equilibrium, being the filament growth the rate determinig step. Assuming that CO adsorbs strongly on the metal sites, the reaction will be zero order with respect to CO. The overall reaction rate will be given by :

The rate of growth of a filament has been related to the diffusion of carbon through the metal crystallite in the tip (64,65). Diffusion cleans the surface, so that the reaction can continue. From these experiments the rate of reaction can be expressed as:

$$r = 2.2E10 \exp(-32{,}000/RT) \text{ (mg C / cm2.min)}$$

The activation energy for the diffusion of carbon on iron has been reported in the range 18 to 34 Kcal/gmole. Since the activation energy observed experimentally is within this range, the above mechanism is a plausible explanation of the results. The experimental data was compared to the values predicted by the model in Fig. 39.

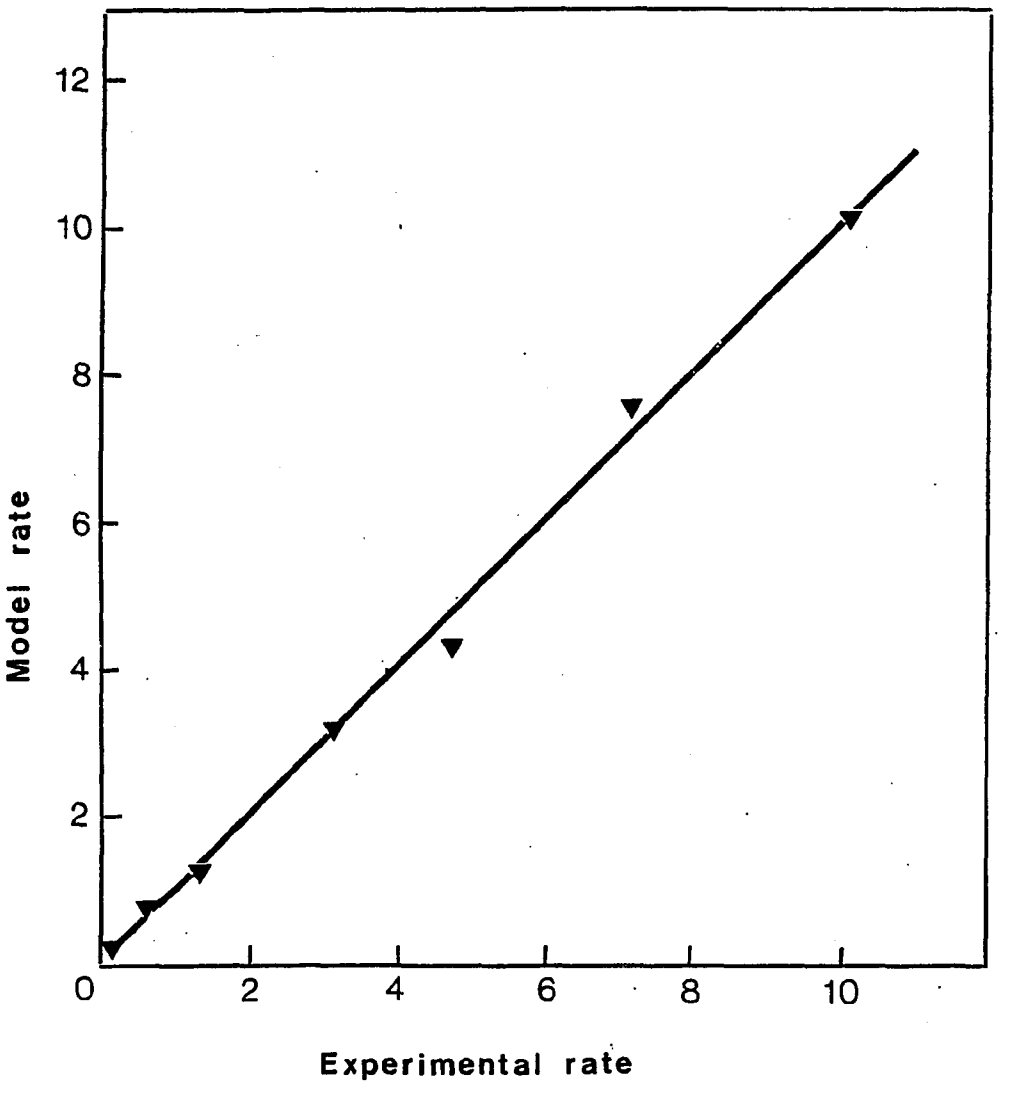

Figure 39. Comparison of experimental data and model prediction for the rate of carbon depostion from CO on non-porous pellets.

4.2 DEACTIVATION OF COMMERCIAL POROUS PELLETS

Carbon deposition from pure CO decreases the activity for the CO decomposition reaction (see Fig. 16). In contrast to previously observed results by Froment et al. (93), this decrease in activity levels off after a certain amount of carbon has been deposited. Constant lower rates of deposition are then achieved. Initially high rates of carbon formation are followed by much lower rates of deposition. The influence of the amount of carbon deposited on the rate of formation (Fig. 17), appears to be confined to the initial period. This suggests a mechanism of pore blockage by the carbon formed at the early stages of deactivation. The activity function plotted vs. the amount of carbon deposited show no dependence on the temperature of reaction in the range studied.

These results suggest that there is only a change in the catalyst active area because of carbon formation. Initial and final areas are the same independently of temperature (Fig. 18). Also, the amount of carbon needed to achieve constant rates of deposition is the same at all temperatures. Taking into account these experimental facts the following explanation can be advanced: initial carbon deposition is high because all the metal area is available for reaction. As soon as some carbon is formed, the smallest pores are blocked. Larger pores are blocked in time as more carbon is

formed. This diminishes the amount of active metal, and therefore the activity. Once all pores are filled with carbon, the reaction will proceed at a constant rate because C deposits now on the filaments formed on the pellet surface and those protruding out off the largest pores.

The experimental data was fitted by the following model:

$$A = (1 - B) \exp (-D.w) + B$$

where A = activity function

B = final area / initial area

D = pellet parameter (1/mg)

w = amount of carbon formed (mg)

A value of B of 0 means total deactivation of the catalyst at infinite time (Froment's model for pore blockage). A value of 1 represents no deactivation (i.e. filaments grow unlimited by pore volume, as in the case of iron foils). A large value of D suggests low pellet porosity. Pores are rapidly filled. The final active area is obtained after a few mg of carbon are formed. Small values of D are consistent with materials with large pores. the model was fitted by a non linear regression computer program. The values of the parameters obtained were D=.42 and B=.19 mg-1. The standard deviation was .04 or 4%. The proposed model becomes:

$$A = .81 \exp (-0.45\ w) + 0.19$$

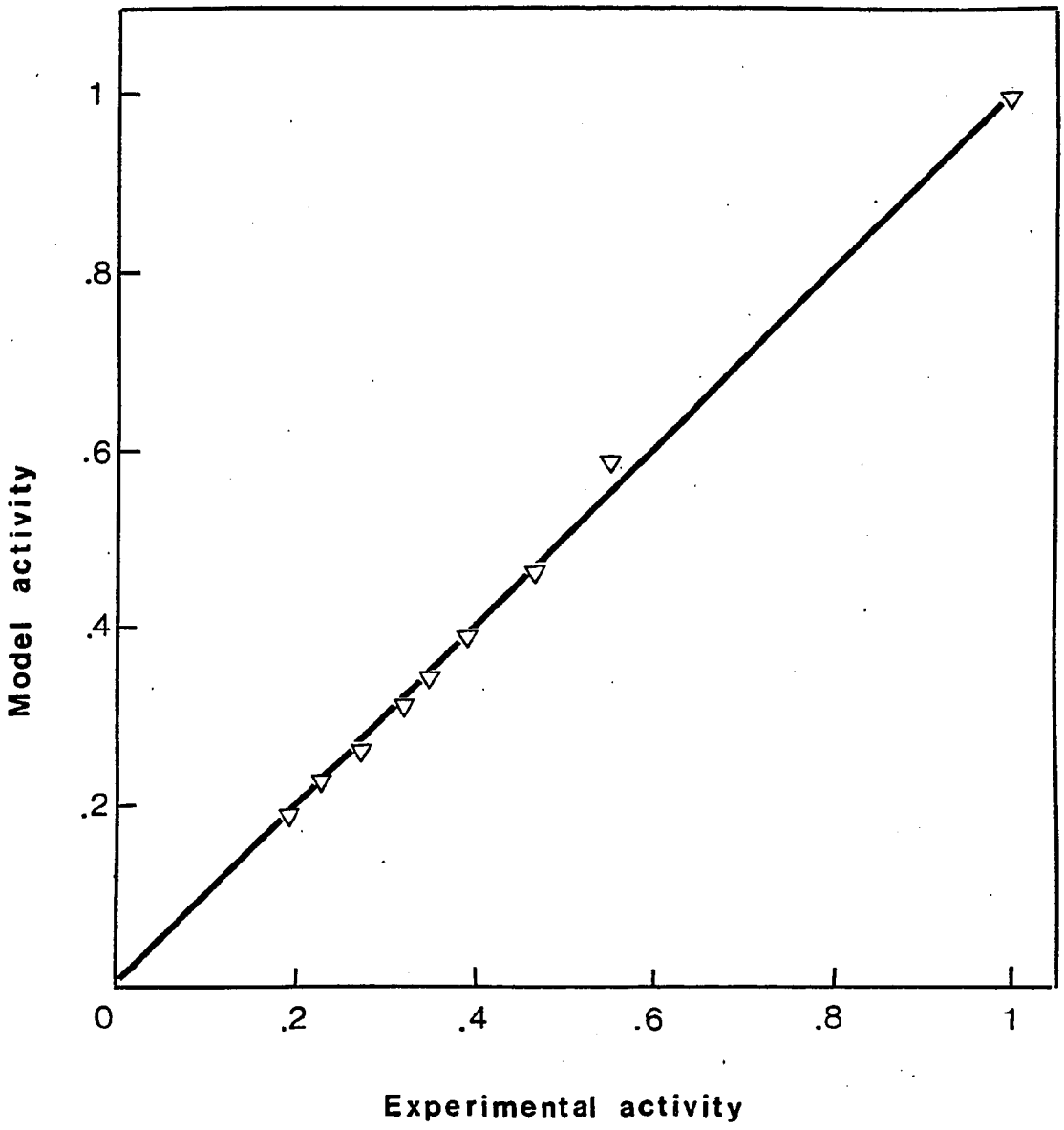

Figure 40. Comparison of experimental and model prediction of the activity function for porous catalyst deactiviation at 300°C.

4.3 DEACTIVATION AND REGENERATION OF NON-POROUS PELLETS

Carbon is formed from pure CO at constant initial rates over non-porous pellets. After a certain amount of carbon is formed deactivation of the catalyst occurs (Fig. 22). This amount of carbon depends on the temperature of reaction. The higher the temperature, the more carbon needed for deactivation to begin. Final constant rates of deposition are achieved after the deactivation process. Initial and final rates of carbon formation follow identical Arrhenius plots. This suggests that the mechanism of carbon formation does not change with time nor with the amount of carbon deposited. What changes is the active area available for reaction.

Hydrogenation of the carbon deposits from the same non-porous pellets show a similar behaviour. An initial constant rate of gasification (Fig. 26) is followed by a deactivation process. Lower final rates of hydrogenation are achieved after a certain amount of carbon has been gasified. The amount of carbon depend on the temperature of reaction. Initial and final rates of gasification follow identical Arrhenius plots. In both cases, deposition and gasification the final activity function is the same.

The following explanation can be advanced. Iron particles are distributed on patches on the pellet surface. Initially, the carbon formation reaction can be produced on all of the patches. Those metal particles that can be lifted off the

pellet surface will form filaments and continue to react. Those particles that cannot be lifted off will reach equilibrium after a certain amount of carbon has been deposited. Equilibrium is a function of the reaction temperature. An Arrhenius plot for the amounts of carbon deposited before deactivation begins is plotted in Fig. 41. When carbon deposits are gasified, initially all area is available for reaction (patches and filaments). After carbon has been depleted from the patches, equilibrium is reached and the total active area reduced to the final value .

The experimental data was fitted with a model similar to that of porous pellets. To allow for an initial constant deposition or gasification rate, a parameter F was introduced. F represents the amount of carbon necessary for equilibrium at the reaction temperature. The model becomes:

for w smaller than F $A = 1$

for w greater than F $A = (1-B) \exp (-D.(w-F)) + B$

The non linear regression method gives values of B=.12 and D=3.5 with a standard deviation of .Ø2 or 2%.

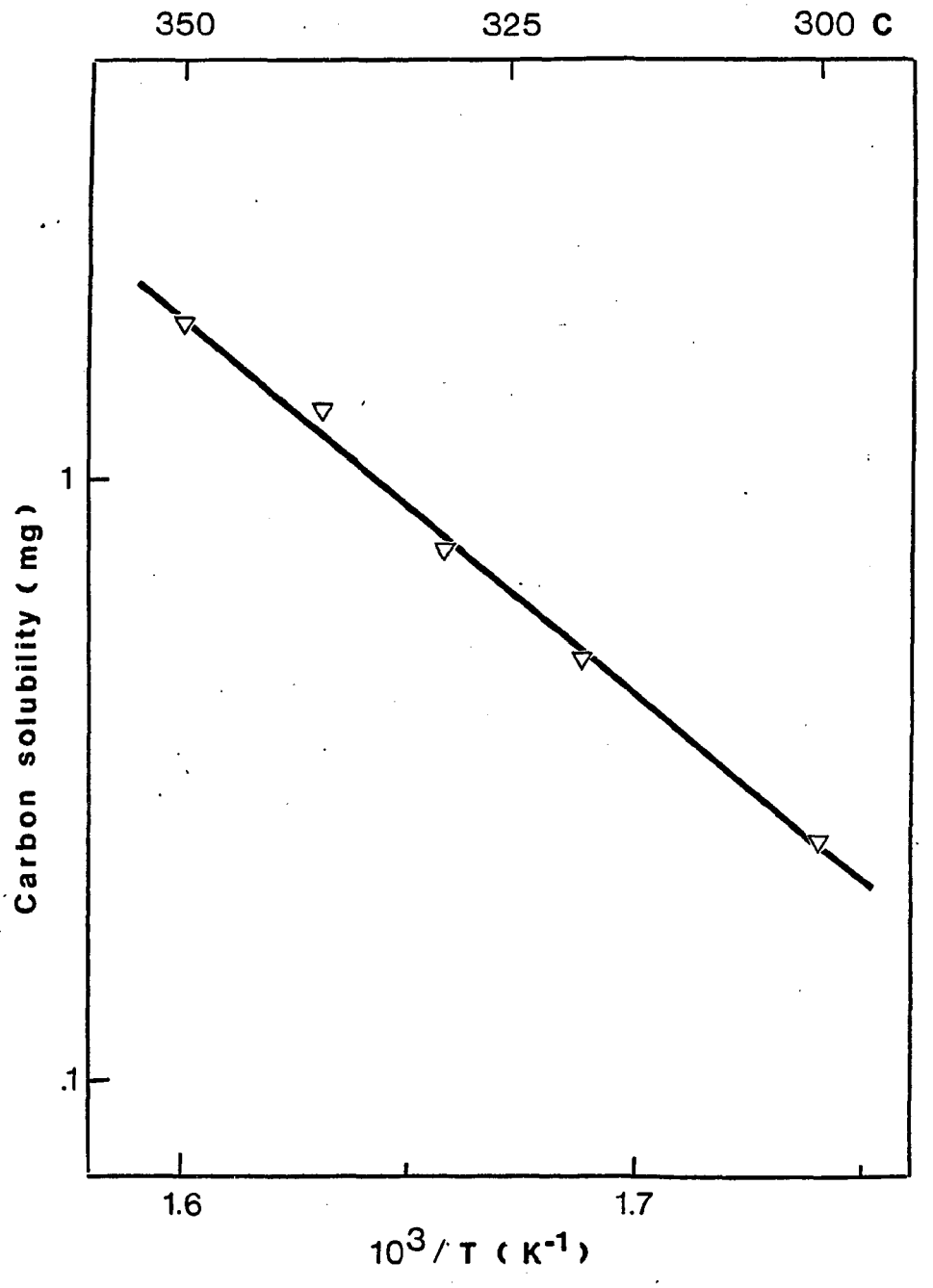

Figure 41. Arrhenius plot for the carbon solubility in iron for non-porous pellets.

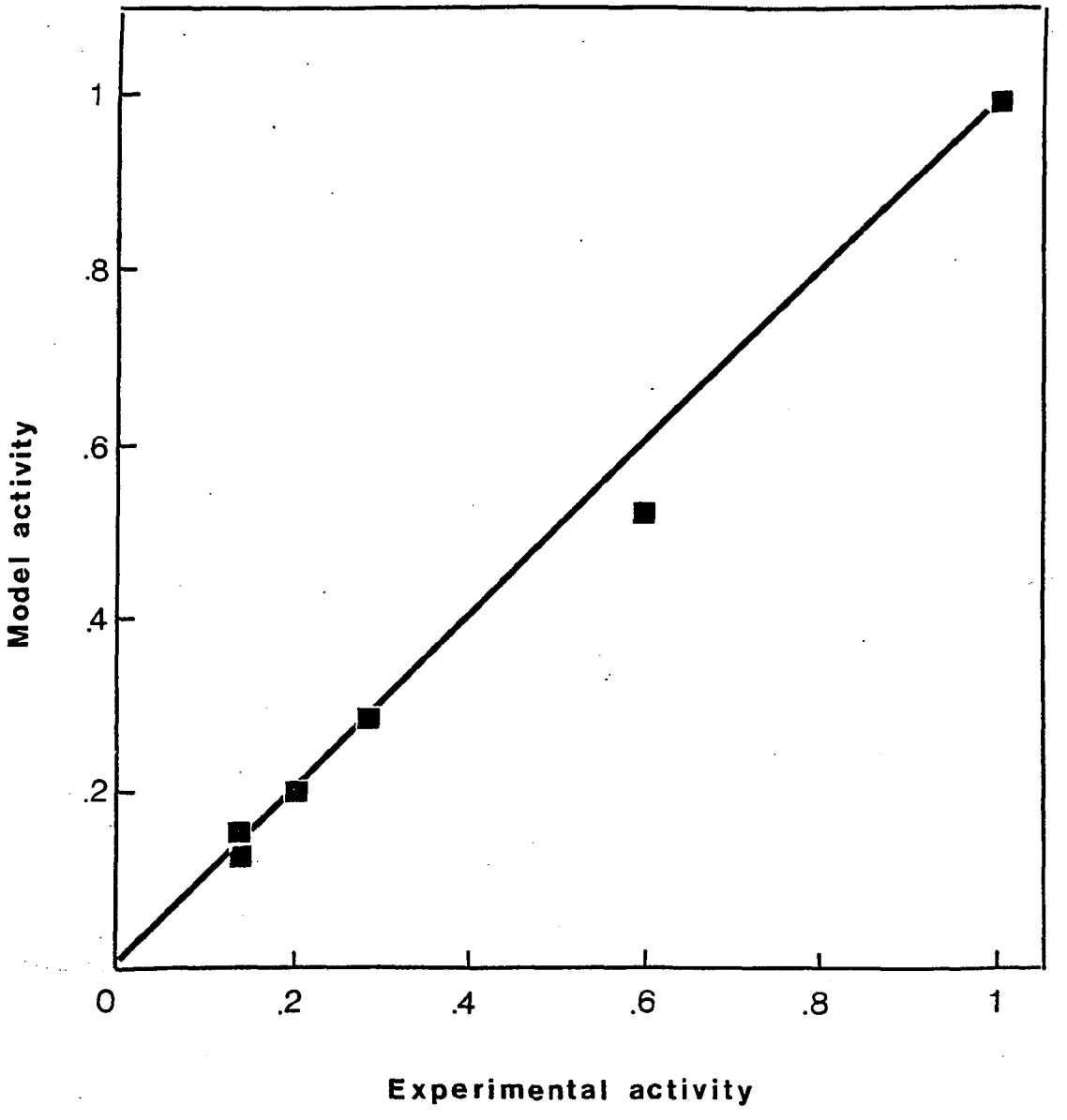

Figure 42. Comparison of experimental and model prediction of the activity function for nonporous pellets at 320°C.

4.4 GASIFICATION OF CARBON DEPOSITS WITH HYDROGEN

After an initial deactivation process, gasification of carbon proceeds at constant rates. Hydrogen gasifies the carbon deposits to methane and possibly higher hydrocarbons. The dependence of the rate with the hydrogen partial pressure is 1 in the range of temperatures of this study. In order to explain this behaviour the following set of reactions is proposed:

$$C\ (\text{filament}) + M \longleftrightarrow CM \qquad (1)$$

$$H_2 + 2M \longleftrightarrow 2HM \qquad (2)$$

$$CM + 2HM \longrightarrow CH_2M + 2M \qquad (3)$$

$$CH_2M + HM \longleftrightarrow CH_3M + M \qquad (4)$$

$$CH_3M + HM \longrightarrow CH_4\ (g) + 2M \qquad (5)$$

Assuming that the rate limiting step is given by reaction (3), (1) and (2) are in quasi-equilibrium, the reaction rate will be order 1 with respect to hydrogen partial pressure. The rate becomes:

$$r = 4.E12 \exp(-48{,}000/RT)\ P \quad (mg/hr)$$

Carbon deposited from CO is readily gasified to methane. This shows that this type of carbon is active and can be considered a precursor for the Fischer-Tropsch synthesis.

Experimental values for the rate of carbon gasification were compared to the ones predicted by the above model. Results can be seen in Fig. 43.

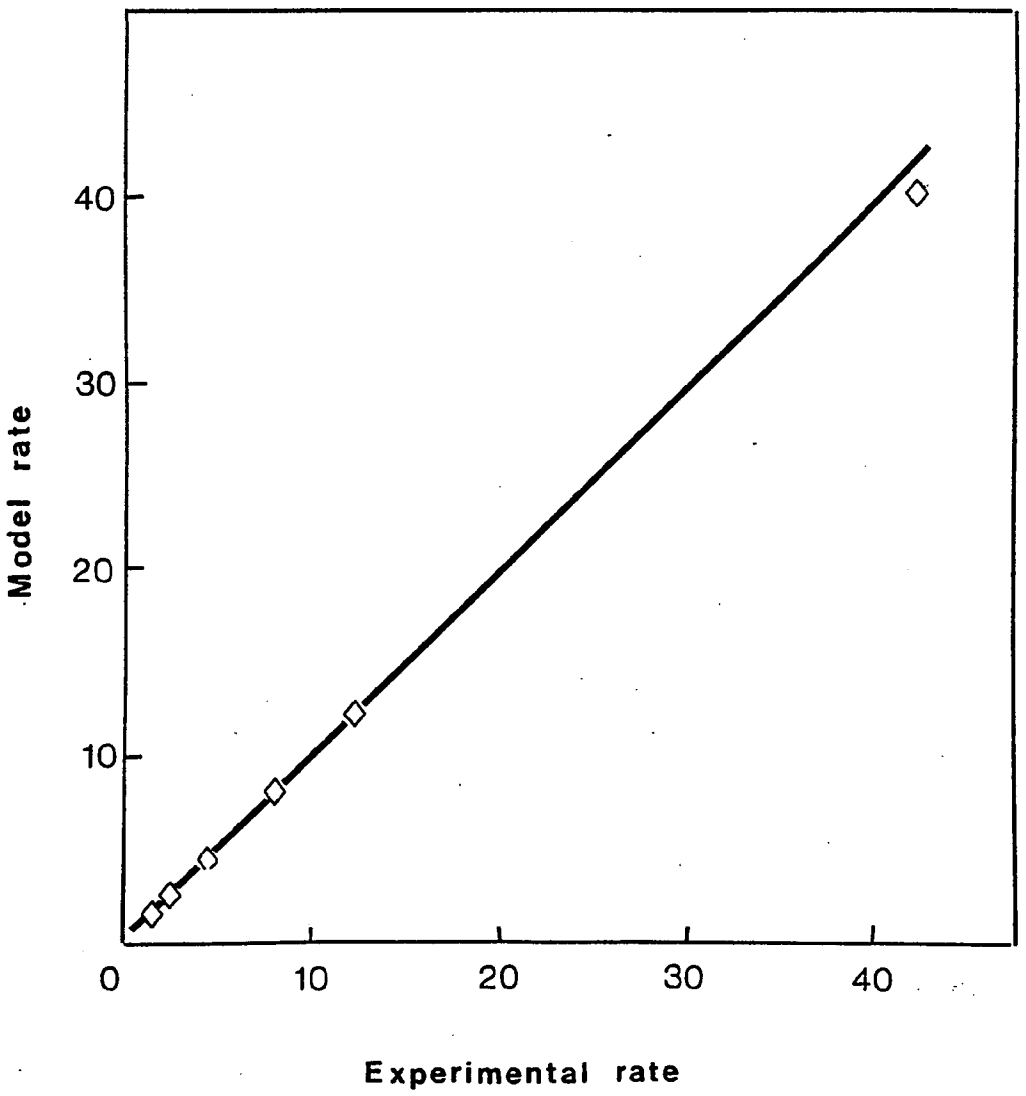

Figure 43. Comparison of experimental and model prediction for the rate of carbon gasification from porous pellets.

4.5 EFFECT OF HYDROGEN ON THE RATE OF C FORMATION

When hydrogen is added to CO it increases the rate of carbon deposition. The order of reaction with respect to CO partial pressure appears to be Ø, as for pure CO. The order with respect to hydrogen partial pressure seems to be Ø at low hydrogen concentrations, approximately .5 at higher concentrations. A mechanism that takes this facts into account is proposed as follows:

$$CO + M \rightleftharpoons COM \qquad (1)$$

$$H_2 + 2M \rightleftharpoons 2HM \qquad (2)$$

$$COM + M \rightleftharpoons CM + OM \qquad (3)$$

$$CM \longrightarrow C\ (filam) + M \qquad (4)$$

$$CM + 2HM \longrightarrow CH_2M + 2M \qquad (5)$$

Reactions (4) and (5) compete for CM intermediate. Making the hypothesis of steady state on CM concentration the rate becomes:

$$r = \frac{k3}{1 + P_{H_2}.k5/k4}$$

By plotting the inverse of the reaction rate vs. the hydrogen partial pressure, a straigh line should be obtained.

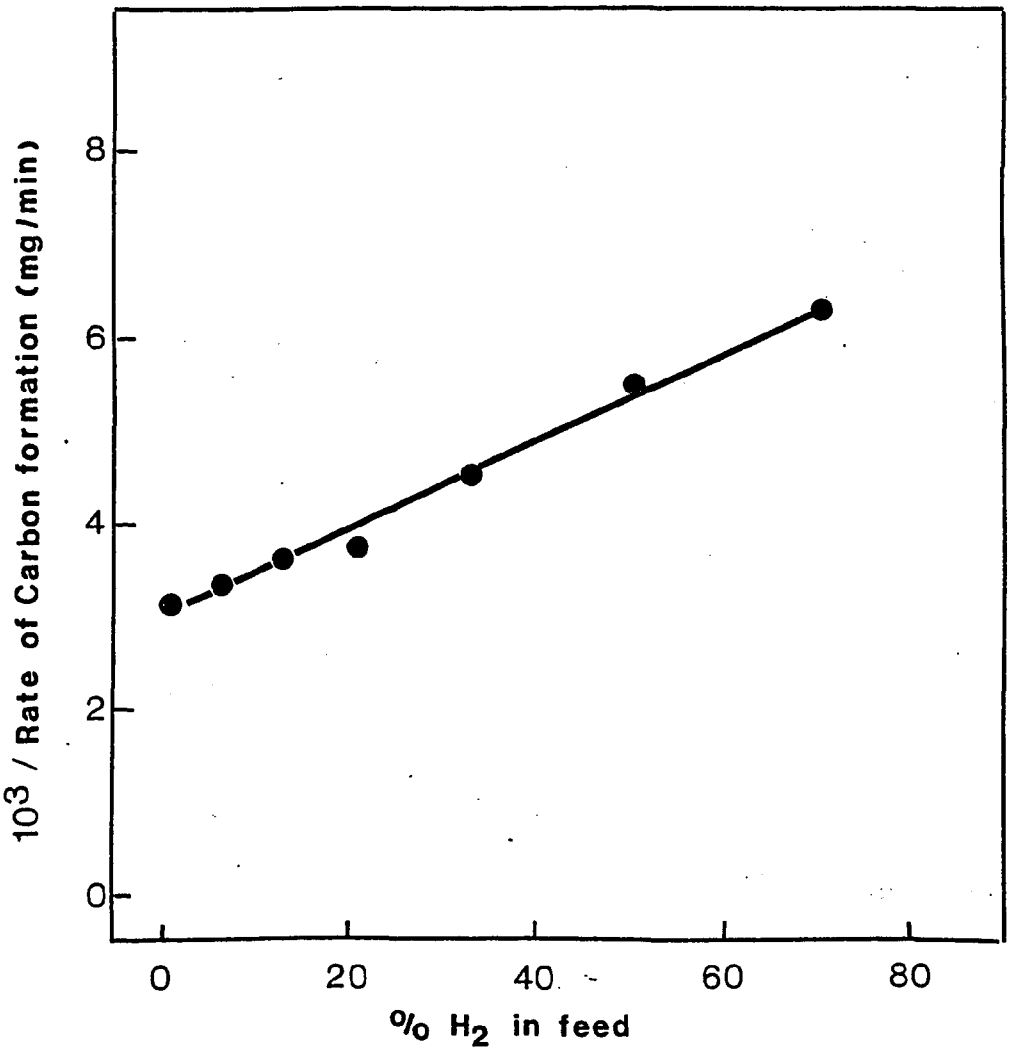

Figure 44. Effect of hydrogen on the inverse of the rate of carbon formation on non-porous pellets at 260°C.

Chapter V

CONCLUSIONS

1- Carbon formation on iron catalysts goes through an induction period prior to filament growth when iron foils, powders and pellets are treated with CO and CO/He mixtures.

2- Iron catalysts produce filamentous growths when contacted with pure CO or CO/He mixtures. This allows for constant rates of carbon formation over the different catalysts tried in this study.

3- The rate of carbon deposition can be approximated by a zero order kinetic equation with respect to CO in the range of partial pressures studied. The rate of carbon deposition is limited by the growth of the filaments.

4- Carbon formation from pure CO deactivates commercial porous pellets. Final constant rates of deposition are achieved through filamentous growths. A pore blocking mechanism appears to be consistent with the experimental data.

5- Carbon fromation from pure CO deactivates non-porous pellets. Hydrogenation of the carbon deposits regenerates

the pellet activity. This behaviour of the pellets suggests that the active iron is distributed in patches on the surface. Some of the patches can be lifted off the surface and form filaments. Others cannot be lifted off and deposit carbon until saturation (equilibrium) is achieved.

6- Carbon deposited from pure CO can be readily gasified with hydrogen. This shows that this kind of carbon is active towards hydrocarbon formation. The order of reaction with respect to hydrogen partial pressure appears to be 1. This is consistent with a mechanism in which the formation of a CH_{2M} group is the rate limiting step.

7- Hydrogen increases the rate of carbon formation from pure CO The order of reaction with respect to CO partial pressure is Ø. That for hydrogen partial pressure varies. At low hydrogen concentrations is Ø, at higher concentrations tends to -1.

REFERENCES

(1) Sabatier,P. and Sandersens,J.P.; Compt.Rend., 134, 514 (1902).

(2) Fischer,F. and Tropsch,H.; Chem.Ber., 4, 276 (1923).

(3) Fischer,F. and Tropsch,H.; Chem.Ber., 59, 830 (1926).

(4) Fischer,F. and Tropsch,H.; Brennst.Chem., 7, 97 (1926).

(5) Dry,M.E.; Catalysis, Vol. I, 159 (1981).

(6) Raupp,G.B. and Delgass,W.N.; J.Catal., 58, 318 (1979)

(7) Goodman,D.W.; Kelley,R.D.; Madey,T.E. and Yates,J.T.; A.C.S. Division of Pet. Chem.-Preprints, 23, 446 (1978).

(8) Martin,G.A.; Primet,M. and Dalmon,J.A.; J.Catal., 53, 321 (1978).

(9) Niemantsverdriet,J.W.; van der Kraan,A.M.; van Dijk,W.L. and van der Baan,H.S.; J. Phys. Chem., 84, 3363 (1980).

(10) Bertolini,J.C. and Imelik,B.; Ned.Tijdschr.Vacuumtech., Vol. 16, 2,24 (1978).

(11) Ott,G.L.; Fleisch,T. and Delgass,W.N.; J.Catal., 65, 253 (1980).

(12) Heal,M.J.; Leisegang,E.C. and Torrington,F.G.; J.Catal., 42, 10 (1976).

(13) Haggin,J.; C&EN, Oct. 26, 22 (1981).

(14) Dwyer,D.J. and Somorjai,G.A.; J.Catal., 52, 291 (1978).

(15) Rabo,J.A.; Risch,A.P. and Poutsma,M.L.; J.Catal., 53, 295 (1978).

(16) Dwyer,D.J. and Somorjai,G.A.; J.Catal., 56, 249 (1979).

(17) Joint Army-Navy Force Thermochemical Tables,2nd Edn.,Nat. Bur. Stand.,Nat. Stand. Ref. Data Service, 37, (1971).

(18) Rossini.F.D.; Selected Values of Properties of Hydrocarbons,Nat. Bur. Stand. Circular C461,1947.

(19) Lozada.I. and LaCava,A.I.; Catalytic Synthesis of Methane, Master's Report, City College, CUNY (1978).

(20) Bond,G.C.; 'Heterogeneous Catalysis', Oxford Chemistry Series, 22 (1974).

(21) Broden,G.; Rhodin,T.N. and Brucker,C.; Surf.Sci., 593 (1976).

(22) Allyn,C.L.; Gustafsson,T. and Plummer,E.W.; Chem.Phys.Lett., 47, 127 (1977).

(23) Batra,I.P.and Robaux,O.; J.Vac.Technol., 12, 242 (1975).

(24) Blyholder,G.; J.Phys.Chem., 74, 4335 (1970).

(25) Cossley.A. and Kine,D.A.; Surf.Sci., 68, 528 (1977).

(26) Lin,K.C.; Witt,J.D. and Hammaker,R.M.; J.Chem.Phys., 55, 1148 (1971).

(27) Eischens,R. and Pliskin,W.A.; Adv. Catalysis, 10, 1 (1958).

(28) Dorgelo,G.J. and Sachtler,W.M.H.; Naturwissenschaften, 20, 576 (1959).

(29) Robertson,J.C. and Wilmsen,C.W.; J.Vac.Sci.Technol., 9, 901 (1972).

(30) Miyazaki,E.; J.Catal., 65, 84 (1980).

(31) Eidus,Y.T.; Izv.Akad.Nauk SSSR, Otd.Khim.Nauk, 129 (1951).

(32) Craxford,S.R.; Fuel, 26, 119 (1946).

(33) Craxford,S.R. and Rideal,E.K.; J.Chem.Soc., 1, 604 (1946).

(34) Craxford,S.R.; Trans.Faraday Soc., 42, 576 (1946).

(35) Anderson,R.B.; Catalysis, Vol. IV, New York, Reinhold, (1956).

(36) Kummer,J.T.; DeWitt,T.W. and Emmett,P.H.; J.Chem.Soc., 70, 2632 (1948).

(37) Kummer,J.T.; Browning,L.C. and Emmett,P.H.; J.Chem.Phys., 16, 739 (1948).

(38) Browning,L.C.; DeWitt,T.W and Emmett,P.H.; J.Am.Chem.Soc., 72, 4211 (1950).

(39) Ekerdt,J.G. and Bell,A.T.; J.Catal., 58, 170 (1979).

(40) Araki,M. and Ponec,V.; J.Catal., 44, 439 (1976).

(41) Matsumoto,M. and Bennett,C.O.; J.Catal., 53, 331 (1978).

(42) Wentrcek,P.R.; Wood,B.J. and Wise,H.; J.Catal., 43, 363 (1976).

(43) Biloen,P.; Helle,J.N. and Sachtler,W.N.H.; J.Catal., 58, 95 (1979).

(44) Ponec,V.; Knor,Z. and Cerny,S.; 'Asorption on Solids', CRC Press, 470 (1974).

(45) Ponec,V.; Knor,Z. and Cerny,S.; J.Catal., 4, 485 (1965).

(46) Ponec,V.; Knor,Z. and Cerny,S.; Discussions Faraday Soc., 41, 149 (1966).

(47) Thomas and Thomas; 'Introduction to the Principles of Heterogeneous Catalysis'; Academic Press, 400 (1967).

(48) Beeck,O.; Advan. Catal., 2, 151 (1950).

(49) Elvins,O.C. and Nash,A.W.; Nature, 118, 154 (1926).

(50) Kolbel,H.; Ralek,M. and Jiru,P.; Brennst. Chem., 9, 580 (1970).

(51) Storch,H.H.; Golumbic,N. and Anderson,R.B.; 'The Fischer-Tropsch and Related Synthesis', New York, John Wiley 1951.

(52) Blyholder,G.; J.Phys.Chem., 70, 893 (1966).

(53) Blyholder.G. and Goodsel,A.J.; J.Catal., 23, 374 (1971).

(54) Heal,M.J.; Leisegang,E.C. and Torrington,R.G.; J.Catal., 51, 314 (1978).

(55) Pichler,H. and Schulz,H.; Chem.-Ing.-Techn., 42, 1162 (1970).

(56) Kolbel,H. and Roberg,H.; Ber.Bunsenges.Phys.Chem., 81, 634 (1977).

(57) Kolbel,H.; Patzschke,G. and Hammer,H.; Brennst.-Chem., 47, 4 (1966).

(58) Karu,A. and Beer,M.; J.Appl.Phys., 37, 2179, (1966).

(59) Lafitu,H. and Jacque,L.; Bull.Soc.Chim.France, 4779 (1968).

(60) Lecoanet,A.; These de L'Universite de Paris (1968).

(61) Tamai,Y.; Nishiyama,Y. and Takahashi,M.; Carbon, 6, 593 (1968).

(62) LaCava,A.I.; Trimm,D.L. and Turner,C.E.; Thermochimica Acta, 24, 273 (1978).

(63) Lahaye,J.; Prado,G. and Donnet,J.; Carbon, 12, 27 (1974).

(64) LaCava,A.I.; Fernandez-Raone,E.D. and Caraballo,M.; 'Coke Formation on Metal Surfaces', ACS Symposium Series, 89 (1981).

(65) LaCava,A.I.; Fernandez-Raone,E.D.; Isaacs,L. and Caraballo,M.; ib., 109 .

(66) Baker,R.; Feates,F. and Harris,P.; Carbon, 10, 93 (1972).

(67) Baker,R.; Barber,M.; Harris,P.; Feates,F. and Waite,R.; J.Catal., 26, 51 (1972).

(68) Smith,G.; Hinckley,C. and Zahraa,O.; J.Catal., 78, 262 (1982).

(69) Wang,C. and Ekerdt,J.; J.Catal., 80, 172 (1983).

(70) Scherzer,J.; J.Catal., 80, 465 (1983).

(71) White,G.A.; Roszkowski,T.R. and Stanbridge,D.W.; Hydroc.Process., 130 (1975).

(72) Greyson,M.; Catalysis Vol. IV, 480, Reinhold, N.Y., 1956.

(73) Greyson,M.; Bureau Mines Report 5137, 1955.

(74) Booth,N.; 'Catalytic Synthesis of Methane', The Gas Research Board, London, England, August 1948.

(75) Boehm,H.P.; Carbon, 11, 583 (1973).

(76) Baker,R.; Alonzo,J.R.; Dumesic,J.A. and Yates,D.J.C.; J.Catal., 77, 74 (1982).

(77) Ruston,W.R.; Warzee,M.; Hennaut,J. and Waty,J.; Carbon, 7, 47 (1969).

(78) Rostrup-Nielsen,J. and Trimm,D.L.; J.Catal., 48, 155 (1977).

(79) Renshaw,G.D.;Roscoe,C. and Walker,P.L.; J.Catal., 22, 394 (1971)

(80) Walker,P.L.;Rakszawski,J.F. and Imperial,G.R.; J.Phys.Chem., 63, 133 (1955).

(81) Nishiyama,J. and Tanai,J.; J.Catal., 33, 98 (1974).

(82) Somorjai,G.; J.Catal., 27, 453 (1972).

(83) Amelse,J.A.; Butt,J.B. and Schwartz,L.M.; J.Phys.Chem., 82, 558 (1978).

(84) Schafer-Stahl,M.; Angew.Che.Int.Ed. (English) 19, 729 (1980).

(85) Manning,M.P. and Reid,R.C.; Ind.Eng.Chem.Process Develop., 16 (3), 358 (1977).

(86) Wheeler,A.; Adv.Catal., 3, 249 (1951).

(87) Levenspiel,O.; 'Chemical Reaction Engineering', 2nd Edition, John Wiley (1972).

(88) Satterfield,C.N.; 'Mass Transfer in Heterogeneous Catalysis', M.I.T. Press (1970).

(89) Petersen,E.E.; 'Chemical Reaction Analysis', Prentice-Hall (1965).

(90) Froment,G. and Bischoff,K.; 'Chemical Reactor Analysis and Design', John Wiley (1979).

(91) Ruckenstein,E. and Pulvermacher,B.; A.I.Ch.E.J., 19, 356 (1973).

(92) Szepe,S. and Levenspiel,O.; 'Proc. 4th European Symp. on Chemical Reaction Engineering', Brussels 1968.

(93) Dumez,F.J. and Froment,G.F.; Ind.Eng.Chem.Proc.Des.Devpt., 15, 291 (1976).